MIT Open Access Articles

Jet substructure at the Large Hadron Collider

Jet substructure at the Large Hadron Collider

Roman Kogler[*]

Universität Hamburg, Hamburg, Germany

Benjamin Nachman[†]

Lawrence Berkeley National Laboratory, Berkeley, California 94720, USA

Alexander Schmidt[‡]

RWTH Aachen University, Aachen, Germany

Lily Asquith and Emma Winkels

University of Sussex, Sussex, United Kingdom

Mario Campanelli

University College London, London, United Kingdom

Chris Delitzsch

University of Arizona, Tucson, Arizona 85719, USA

Philip Harris

Massachusetts Institute of Technology, Cambridge, Massachusetts 02142, USA

Andreas Hinzmann

Universität Hamburg, Hamburg, Germany

Deepak Kar

University of Witwatersrand, Johannesburg, South Africa

Christine McLean and Justin Pilot

University of California, Davis, Davis, California 95616, USA

Yuta Takahashi

Universität Zürich, Zürich, Switzerland

Nhan Tran and Caterina Vernieri

Fermilab, Batavia, Illinois 60510, USA

Marcel Vos

IFIC Valencia, Valencia, Spain

(published 12 December 2019)

Jet substructure has emerged to play a central role at the Large Hadron Collider, where it has provided numerous innovative ways to search for new physics and to probe the standard model, particularly in extreme regions of phase space. This review focuses on the development and use of state-of-the-art jet substructure techniques by the ATLAS and CMS experiments.

[*]roman.kogler@uni-hamburg.de

[†]bpnachman@lbl.gov

[‡]alexander.schmidt@physik.rwth-aachen.de

CONTENTS

I. INTRODUCTION

Jets are collimated sprays of particles, produced in abundance in high energy particle collisions. They are ubiquitous in particle collider experiments and indispensable to study the underlying dynamics and interactions. Jets have played a central role in the discovery and property measurements of many fundamental particles like the gluon (g) (Barber *et al.*, 1979; Berger *et al.*, 1979; Brandelik *et al.*, 1979; Bartel *et al.*, 1980) and the top quark (t) (Abe *et al.*, 1995; Abachi *et al.*, 1995a). They have provided key insight into the structure of the strong force and were indispensable in the study of Higgs boson (H) couplings to heavy third generation quarks (Aaboud *et al.*, 2018a, 2018b; Sirunyan *et al.*, 2018a, 2018b). Because of their large production rate at the Large Hadron Collider (LHC), jets feature prominently in searches for new particles and precision measurements of standard model (SM) properties. However, important information on the underlying particle dynamics is not only carried by the total four-momenta of jets, but also by their internal structure. Investigations of this jet substructure reveal a wealth of physical processes and pose interesting theoretical and experimental challenges. While relatively young, the field of jet substructure has become an important field of research over the last decade and will gain further importance with the future data taking periods at the LHC.

With the advent of the LHC it was realized that decays of hypothetical, very heavy resonances can lead to highly Lorentz-boosted heavy SM particles, W, Z, H bosons and top quarks (Seymour, 1994; Butterworth, Cox, and Forshaw, 2002; Agashe *et al.*, 2008; Butterworth *et al.*, 2008; Kaplan *et al.*, 2008). Since these particles feature the largest branching fractions into hadrons, final states with fully hadronic decays have high sensitivity in LHC analyses. The large boost leads to very collimated decays, where particle masses of $\mathcal{O}(100)$ GeV are not large enough for the outgoing quarks to be sufficiently separated relative to each other to be resolved into individual jets. It is this small opening angle between the decay products which leads to fully merged particle decays. The following experimental overview describes techniques for measuring jets as proxies for hadronic decays of W, Z, H bosons and top quarks. However, this review is not limited to these methods but covers also precision jet substructure measurements and the discrimination of quark and gluon jets, reflecting the versatility of jet substructure. The scientific gains from these measurements are manifold, reaching from precision studies of QCD over the determination of fundamental parameters of the standard model to searches for new physical phenomena at the highest energy scales. A recent review on the theoretical aspects of jet substructure was given by Larkoski, Moult, and Nachman (2017).

Since the first evidence for jets in e^+e^- collisions at SPEAR (Hanson *et al.*, 1975), jets have had a significant impact on the research program of every particle collider since DORIS through the LHC and beyond to the design of future colliders. There is no single, universal definition of a jet—which particles belong to a jet depend on the algorithm used to combine particles into jets. In the beginning of jets from the mid-1970s, there were no jet clustering algorithms; information from the whole event was used instead of localized energy flows. The sphericity tensor (Bjorken and Brodsky, 1970) was typically used to obtain a jet axis for events with a back-to-back dijet topology. Quantitative statements about data were obtained from event shapes, like the sphericity or thrust (Brandt *et al.*, 1964; Farhi, 1977). Sphericity is a measure for the isotropy of the produced particles and thrust is a measure of the directed energy flow along an axis that maximizes this flow in an event. These event shapes can be used to characterize how compatible events are with the assumption of two oppositely directed, collimated jets. A clear theoretical advantage of these event shapes is that they are calculable in perturbative quantum chromodynamics (pQCD). This was realized early on and the calculability ultimately resulted in the confirmation of the parton model and, with data from experiments at higher $\sqrt{s}$, the discovery of the gluon in three jet events at PETRA (Barber *et al.*, 1979; Berger *et al.*, 1979; Brandelik *et al.*, 1979; Bartel *et al.*, 1980).

When studying the dynamics of quark and gluon scattering, it became necessary to perform quantitative analyses and calculations that go beyond event shapes. For these to be possible, it was realized that it is mandatory to define a deterministic set of rules on how particles are combined into jets. A schematic drawing depicting this problem is shown in Fig. 1. While the sphericity axis is uniquely defined and easily calculable, the direction and magnitude of the jet axes depend
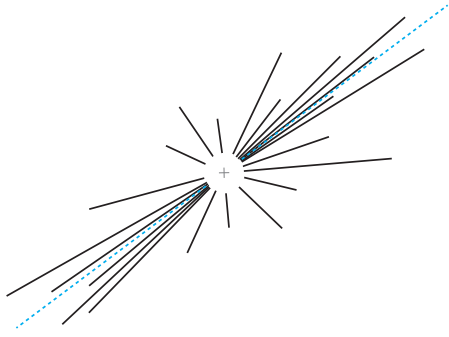
FIG. 1. Schematic drawing of particles emerging from the hard scattering of a high energy particle collision. The sphericity axis is shown as a dashed line.

on which particles should be combined into a given jet, and how the particles are combined to obtain the axes. An intuitive definition for a jet algorithm consists of summing the momenta of all particles within a cone with fixed size (Sterman and Weinberg, 1977). Naive cone algorithms are not infared and collinear (IRC) safe—the requirement that the resulting jets be insensitive to arbitrarily low energy particles and collinear splittings. IRC safety is a useful theoretical requirement for making calculations in pQCD and is also a convenient language for describing the experimental robustness to noise and detector granularity.

There exist many variants of cone-type algorithms, developed in the attempt to solve the IRC unsafety of naive cone jet algorithms. This stems from the necessity of an initial axis, which was eventually solved with the formulation of the SISCone algorithm (Salam and Soyez, 2007). Although this algorithm is IRC safe, it is not widely used today because it was found that sequential recombination algorithms have several advantages over cone-type algorithms. First used by the JADE Collaboration (Bartel *et al.*, 1986; Bethke *et al.*, 1988), the initial version of a recombination algorithm defined for e^+e^- collisions was improved in several steps (Catani *et al.*, 1991; Catani, Dokshitzer, and Webber, 1992) to finally arrive at the longitudinally invariant k_T-clustering algorithm for hadron-hadron collisions (Catani *et al.*, 1993). A generalization of this algorithm leads to three classes, distinct only by the sign of the exponent of the transverse momentum $p_{T,i}$ in the inter-particle distance measure

$$d_{ij}(p_i, p_j) = \min(p_{T,i}^{2k}, p_{T,j}^{2k}) \frac{\Delta R^2}{R^2}, \qquad (1)$$

where[1] $\Delta R^2 = \Delta\phi^2 + \Delta y^2$ and R is typically called the *jet radius*. The original k_T algorithm, with $k = 1$ in Eq. (1), clusters soft and collinear particles first, the Cambridge/Aachen (CA) algorithm (Dokshitzer *et al.*, 1997; Wobisch and Wengler, 1998), with $k = 0$, prioritizes particles in the clustering solely by their angular proximity, and the anti-k_T algorithm (Cacciari, Salam, and Soyez, 2008a), with $k = -1$, combines the hardest particles first. The proposal of the latter algorithm is also

responsible for the disappearance of cone-type algorithms in experimental studies. When it was realized that the anti-k_T algorithm results in nearly perfect conical jets the LHC Collaborations made a transition to this algorithm. Today, almost all studies involving jets performed at the LHC use this algorithm. Even when analyzing the substructure of jets with advanced grooming or tagging techniques, the initial step often consists of building an ensemble of particles that were clustered with the anti-k_T algorithm.

So far, it has not been specified what the term particle refers to when using particles as input to jet clustering. In fact, in jet physics the term particle is often used generically for different sorts of objects, whose ensemble comprises the input to a given jet algorithm. Three different ensembles are commonly used. The partonic final state includes all particles resulting from the parton shower before the hadronization starts (which is unphysical). This also includes photons when these were created in the hard interaction or emitted from charged particles during the parton shower. The ensemble on the particle level, also called the hadron level, consists of hadrons and their decay products, including photons and leptons. The detector-level input consists of calorimeter clusters, reconstructed particle tracks, or combinations thereof. Jet algorithms using these different ensembles as input result in parton-, particle-, or detector-level jets, respectively. Ideally, in any given event, the jets obtained on parton, particle, and detector levels are as similar as possible. Realistically, agreement cannot be achieved, but a close correspondence ensures the possibility to study the underlying partonic dynamics with the use of jets. It is this correspondence, paired with calculability in pQCD, that makes jets indispensable tools at high energy particle colliders.[2]

Soon after their discovery, it was realized that not only the kinematics of jets but also their internal structure carries information. The parton shower and subsequent hadronization leads to a characteristic multiplicity, as well as angular and momentum distributions of hadrons inside jets, which depend on the parton that initiated the shower. For example, the probability of a $q \to qg$ splitting is proportional to the color factor $C_F = 4/3$ at leading order in QCD, while the probability of $g \to gg$ is proportional to $C_A = 3$. The larger value of C_A results in a larger multiplicity of hadrons and in broader jets. This leads to the suggestion of measuring jet shapes, defined as the fractional transverse momentum profile of particles within a concentric inner cone, smaller than the jet cone of the original jet, and pointed to their usefulness for distinguishing quark jets from gluon jets (Ellis, Kunszt, and Soper, 1992). Experimental results from LEP (Alexander *et al.*, 1991; Buskulic *et al.*, 1995; Abreu *et al.*, 1996; Acciarri *et al.*, 1997), Tevatron (Abe *et al.*, 1993; Abachi *et al.*, 1995b), and HERA (Breitweg *et al.*, 1998, 1999; Adloff *et al.*, 1999) confirmed this and can be considered as the starting point of physics with jet substructure in particle physics.

At the LHC, jet substructure is used to identify highly boosted heavy SM particles in fully hadronic decays. An

---

[1] Sometimes the rapidity (y) is used and sometimes the pseudorapidity (η) is used depending on the application. See Gallicchio and Chien (2018) for a detailed discussion.

[2] For a theoretical introduction to jets, we recommend the reviews of Ellis, Stirling, and Webber (1996) and Salam (2010) as well as the theory companion, the experimental review of Larkoski, Moult, and Nachman (2017).
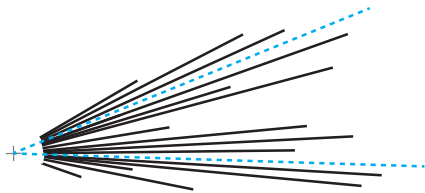
FIG. 2.   Schematic drawing of particles clustered into a single jet. Two subjet axes are shown as dashed lines.

example of a jet with substructure from a two-prong decay is shown schematically in Fig. 2. The difficulty lies in identifying the underlying process that led to the final state, for example, distinguishing $W \to q\bar{q}'$, $Z \to q\bar{q}$, or $H \to b\bar{b}$ from QCD splittings like $q \to qg$, $g \to gg$, or $g \to q\bar{q}$. Numerous algorithms have been suggested to identify specific decays, which are part of a class of *jet substructure taggers*. The idea behind many of these algorithms is related to event shapes in e^+e^- collisions. By defining N axes within a jet, it is possible to check for the compatibility of a fully merged N-prong decay. How these axes are found typically differs from algorithm to algorithm, and some techniques do not even explicitly require axes. Popular concepts are an exclusive jet clustering using the particles inside a jet as input, or the maximization of the projection of the jet constituents' momenta onto the desired number of axes, as illustrated in Fig. 2. Since the opening angle between the quarks depends on the momentum of the parent particle and its mass, larger jets ($R \sim 1$) than normally employed in LHC analyses ($R \sim 0.4$) are used to reconstruct boosted heavy particle decays. A larger distance parameter is chosen to capture the full kinematics of the decay already at moderate momenta of 200–400 GeV. The drawback of jets with large areas is unwanted contributions from the underlying event and from multiple proton-proton collisions in a single bunch crossing (pileup). These lead to a worsening of the resolution in quantities used to identify the substructure of jets, like the jet mass. Jet *grooming* and pileup removal algorithms have been developed to mitigate these effects. Grooming algorithms aim at removing soft and wide-angle radiation, therefore not only reducing the effects from the underlying event but also reducing the sensitivity to the details of fragmentation. Pileup removal algorithms are designed to identify and subtract contributions from a different interaction vertex, by eliminating uncorrelated radiation from jets. A combination of these techniques often leads to the best overall performance and it is an ongoing effort to understand the interplay of pileup removal, grooming, and tagging algorithms.

The theoretical and algorithmic developments are possible due to advances in experimental methods. New technologies, like silicon pixel detectors, high-resolution tracking detectors in conjunction with strong magnetic fields, highly granular calorimeters with low electronic noise, and lightweight materials for detector structures with little dead material inside the active detector volume, have enabled increasingly precise jet measurements and studies of internal jet structure. Modern particle detectors at the LHC are equipped with many layers of high-resolution tracking detectors, strong and very homogeneous magnetic fields, and finely segmented

calorimeters with an excellent energy resolution. With these technologies, the ATLAS and CMS detectors[3] are equipped to track and reconstruct individual particles produced in high energy collisions. On average about 60% of a jet's momentum is carried by charged hadrons, photons account for about 25% of the total jet momentum, and the remaining 15% can be attributed to long-lived neutral hadrons (Khachatryan *et al.*, 2017a). With increasing jet energy, the particle multiplicity increases and also the fraction of the jet's momentum carried by soft particles. For example, on average 50% of the momentum of a 50 GeV jet is carried by particles with a momentum less than 5% of the jet's momentum. It is therefore crucial to ensure that particles with energies down to $\mathcal{O}(100 \text{ MeV})$ can be reconstructed in order to retain the full information on a jet's kinematics and internal structure.

As important as the reconstruction of the total jet energy is the measurement of the jet constituent multiplicity and their angular distributions. While charged particles can be efficiently reconstructed as tracks, neutral particles develop showers in the calorimeters and the possibility to resolve two separate showers depends on the granularity of the calorimeter and the lateral shower development. Hence, it becomes more difficult to separate two adjacent particles in dense environments, such as high-momentum jets, and the situation is aggravated by the presence of hadronic showers from charged hadrons. Often it is impossible to build one calorimeter cluster per neutral particle. A way to improve the angular resolution in jet substructure analyses is to combine measurements from the tracking detectors and calorimeters. Using combined detector measurements as input to jet algorithms, for example, using a particle-flow (PF) approach, results in improved resolutions of jet substructure observables, compared to using only tracks or only calorimeter clusters.

An important aspect of experimental analyses at the LHC is the calibration of jets, necessitated by the noncompensating nature of hadron calorimeters, suppression of electronic noise, tracking inefficiencies, dead material in front of calorimeters, the influence of pileup, and other effects. While the calibration of the total jet energy scale is an important aspect in all analyses using jets, the precise knowledge of the jet mass scale and the detector response to jet substructure observables and jet tagging algorithms is specific to jet substructure analyses. Calibrating the jet energy scale results in a change of the magnitude of the jet's four-momentum, where the jet mass scale comprises an additional degree of freedom that cannot be constrained by the typical methods of balancing a jet with a well-calibrated reference object. The jet mass scale is usually calibrated using jets from fully merged, highly boosted $W \to q\bar{q}'$ decays, facilitating a calibration of the peak position in the jet mass distribution. Measurements of the jet mass distribution from light quark and gluon jets, as well as from

---

[3]The ALICE and LHCb detectors are also well equipped to perform jet substructure studies. While these experiments do not have access to boosted massive particles due to their data rate (ALICE) or acceptance (LHCb), they are performing many interesting QCD studies with jet substructure. This review will be focused on ATLAS and CMS, but the future of jet substructure will involve key contributions from all four LHC experiments.

fully hadronic highly boosted *W*, *Z*, and *t* decays allow for precise tests of the modeling of perturbative and nonperturbative effects in jet production. Similar measurements can also be used to study the detector response to jet substructure observables and their modeling in simulation. A mismodeling of variables used for tagging, either in the detector simulation or on the level of the underlying physics, can result in a wrong estimation of the tagging efficiency or the misidentification rate, with important consequences for measurements. In order to overcome this limitation, measurements of tagging efficiencies and misidentification rates are performed in samples enriched with the particle decays in question. While these measurements do not help to understand the cause of the mismodeling or to improve the description of jet substructure distributions, these can be used to correct the efficiencies in simulation. It is these measurements that have enabled the use of jet substructure taggers in numerous physics analyses since the beginning of data taking at the LHC. The increased statistics from a data sample corresponding to about 150 fb^{-1} per experiment at a center-of-mass energy of 13 TeV can now be used to improve our understanding of the detector response to jet substructure algorithms, the underlying physics, and the performance differences of taggers. These studies and measurements represent the continuation of an exciting physics program at the LHC in a field which reached its adolescence in the past few years. In the years to come, the field of jet substructure will evolve and mature through precision measurements and the exploration of unknown territory.

We begin this review with a brief overview of the ATLAS and CMS detectors in Sec. II, followed by a description of the input to jet reconstruction and jet calibration in Sec. III. Important aspects of jet reconstruction at the LHC, and jet substructure, in particular, are algorithms to mitigate the effects of pileup. Recent experimental advancements and algorithms employed in ATLAS and CMS analyses are discussed in Sec. IV. In Sec. V we review jet grooming techniques in use in experimental analyses and discuss their impact on jet substructure observables. A special emphasis is given on the jet mass calibration and jet mass measurements in different final states. Measurements of other jet substructure distributions are described as well. One of the key developments within the field of jet substructure is tagging algorithms, which are described in detail in Sec. VI. Theoretical and experimental developments have resulted in large performance gains of substructure taggers in the last years, relevant for a large number of present and future physics analyses. We highlight the main developments and improvements and give an overview of relevant experimental studies. The use of jet substructure taggers in existing cross section measurements is reviewed in Sec. VII. So far, the major beneficiaries of jet substructure methods have been analyses in search for new physical phenomena. We review the application of these methods to searches for new physics in Sec. VIII and conclude in Sec. IX.

II. ATLAS AND CMS DETECTORS

The ATLAS (Aad *et al.*, 2008) and CMS (Chatrchyan *et al.*, 2008) detectors are designed to observe leptons, photons, and hadrons resulting from LHC *pp* collisions. The physics of the hard reaction takes place at the point of collision (the primary vertex) within the beam pipe. Beyond the beam pipe,[4] at 4.4 cm (3.3 cm) in CMS (ATLAS), the first cylindrical layers of detectors encountered are silicon pixels and strips for identification of charged particles. CMS provides a 3.8 T magnetic field via a solenoid positioned outside the silicon tracking detector, the electromagnetic calorimeter (ECAL), and most of the hadronic calorimeter (HCAL). ATLAS has an additional tracking layer composed of straw drift tubes [transition radiation tracking (TRT)], with a 2 T magnetic field encompassing the silicon and TRT detectors, while the ECAL and HCAL are situated outside the solenoidal magnet. The calorimeters are surrounded by muon spectrometers which build the outermost part of the ATLAS and CMS detectors. Both detectors are nearly hermetic and can therefore measure the missing transverse momentum.

The energy and momentum ranges and resolutions for the barrel regions[5] of ATLAS and CMS are shown in Table I along with the measurement granularity, which limits the angular resolution. The better energy resolution of the CMS ECAL is due to the use of lead tungstate (PbWO$_4$) crystals, as opposed to the liquid argon (LAr) used by ATLAS. The differences in the ATLAS and CMS calorimeter designs are a result of the different ranking of priorities decided by the two collaborations; ATLAS chose a radiation-hard technology with sufficient resolution in a fine sampling LAr calorimeter, while CMS prioritized the excellent resolution of a total absorption crystal calorimeter (the focus was Higgs mass reconstruction), and accepted the accompanying limitations in radiation hardness associated with this technology. The CMS ECAL crystal response varies under irradiation, which is partially recovered in a few hours at room temperature.

The ATLAS ECAL is segmented into three (two) longitudinal layers for $|\eta| < 2.5$ ($|\eta| > 2.5$). The granularity of the ATLAS ECAL in Table I refers to its second layer (as most of the electromagnetic energy is deposited there); the first layer has a finer granularity in η. The multiple layers allow for a finer granularity than the cell size in any of the individual layers, being advantageous over a laterally segmented calorimeter, and additionally provide pointing information. The difference between ATLAS and CMS for the HCAL resolution is particularly large at higher energies: a 1 TeV jet has $\sigma(E)/E \sim 2\%$ in ATLAS, in contrast to $\sigma(E)/E \sim 5\%$ in CMS. This is one reason why CMS fully adapted a particle-flow technique since the beginning of the LHC (see Sec. III.A).

---

[4]The LHC Collaborations are continuously working to improve the detectors; the numbers given here are for the detectors that operated in 2015–2017. Before and after this time, the exact values are not the same as reported here.

[5]For example, the ATLAS ECAL barrel covers the pseudorapidity range $|\eta| < 1.475$, the end caps cover $1.375 < |\eta| < 3.2$, and the forward ECAL layer extends the coverage up to $|\eta| < 4.9$. The CMS ECAL barrel covers $|\eta| < 1.48$, and the end caps extend the coverage up to $|\eta| < 3$.

TABLE I. ATLAS and CMS detectors in the barrel regions. The granularity is in pseudorapidity and azimuth ($\eta \times \phi$) and d_0 is the transverse impact parameter resolution with respect to the beam line. The tracker momentum resolution is from muons while the d_0 resolution is from generic charged particles (mostly pions) in $t\bar{t}$ events. The ECAL energy resolution is presented for electrons. The granularity for the ATLAS calorimeters is for the middle layers only, which collect the largest amount of energy. For the ATLAS EM calorimeter, the innermost layer has $\Delta\eta = 0.0031$ for γ/π^0 separation.

	ATLAS	CMS
Tracking		
$1/p_T$ resolution	$0.05\% \times p_T/\text{GeV} \oplus 1\%$	$0.02\% \times p_T/\text{GeV} \oplus 0.8\%$
	(Aad *et al.*, 2010)	(CMS Collaboration, 2014a)
d_0 resolution (μm)	20	20
	(Abbott *et al.*, 2018)	(CMS Collaboration, 2014a)
ECAL		
E resolution	$10\%/\sqrt{E} \oplus 0.2\%$	$3\%/\sqrt{E} \oplus 12\%/E \oplus 0.3\%$
	(Aad *et al.*, 2008)	(Chatrchyan *et al.*, 2008)
Granularity	0.025×0.025	0.017×0.017
HCAL		
E resolution	$50\%/\sqrt{E} \oplus 5\%$	$100\%/\sqrt{E} \oplus 5\%$
	(Aad *et al.*, 2008)	(CMS Collaboration, 1997)
Granularity	0.1×0.1	0.087×0.087

III. JET RECONSTRUCTION

A. Inputs

Both experiments have dedicated algorithms to reconstruct particle kinematics from calorimeter and tracker information designed to minimize the fake rate, maximize the efficiency, and minimize the bias and resolution of the particle candidate parameters. As there is no algorithm that can simultaneously optimize all of these objectives, the various approaches trade off optimality under one metric for improvements under another. ATLAS and CMS have also developed different algorithms that cater to the experiment's hardware as well as the collaboration's goals for the tradeoffs. By default, CMS combines tracker and calorimeter information into unified particle-flow objects as inputs to jet reconstruction (CMS Collaboration, 2009a, 2010; Sirunyan *et al.*, 2017a). ATLAS has traditionally used calorimeter-only information for jet reconstruction, with tracking information used to augment or enhance the performance. While ATLAS is currently migrating to a variation of particle flow (Aaboud *et al.*, 2017a), most of this review focuses on calorimeter-only jets as they are still the most widely used setup. ATLAS benefits less than CMS from particle flow because of its weaker magnetic field and longitudinally segmented calorimeter.

ATLAS and CMS combine calorimeter cells using topological clusters (Aad *et al.*, 2017; Sirunyan *et al.*, 2017a). These clusters are three dimensional in ATLAS as a result of the longitudinal segmentation. Cluster seeds are started from highly significant energy (high cell signal to average electronic $\oplus$ pileup noise) deposits which are combined (or split) based on the distribution of the significance of energy in nearby cells. Calorimeter-cell clusters in CMS are obtained using a Gaussian-mixture model, which results in one or more calorimeter clusters within each topological cluster. HCAL clusters can be split according to the number and energy distribution of associated ECAL clusters. Cluster splitting is critical to achieve a better estimate of the spatial energy distribution as input to jet substructure algorithms (CMS Collaboration, 2014b; ATLAS Collaboration, 2017h).

The topological clusters are calibrated using simulations to account for the noncompensating calorimeter response to hadrons, signal losses due to energy deposited in inactive detector material, and signal losses on cluster boundaries caused by the topological clustering algorithms. In ATLAS, the calibration scheme relies on a classification of clusters as hadronic or electromagnetic in origin based on the energy and position of the cluster, the longitudinal depth (λ_{clus}), and normalized signal energy density; hadronic showers tend to occur deeper in the calorimeter and be less dense (Aad *et al.*, 2017). Charged and neutral pions are used to derive this classification and calibration, called the local cell weighting (LCW). In CMS, dedicated ECAL (based on photons) and HCAL (based on neutral kaons) calibrations are combined to account for energy and $|\eta|$-dependent nonlinearities in the hadron calorimeter response (Sirunyan *et al.*, 2017a). Both ATLAS and CMS validate the performance of these calibrations with single particle studies in data (Aaboud *et al.*, 2017b; Sirunyan *et al.*, 2017a).

Different strategies are used by ATLAS and CMS to reconstruct tracks from their inner detectors. ATLAS focuses first on maintaining a high efficiency with a rather inclusive first pass through inner detector hits. A second step known as ambiguity solving reduces the fake rate. In contrast, CMS uses a sequential approach with multiple passes through the remaining inner detector hits. With each pass, the efficiency increases while maintaining a low fake rate. Both procedures are effective at identifying about 90% of charged pions above 1 GeV with a percent-level (or smaller) fake rate. Lower momentum particles can be reconstructed at the cost of a higher fake rate and lower efficiency. Because of its weaker magnetic field, ATLAS is able to reach low track momentum of 100 MeV for physics analysis (Aaboud *et al.*, 2016b), although most jet substructure measurements and searches use a threshold of 500 MeV. In contrast, the momentum resolution in CMS is excellent up to higher momenta than in ATLAS. The TRT can be used to improve the momentum resolution of high p_T tracks (Aaboud *et al.*, 2017d), but the weaker magnetic field despite a comparable inner detector radius is a fundamental limitation.

Both experiments have implemented dedicated strategies for track reconstruction in high density environments such as the core of high-p_T jets. In such environments, pixel and strip clusters can merge resulting in a loss in tracking efficiency and degraded resolution. ATLAS has implemented a stacked neural network (NN) approach to examine pixel clusters to identify multiparticle clusters, estimate the position of the particles passing through the clusters, and also predict the residual resolution of the position estimates (ATLAS Collaboration, 2014a, 2015a, 2016b, 2017a; Aaboud *et al.*, 2017e). CMS has introduced a dedicated tracking step in which a cluster splitting procedure attempts to split merged clusters exploiting the information of the jet direction, predicting the expected cluster shape and charge (CMS Collaboration, 2014c).

For particle flow in CMS, tracks and calibrated clusters are combined taking the tracking and calorimeter resolutions into account. First, a link is created between tracks in the central tracker and calorimeter clusters. Links are also created between clusters in the ECAL and HCAL, when the cluster position in the ECAL is within the cluster envelope in the less granular HCAL. Tracks with a p_T uncertainty in excess of the calorimetric energy resolution expected for charged hadrons are masked, which allows the rate of misreconstructed tracks at large p_T to be reduced.

The ECAL and HCAL clusters not linked to any track give rise to photons and neutral hadrons. Charged hadrons are created from the remaining ECAL and HCAL clusters, linked to tracks. If the calibrated calorimetric energy is compatible with the corresponding track momenta under the charged-pion hypothesis, no neutral particles are created. Otherwise, the excess energy is interpreted to originate from photons and neutral hadrons for deposits in the ECAL and HCAL, respectively. The particle-flow algorithm in ATLAS is similar to the one used by CMS and is described in more detail by Aaboud *et al.* (2017a).

The combination of tracking and calorimetric measurements results in an optimal input for jet substructure measurements, making use of the superior angular resolution from the tracking detector and calibrated calorimeter clusters. Once the calibrated PF objects are clustered into jets, their relative momenta and angular distances are kept constant, and only the total energy response of jets is corrected with factorized jet energy scale (JES) calibrations (see Sec. III.B).

The particle-flow algorithm improves the energy resolution as shown in Fig. 3. A similar performance gain is observed in ATLAS, but the weaker magnetic field means that the point where calorimetery and tracking are comparable is lower (about 100 GeV).

B. Calibration

The ratio of the measured energy E_{reco} to the deposited energy E_{true} is the jet energy *response* which depends on the energy, pseudorapidity, and other features of the jet. Because of the properties of tracking detectors and calorimeters, the average response is not unity. For example, calorimeter jets in ATLAS with $E_{true} = 30$ GeV may have responses below 0.3, while jets of higher energies may have responses above 0.8. For this reason, the JES is calculated in bins of the particle-level jet energy E_{true} and η_{det} as the mean
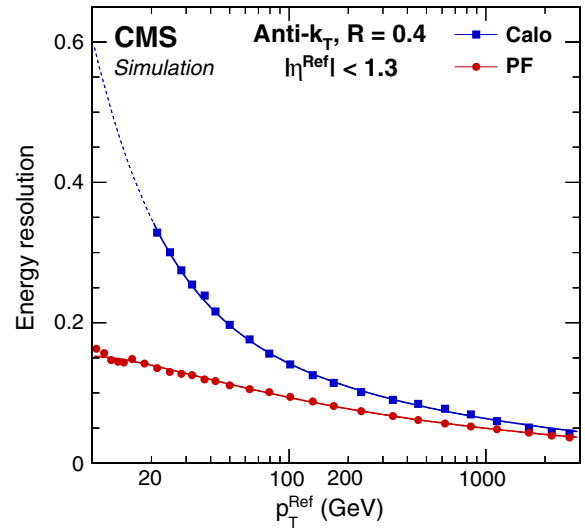

FIG. 3. Jet energy resolution for particle flow (red, lower line) and calorimeter-only (blue, upper line) jets in the barrel region in CMS simulation, with no pileup, as a function of the p_T of the reference jet. From Sirunyan *et al.*, 2017a.

of a Gaussian fit to the response distribution and a numerical inversion procedure is used to derive calibration factors in bins of the reconstructed jet energy from E_{true} (CMS Collaboration, 2011b; Aad *et al.*, 2015b; Aaboud *et al.*, 2017c; Cukierman and Nachman, 2017).

In ATLAS, the calibration of the JES is undertaken in several stages, starting from jets at either the electromagnetic (EM) or LCW (built from calibrated inputs) scale. Using calibrated inputs bring the JES to within 10% of unity for $E = 30$ GeV and $|\eta| < 0.3$ (Aad *et al.*, 2015b). The global sequential calibration (ATLAS Collaboration, 2015b; Aaboud *et al.*, 2017c) was introduced for run 2 and reduces the sensitivity to differences in the responses of quark versus gluon-initiated jets (quark/gluon separation is also discussed in Sec. VI.A). This additional calibration results in a significant jet p_T resolution improvement of up to 35% depending on the p_T and η of the jet (ATLAS Collaboration, 2015b). The JES uncertainty varies between 1% and 6% in the central region with $\eta = 0$ as shown in Fig. 4 (Aaboud *et al.*, 2017c).
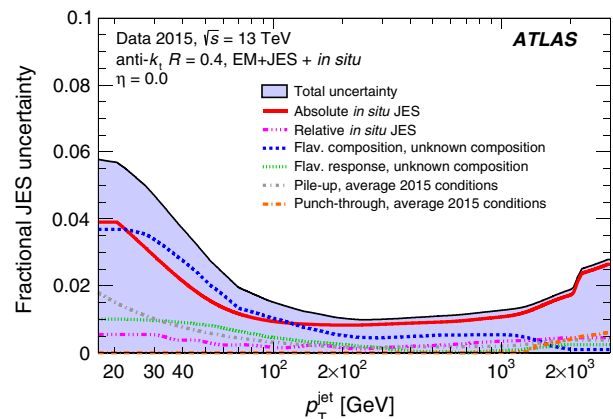

FIG. 4. ATLAS jet energy scale uncertainty. Adapted from Aaboud *et al.*, 2017c.
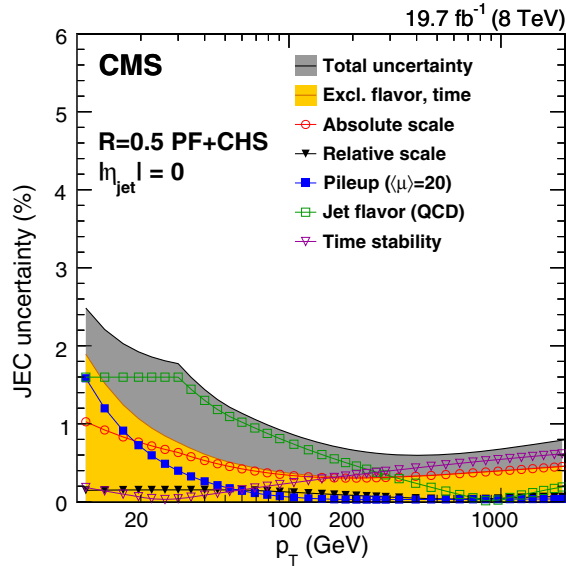
FIG. 5. CMS jet energy scale uncertainty. JEC means jet energy correction, which has the same meaning as JES. From Khachatryan *et al.*, 2017a.

FIG. 6. Average pileup contribution to the jet p_T, ρ, as a function of the average number of pileup interactions per bunch crossing μ for data (circles) and simulation (diamonds) at the CMS experiment. From Khachatryan *et al.*, 2017a.

In CMS, jets are clustered from calibrated particle flow objects, thus the uncalibrated JES is within 6% of the expected value of 1 for central jets with $\eta < 0.7$ and $p_T > 30$ GeV (Khachatryan *et al.*, 2017a). To account for deviations from unity, factorized JES calibrations are applied in multiple stages (CMS Collaboration, 2014d) including pileup corrections, simulation-based response corrections, and small residual corrections for tracking inefficiencies and threshold effects, derived *in situ* from $\gamma + $ jet, $Z + $ jet, and dijet samples (CMS Collaboration, 2011b). This additional correction is not used when jet substructure observables are constructed, but dedicated corrections are derived as described in Sec. V.B. Figure 5 shows the calibrated JES uncertainty obtained in CMS, which is below 1% for jets with $p_T > 100$ GeV in the central region with $\eta = 0$. Even for jet p_T as low as 10 GeV the uncertainty is below 3%, owing to the excellent performance of the particle flow reconstruction.

A detailed discussion of the different approaches for deriving jet energy scale uncertainties in ATLAS and CMS can be found in CMS Collaboration (2014d).

IV. PILEUP MITIGATION

A. Definition

Pileup originates from simultaneous proton-proton (pp) collisions that occur in addition to a hard scattering collision of interest. The hard scattering event of interest is referred to as the primary vertex (PV). Pileup is uncorrelated with the PV and typically consists of an admixture of inelastic, elastic, and diffractive pp processes which are separated in the longitudinal direction. As the detector response is not instantaneous, pileup events from both the same (*in-time*) and neighboring (*out-of-time*) bunch crossings can contribute. This review focuses on the mitigation of in-time pileup, although out-of-time pileup is also mitigated to differing degrees due to the specifics of the ATLAS and CMS detector technologies and reconstruction algorithms.
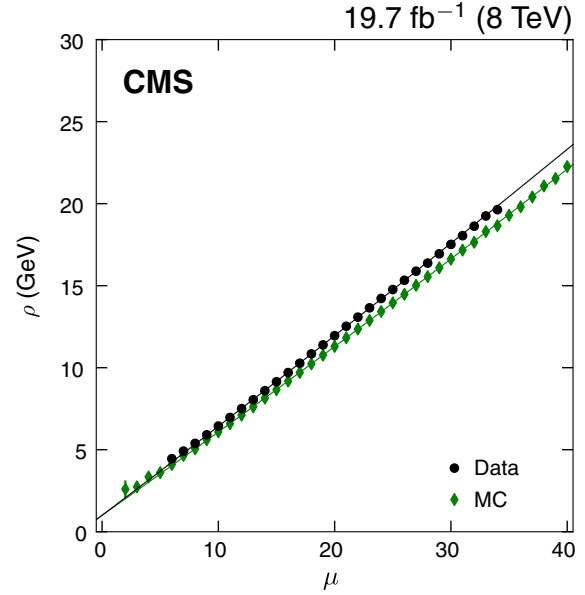
During the LHC run 1 the mean number of pileup interactions reached $\langle\mu\rangle = 21$, and μ values up to 60 were attained in certain runs of 2017 (run 2) with possibly even higher values in run 3, and culminating at the high luminosity LHC (HL-LHC) reaching up to $\langle\mu\rangle = 140$–200.

Pileup typically leaves about 0.5 GeV of energy in the detector per unit area (η, ϕ), per pileup vertex; the effects of this are present in all aspects of LHC physics, from detector design and software performance to the final sensitivity of measurements and searches.

B. Mitigation methods

Properties of pileup interactions are exploited to discriminate pileup particles from particles originating from the primary vertex or to remove energy contributions from pileup to the individual jet.

Pileup can be approximated as a spatially uniform deposition of energy. The so-called *area subtraction* uses a pileup p_T density per unit area estimator ρ and defines a jet catchment area A to remove energy that is assumed to originate from pileup interaction. This approach corrects the jet in the following way: $p_T^{corr} = p_T^{orig} - \rho A$. An example of ρ is shown in Fig. 6. There are many subtleties in defining both ρ and A, which have been discussed by Cacciari, Salam, and Soyez (2008b), CMS Collaboration (2014e), and Aad *et al.* (2016d). An extension to this method is *shape subtraction* (Soyez *et al.*, 2013), where randomly distributed ghost particles are used to calculate a jet shape's sensitivity to pileup, which can then be corrected for nonuniformities in the spatial distribution of pileup particles.

Instead of a global, collective treatment of pileup for the whole jet, the individual particles within the jet can be classified to whether they belong to the actual jet or to the
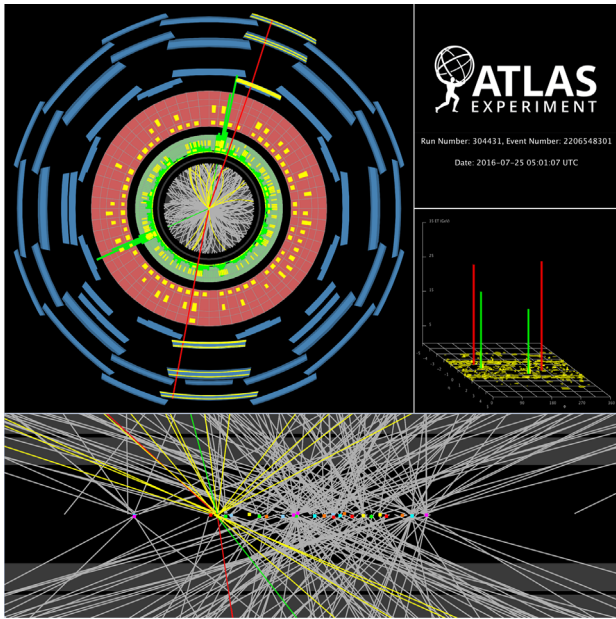
FIG. 7. $H \to 2e2\mu$ candidate event with 25 additional reconstructed vertices recorded in 2016. From ATLAS Collaboration, 2016c.

underlying pileup. Charged particles leave tracks in high granularity tracking detectors at the heart of multipurpose detectors like ATLAS and CMS and can be separated based on their longitudinal position $\hat{z}$ (along the beam line) within the luminous region; see Fig. 7. The *charged-hadron subtraction* (CHS) (CMS Collaboration, 2014e) method identifies each pileup track individually. Used in concert with particle-flow concepts which attempt to identify each particle in the event uniquely, CHS can effectively remove all charged pileup radiation from the event, including calorimeter signals that are linked to tracks through the particle-flow algorithm. Identification of pileup jets, formed predominantly from the energy of one or many pileup vertices, is another technique for removing pileup using charged particles; by determining the fraction of energy of the jet from the primary vertex, one can distinguish such pileup jets from the PV jets (CMS Collaboration, 2013a; Aad *et al.*, 2016d).

The two methods discussed can be combined. First the more precise CHS method subtracts the pileup contribution from charged particles. In the second step, the remaining contributions from neutral particles are removed with the area subtraction method.

In a more advanced approach, local, topological information is used, as QCD radiation from pileup vertices is often uncorrelated and soft. It can thus be removed based on the local energy profile, i.e., if the radiation is not consistent with hard scattering radiation from the PV. This can be done in the transverse plane η, ϕ and also as a function of radiation depth. The jet grooming technique is such an example to clean the jet of soft and wide-angle radiation which incidentally removes pileup radiation. It is discussed in more detail in Sec. V.A. Topoclustering (Aad *et al.*, 2017), used by the ATLAS Collaboration, is deployed at the formation of clusters in the calorimeter requiring radiation to have a certain topological profile. In the forward region, where no

tracking information is available, jet shapes and topological correlations can be used to identify pileup (Aaboud *et al.*, 2017f).

While the previous methods have been successfully deployed in the LHC experiments, they each have some deficiencies as well. Ideally, one wants to effectively combine all pileup mitigation handles in order to maximally distinguish pileup from PV radiation and to remove pileup at the most granular level possible, i.e., at the particle or constituent level, in order to be as generic as possible. For example, while area subtraction is effective for correcting the jet p_T, it is not used to mitigate the pileup dependence of jet substructure observables as it is only able to correctly remove pileup contributions on average. In fact, jet substructure variables are among the most difficult to correct for pileup because they are so reliant on radiation profiles. A number of hybrid methods have been proposed operating at the event constituent level. One example is the Pileup Per Particle Identification (PUPPI) (Bertolini *et al.*, 2014) algorithm which is extensively used in CMS. The PUPPI algorithm uses both event energy density and local topological information incorporated in an event-by-event particle-level discriminator to determine if a particle is from pileup. The algorithm defines a shape which attempts to distinguish parton showerlike radiation from pileuplike radiation. The shape is calculated from p_T, the angular distance to nearby particles, and other information. Particle four-vectors are then weighted proportional to the value of the discriminator value. Ideally, particles from the hard scatter would get a weight of 1 and pileup particles would get a weight of 0. Almost all pileup particles have values within a few standard deviations of the median and are assigned small weights. Values that deviate far from the charged pileup are indicative of a hard scatter, and these particles are assigned large weights. This weighting method allows for experimental information, such as tracking, vertexing, and timing information, to be included.

Other examples of such hybrid methods are constituent subtraction (Berta *et al.*, 2014; Bertolini *et al.*, 2014; Cacciari, Salam, and Soyez, 2015), SoftKiller (Cacciari, Salam, and Soyez, 2015), and PUMML (Komiske *et al.*, 2017). Precursor hybrid methods include *jets without jets* (Bertolini, Chan, and Thaler, 2014) and *jet cleansing* (Krohn *et al.*, 2014).

C. Performance studies

Pileup removal algorithms are commissioned for use in ATLAS and CMS via detailed studies of jet observables in terms of the resolution and absolute scale, pileup dependence, and the background rejection versus signal efficiency for boosted heavy particle taggers.

For observables like jet p_T, dependencies on the number of reconstructed vertices and μ are observed even with area subtraction methods for the pileup levels currently observed at the LHC, $\langle\mu\rangle \sim 25$. To correct for these effects, an additional residual correction is applied (Aaboud *et al.*, 2017c; Khachatryan *et al.*, 2017a). Enhancements are also possible from combining area subtraction methods with CHS.

For jet substructure observables, particle- or constituent-level pileup mitigation strategies have been shown to improve performance, especially in simulation studies for up to $\langle\mu\rangle \sim 40$. An example is given in Fig. 8, where the
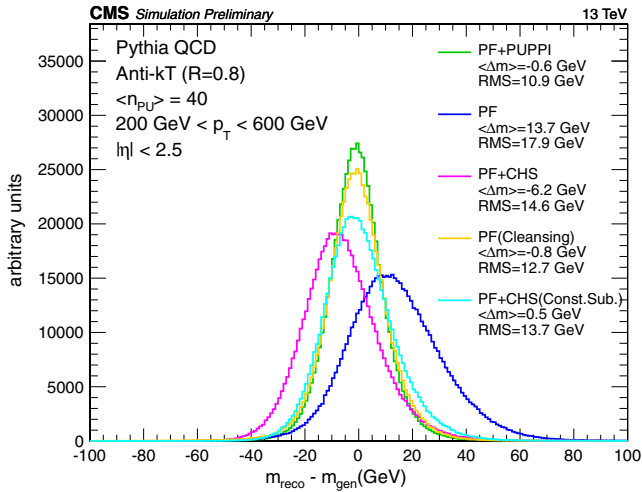
FIG. 8. Comparison of different pileup removal algorithms for the leading ungroomed jet mass response in simulated QCD multijet events with CMS. From CMS Collaboration, 2014e.

ungroomed jet mass of the leading jet in p_T in simulated QCD multijet events is corrected with different pileup removal techniques. The jet mass resolution can be improved further when using a grooming algorithm. The effect of different pileup removal techniques on the groomed jet mass depends however strongly on the choice of the grooming algorithm as discussed in detail by CMS Collaboration (2014e) and ATLAS Collaboration (2017b). The improved performance observed in simulation has also been verified in collision data (CMS Collaboration, 2017a).

Generally these techniques, particularly those which operate at particle level, can also be used to improve performance of nonjet objects such as missing transverse energy and lepton isolation. In the latter case, where the energy in a small cone around the lepton is summed, pileup mitigation techniques help to reduce the isolation's susceptibility to pileup.

Preliminary studies (detector configurations have not yet been finalized) into the application of these advanced hybrid techniques at the higher pileup levels anticipated at the HL-LHC suggest that they are effective in the $\langle \mu \rangle = 140$–200 range (Contardo *et al.*, 2015; ATLAS Collaboration, 2017c).

V. JET SUBSTRUCTURE METHODS AND OBSERVABLES

A. Jet grooming

Jet grooming techniques have seen a particularly high level of interest from the experimental and theoretical communities alike. Jet grooming is an additional "postprocessing" treatment of large radius jets, an extra step used to remove unwanted soft radiation and to allow the underlying hard substructure associated with a two-prong (e.g., W boson) or three-prong (e.g., top quark) decay to be identified more efficiently.

In particular, grooming is the systematic removal of radiation from within a jet, often targeting soft and wide-angle radiation. There are a variety of techniques and each one has tunable parameters that are chosen to suit the particular needs of the application. The three main algorithms used by ATLAS and CMS are trimming (Krohn, Thaler, and Wang,

2010), pruning (Ellis, Vermilion, and Walsh, 2010), and soft drop (Larkoski *et al.*, 2014). In each of these cases, the constituents of a jet are reclustered and soft or wide-angle radiation is rejected in this process. For trimming, the k_T algorithm is used to recluster and the radius parameter of the reclustering is called R_{sub}. Those smaller-radius jets with a momentum fraction $f < f_{cut}$ are removed to produce the trimmed jet. The two other algorithms impose a condition on each $2 \to 1$ clustering step, by going backward in the sequence in which the particles were combined in the reclustering. The transverse momentum fraction of the softer particle to the merged system $z = \min(p_{T,1}, p_{T,2})/(p_{T,1} + p_{T,2})$ is a natural choice for determining the scale of the soft radiation, and the angular distance ΔR between the two particles for identifying wide-angle radiation. The difference between pruning and soft drop lies in the way how particles and their combinations get rejected based on the values of z and ΔR. For pruning, the softer particle of the $2 \to 1$ clustering step is discarded if $z < z_p$ and $\Delta R < d_p$. For soft drop, the softer particle is discarded if $z < z_{cut}(\Delta R/R)^\beta$, where z_{cut} and the angular exponent β are free parameters.[6]

The role of grooming has traditionally satisfied two purposes in ATLAS, being the mitigation of pileup effects on jets, and the removal of soft or wide-angle radiation. The particle flow algorithm employed in CMS in conjunction with CHS or PUPPI allows for a correction for pileup effects. This reduces the usefulness of grooming for pileup mitigation, but retains its advantage for the removal of soft or wide-angle radiation.

ATLAS performed a broad study of the relative performance of different grooming techniques for boson-tagging (ATLAS Collaboration, 2015c, 2017b; Aad *et al.*, 2016e), top-tagging (ATLAS Collaboration, 2015d; Aad *et al.*, 2016k), and SM measurements (Aad *et al.*, 2014d; Aaboud *et al.*, 2018c), using the removal of pileup dependence, the jet mass resolution, and the tagging efficiency versus background rejection as performance metrics. The "standard" grooming procedure adopted by ATLAS is trimming with $f_{cut} = 0.05$ for boson tagging in both run 1 ($R_{sub} = 0.3$) and run 2 ($R_{sub} = 0.2$). The trimming algorithm with the same parameters was adopted for top tagging, along with several other techniques (see Sec. VI.C). Another technique currently in use by ATLAS is the *reclustering* of small-R jets (Nachman *et al.*, 2015), which uses fully calibrated anti-k_T, $R = 0.4$ jets as inputs to the anti-k_T algorithm with a larger distance parameter (typically $R = 1.0$). This has proven a popular method in ATLAS analyses due to the flexibility of optimizing the jet distance parameter depending on the considered phase space of the analysis (Aad *et al.*, 2016g; Aaboud *et al.*, 2016c, 2017h). A recent study of *in situ* measurements (ATLAS Collaboration, 2017d) (including "close-by" effects) confirms that the differences between data and simulation observed with reclustered jets are indeed covered by simply

---

[6]Most applications of soft drop use $\beta = 0$, in which case it is equivalent to an earlier algorithm known as modified mass drop tagger (mMDT) (Dasgupta *et al.*, 2013). Since both collaborations call this soft drop, we also refer to the algorithm by this name, but encourage the users to cite the mMDT publication in addition to the soft drop one.

propagating the uncertainties associated with the input anti-k_T, $R = 0.4$ jets.

CMS studied a large number of grooming techniques in the context of boosted boson-tagging (CMS Collaboration, 2014b; Khachatryan *et al.*, 2014a), top-tagging (CMS Collaboration, 2014f, 2016a), and SM measurements (Chatrchyan *et al.*, 2013b; Sirunyan *et al.*, 2018o). During run 1 the grooming techniques were used together with charged-hadron subtraction for pileup mitigation (see Sec. IV). All groomers studied showed reasonable or good agreement between data and simulation and the pruning algorithm ($R = 0.8$, $z_p = 0.1$, and $d_p = 0.5$) showed the best performance for boson tagging (Khachatryan *et al.*, 2014a). For run 2, soft drop ($z_{cut} = 0.1$ and $\beta = 0$) is used for jets with $R = 0.8$ in jet substructure analyses in CMS together with the pileup removal algorithm PUPPI (Bertolini *et al.*, 2014) (see Sec. IV). Soft drop jets in combination with PUPPI show a similar performance as pruning when comparing signal efficiency versus background rejection (CMS Collaboration, 2016a, 2017a), but allow for better theoretical control. While grooming techniques were found to improve the performance (higher background rejection at fixed signal efficiency) of the jet mass, N-subjettiness ratios (Thaler and Van Tilburg, 2011, 2012) were found to perform better without grooming for boosted boson tagging (Khachatryan *et al.*, 2014a). For top-tagging applications, however, soft drop groomed N-subjettiness ratios improved the performance with respect to ungroomed ones for jets with $p_T < 400$ GeV. For higher p_T jets there was no significant gain observed with grooming for N-subjettiness ratios (CMS Collaboration, 2016a).

B. Jet mass

The reconstruction of jet energies mainly relies on the capability of a detector to measure the total energy of all particles deposited in the detector; however, the measurement of jet mass requires detection of the deposited energy with a granularity that is finer than the size of a jet. The mass of a jet can be estimated only if the energy is deposited in at least two detector elements, as it depends on both the energy and opening angle between the jet constituents. For jet substructure techniques that rely on the rejection of soft particles, it is also important to be able to reconstruct particles with low p_T separately from harder particles in a jet.

The jet mass *response* distribution R_{reco} is constructed from the calibrated, reconstructed jet mass M_{reco} divided by the particle-level jet mass M_{true}. The mass response distribution is calculated in bins of reconstructed jet $p_{T,reco}$ and η_{reco}. In ATLAS, the jet mass scale (JMS) is defined as the mean of this response distribution. The jet mass resolution (JMR) is then defined as half the 68% interquartile range (IQnR) of the response distribution as

$$r = 0.5 \times 68\% \, \text{IQnR}(R_{reco}). \qquad (2)$$

This is robust to large non-Gaussian tails but, if the distribution is Gaussian is equal to its 1σ width. The fractional JMR is expressed as the JMR divided by the *median* of the response distribution.
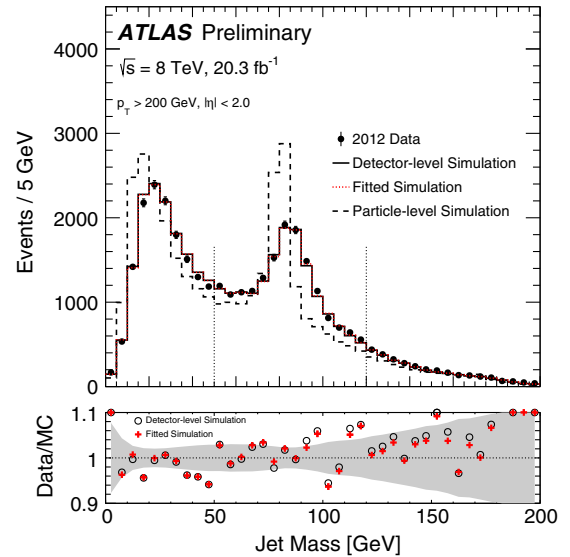

FIG. 9. The trimmed jet mass before (detector-level) and after (fitted) determining s and r. The particle-level distribution is shown for comparison. Jets are required to have $p_T > 200$ GeV. Adapted from ATLAS Collaboration, 2016e.

ATLAS has recently developed a data-driven approach to extract the JMS and JMR from an enriched sample of boosted $t\bar{t}$ events; however, the method can also be extended to other final states. This *forward-folding* approach folds the particle-level mass spectra by a modified response function such that the JMS in a given bin of particle-level jet mass and reconstructed jet p_T is scaled by the scale parameter s and the JMR is scaled by the resolution parameter r:

$$M_{fold} = s M_{reco} + (M_{reco} - \langle M_{reco}^{m,p_T} \rangle)(r - s). \qquad (3)$$

The values of r and s for which the M_{fold} distribution best matches the data are extracted from a two-dimensional χ^2 fit as shown in Fig. 9 and detailed by ATLAS Collaboration (2016d, 2016e).

With the forward-folding approach, the JMS and JMR for hadronically decaying boosted W bosons with $p_T \gtrsim 200$ GeV are determined with 2%–3% and 20% systematic uncertainties, respectively; see Fig. 10. As the jet mass and its detector response depend on kinematics and jet substructure, the measurement was repeated differentially with an increased luminosity for boosted W and top quarks in ATLAS Collaboration (2017e). It will be important to extend the technique to other final states in the future. This may require hybrid data or simulation methods. A detailed study of the various contributions to the JMS and JMR has been performed in context of the soft drop mass measurement (Aaboud *et al.*, 2018c), described in Sec. VII.A.1, by propagating experimental uncertainties on the inputs to the jet reconstruction to the jet mass. The dominating uncertainties are due to the theoretical modeling of jet fragmentation and the cluster energy scale.

As the forward-folding method is currently restricted to jets with $p_T < 350$ and 500 GeV for boosted W bosons and top quarks, respectively, the results are combined with the
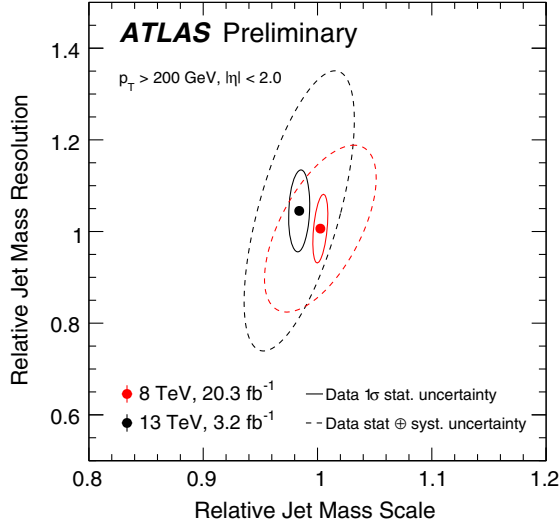
FIG. 10. The fitted values of the relative jet mass scale (*s*) and resolution (*r*) for trimmed anti-k_T, $R = 1.0$ calorimeter jets from the 2012 and 2015 ATLAS datasets and the 1σ statistical and total uncertainty ellipses. The $\sqrt{s} = 8$ and 13 TeV selections are similar, although the trimming definition slightly changed between runs ($R_{sub} = 0.3$ to 0.2). Adapted from ATLAS Collaboration, 2016d.

FIG. 11. The ATLAS combined jet mass resolution. Adapted from ATLAS Collaboration, 2016d.

so-called R_{trk} method which constrains the mass scale by comparing the calorimeter jet mass to the mass calculated from track jets and extends up to $p_T = 3000$ GeV (ATLAS Collaboration, 2017e). The R_{trk} method can also be generalized to other variables and is used in ATLAS to constrain the p_T scale of large-R jets as well as to derive systematic uncertainties on jet substructure variables.

The concept of a *track-assisted mass* for trimmed, large-R jets has been studied by ATLAS Collaboration (2016d) to maintain performance for highly boosted particles due to the limited granularity of the calorimeter. The track-assisted mass is defined as

$$m^{TA} = \frac{p_T^{calo}}{p_T^{track}} m^{track}, \qquad (4)$$

where p_T^{calo} is the transverse momentum of the calorimeter jet, p_T^{track} is the transverse momentum of the four-vector sum of tracks associated with the calorimeter jet, and m^{track} is the invariant mass of this four-vector sum, where the track mass is set to the pion mass m_π. The track-assisted mass exploits the excellent angular resolution of the tracking detector and the ratio p_T^{calo} to p_T^{track} corrects for charged-to-neutral fluctuations. The combined mass is defined as

$$m^{comb} = \left(\frac{\sigma_{calo}^{-2}}{\sigma_{calo}^{-2} + \sigma_{TA}^{-2}}\right) m^{calo} + \left(\frac{\sigma_{TA}^{-2}}{\sigma_{TA}^{-2} + \sigma_{calo}^{-2}}\right) m^{TA}, \qquad (5)$$

where σ_{calo} and σ_{TA} are the calorimeter-based jet mass resolution and the track-assisted mass resolution, respectively. The jet mass resolutions for the calorimeter mass, track-assisted mass, and combined mass are shown in Fig. 11 for W/Z boson jets as a function of jet p_T. Similar techniques that take advantage of the excellent angular resolution of the tracking detector at high p_T have been developed to correct
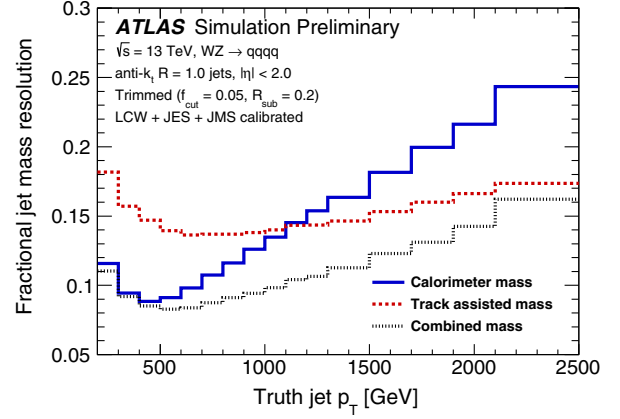
topoclusters to improve the resolution of jet substructure variables (ATLAS Collaboration, 2017h).

It is important to point out that in ATLAS, unlike in CMS, the jet energy scale directly impacts the jet mass scale. As opposed to the description of the JES calibration for small-R jets in Sec. III.B, the area subtraction, residual correction, and global sequential calibration (GSC) (see Sec. VI.A) are not applied to large-R jets.

In CMS, the jet mass is by default reconstructed as a combination of track and calorimeter measurements via the virtues of the particle flow algorithm. Thus the strategy for calibrating the jet mass in CMS differs from the one in ATLAS. In CMS, the individual PF objects are input to the jet reconstruction and are locally calibrated to account for the detector's single particle response (see Sec. III.A). After correcting the individual inputs, the jet four-vector is corrected using JES corrections and small residual differences in the jet mass between data and simulation are corrected using dedicated samples.

The residual *in situ* jet energy corrections are not applied when reconstructing jet masses. Therefore, dedicated corrections are derived from simulation and data. First, the jet mass response is corrected as a function of p_T and η using simulation of W jets from boson pair production. Second, residual corrections are obtained from a data sample enriched in lepton + jets $t\bar{t}$ production where the hadronic W jet can be studied in data (Khachatryan *et al.*, 2014a; CMS Collaboration, 2017a). The selection is optimized for fully merged hadronic W decays. Large-R jets in this sample show a peak at the W mass in the jet mass distribution, as shown in Fig. 12 for the soft drop grooming case. The excellent performance of the PF algorithm results in a JMR of about 10%. The absolute response and the resolution are well described by the simulation, within 1%–2% for the JMS and about 10% for the JMR, which is about the same size as the statistical uncertainty of this measurement. Residual differences in this distribution are used to calibrate the JMS and JMR in simulation and can also be used for dedicated efficiency corrections on other jet substructure observables, such as the N-subjettiness ratio $\tau_{21} = \tau_2/\tau_1$.

Since these measurements are performed in samples of W jets with $p_T \approx 200$ GeV, additional systematic uncertainties apply at higher p_T (Sirunyan *et al.*, 2018j). A detailed
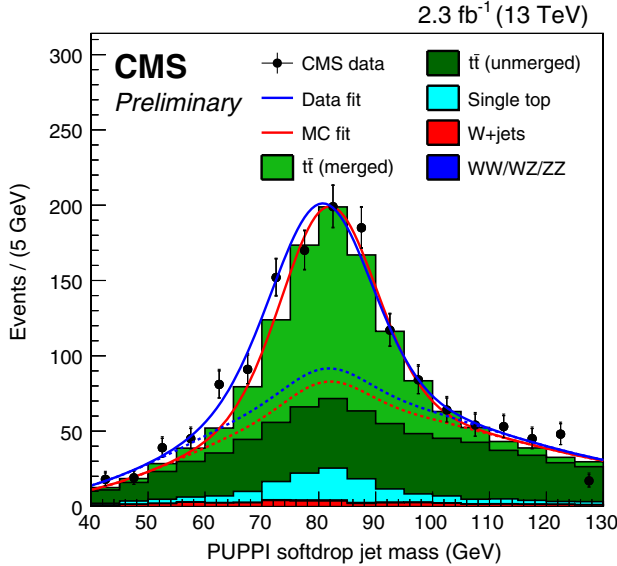
FIG. 12. Jet mass distribution in a sample enriched with lepton + jets $t\bar{t}$ events, where the hadronic W jet with $p_T > 200$ GeV is selected. From CMS Collaboration, 2017a.

FIG. 13. The CMS jet mass resolution as a function of the ungroomed jet mass m_u in different generated p_T bins. Adapted from Sirunyan *et al.*, 2018o.

study of the various contributions to the JMS has also been performed for fully merged top jets in the context of an unfolded top-jet mass measurement (Sirunyan *et al.*, 2017e). To summarize the impact of the various sources of systematic uncertainty to the measurement of residual corrections for jet substructure observables, we quote here the dominant uncertainties related to the scale factor measurement of an N-subjettiness ratio $\tau_{21} < 0.4$ selection (CMS Collaboration, 2017a). The statistical uncertainty of 6% (with 2.3/fb of data) is comparable to the systematic uncertainties related to the simulation of the $t\bar{t}$ topology (nearby jets, p_T spectrum) contributing 4%, the choice of method to derive the scale factors contributing 6% and the modeling of the p_T dependence that rises from 5% at $p_T = 500$ GeV to 13% at $p_T = 2000$ GeV.

The relative JMR in CMS is shown in Fig. 13 as a function of the ungroomed jet mass m_u for anti-k_T, $R = 0.8$ jets. The JMR is obtained from a sample of jets initiated by quarks and gluons. The resolution improves with increasing m_u and is around 9%–13% for the most probable value of $m_u \approx 100$–150 GeV. For a given value of $m_u < 200$ GeV, the resolution worsens with increasing jet p_T due to a higher degree of collimation. Remarkably, the resolution obtained in CMS is comparable to the one for the combined mass in ATLAS (Fig. 11), even though quark/gluon jets are compared with W/Z jets and very different technologies are used to reconstruct the jet mass.

C. Other jet substructure observables

Additional jet substructure observables are used for a variety of purposes, often to complement the jet mass. Most uses of these observables are within the context of a dedicated tagger, described in the next section. These observables can generally be classified into two categories: prong taggers and haze taggers. The most widely used prong taggers
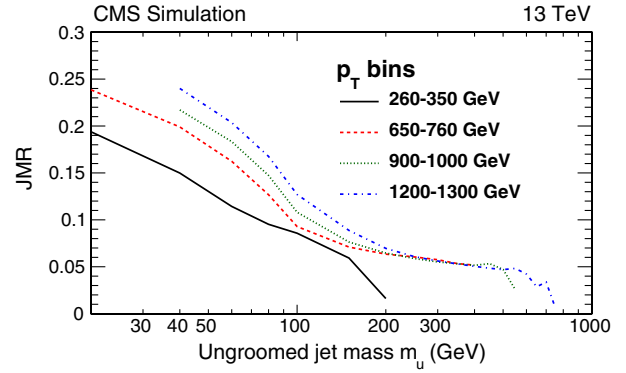
are the N-subjettiness ratios τ_{ij}^{β} (Thaler and Van Tilburg, 2011, 2012), C_2^{β} (Larkoski, Salam, and Thaler, 2013), D_2^{β} (Larkoski, Moult, and Neill, 2014, 2016), and N_2^{β} (Moult, Necib, and Thaler, 2016). The latter three are ratios of energy correlation functions, which are sums over constituents inside jets weighted by the momentum fractions and pairwise opening angles to the power β. For example,

$$N_2 = \frac{_2e_3^{(\beta)}}{(_1e_2^{\beta})^2}, \tag{6}$$

where

$$_1e_2^{(\beta)} = \sum_{1 \le i < j < k \le n_J} z_i z_j z_k \min\{\Delta R_{ij}^{\beta}, \Delta R_{ik}^{\beta}, \Delta R_{jk}^{\beta}\}, \tag{7}$$

$$_2e_3^{(\beta)} = \sum_{1 \le i < j < k \le n_J} z_i z_j z_k$$
$$\times \min\{\Delta R_{ij}^{\beta}\Delta R_{ik}^{\beta}, \Delta R_{ij}^{\beta}\Delta R_{jk}^{\beta}, \Delta R_{ik}^{\beta}\Delta R_{jk}^{\beta}\}, \tag{8}$$

where the sums run over the n_J jet constituents with momentum fractions z_i and opening angles ΔR_{ij}.

The goal of haze taggers is to generally characterize the radiation pattern within a jet without explicitly identifying the number of prongs. The prong taggers also are sensitive to the distribution of radiation around the subjet axes and so the distinction is not strict. Popular haze taggers include jet width $n_{constituents}$ (or n_{tracks}) and p_T^D.

In applications of jet substructure taggers based on these variables the description of data by simulation is a crucial aspect. Differences in the distributions lead to differences in efficiencies and misidentification rates, which need to be quantified in dedicated measurements. Measurements of jet substructure observables, their calibration, and improving their description by adjusting free parameters in event generators is an important step in every analysis.

As an example for three-prong taggers, the N-subjettiness ratio $\tau_{32} = \tau_3/\tau_2$ for $\beta = 1$ is shown here. It is used in ATLAS and CMS for top tagging and studied in light quark and gluon jets from dijet production, as well as in fully merged top quark jets from dedicated $t\bar{t}$ samples. The distribution of τ_{32} with run 2 data is shown in Fig. 14 for a dijet selection and in Fig. 15 for a $t\bar{t}$ selection. Overall good agreement between
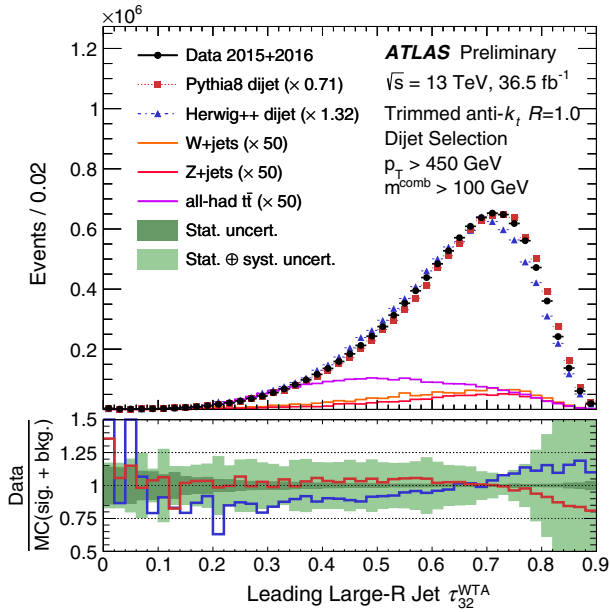
FIG. 14. Measured distribution of the *N*-subjettiness ratio τ_{32} calculated on trimmed anti-k_T, $R = 1.0$ jets for a dijet selection with $p_T > 450$ GeV and $p_T > 200$ GeV for the leading and subleading jets, respectively. The data are compared to simulated events, where the dijet samples have been normalized to the signal-subtracted data. From ATLAS Collaboration, 2017f.

data and simulation is observed, which leads to data-to-simulation scale factors for top-tagging compatible with unity (CMS Collaboration, 2017b).

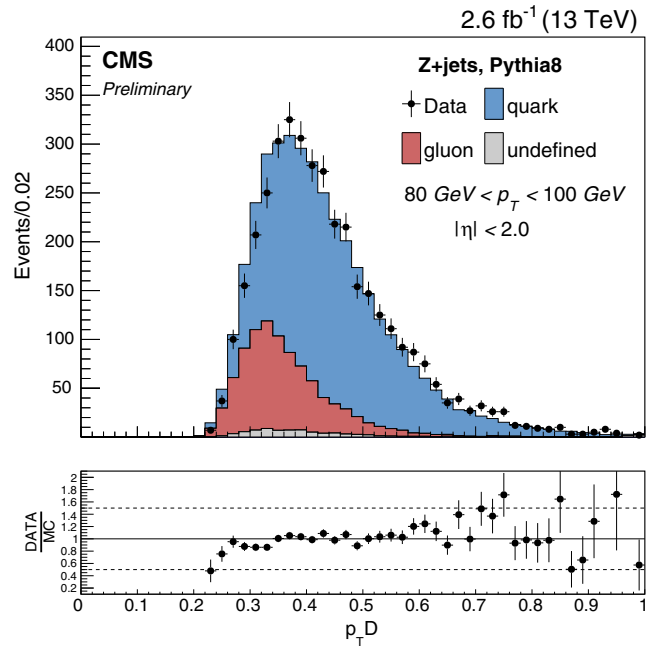As an example for a haze-tagger distribution, the p_T^D distribution is shown in Fig. 16. The distribution from $Z + \text{jets}$

FIG. 15. Measured distribution of the *N*-subjettiness ratio τ_{32} calculated on anti-k_T, $R = 0.8$ jets with $p_T > 400$ GeV corrected with PUPPI in a $t\bar{t}$ sample. The data are compared to simulated events, where the "Merged QB" $t\bar{t}$ contribution consists of events in which the *b* quark from the top quark decay and just one of the quarks from the *W* boson decay is clustered into the jet. From CMS Collaboration, 2017b.

FIG. 16. Distribution of p_T^D calculated on anti-k_T, $R = 0.4$ jets with $80 < p_T < 100$ GeV a $Z + \text{jets}$ sample. From CMS Collaboration, 2017a.

production is well described by simulation, but a significant discrepancy is observed when selecting dijet events. This has important consequences for quark/gluon tagging, where dedicated template fits to data are performed to extract weights to correct the simulation (see Sec. VI.A). Similar conclusions are found for the jet width and constituent multiplicity distributions (CMS Collaboration, 2017a).
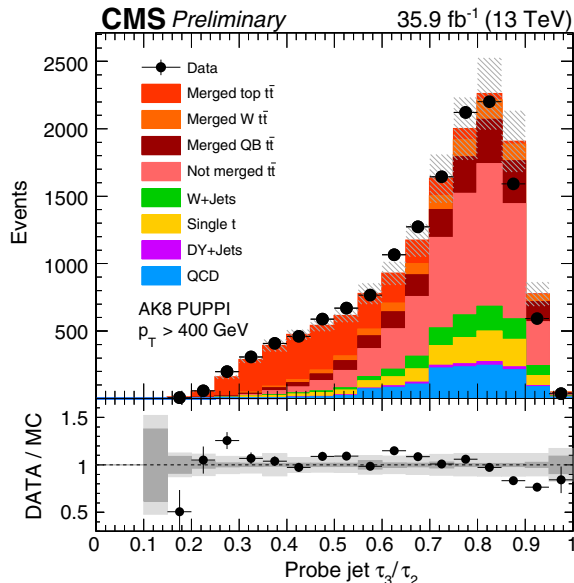
VI. JET TAGGING

Particle identification is an experimental challenge that is traditionally met using custom-designed charged-particle detectors, muon chambers, and calorimeters with granularity fine enough to allow shower shape measurements. Particle identification played an important role in the design considerations for the ATLAS and CMS detectors. Jet substructure techniques used for the identification of the particle origin of jets are a recent development though. Several substructure variables have been developed by the theoretical community that can be used along with the jet mass for jet classification. The term "tagger" indicates the use of one or more of these variables (sometimes after grooming has been applied) to discriminate between jets coming from different types of particles.

A rule of thumb for the decay of a massive object such as a *W*, *Z*, or *H* boson is that the decay products lie within a cone of radius $\Delta R = 2M/p_T$ in the laboratory rest frame, where *M* and p_T are the mass and transverse momentum of the object.[7] Using this for the example of a *W* boson decay, a *W* boson with $p_T = 200$ GeV will have its decay products captured by

---

[7] Note that this rule of thumb gives only a lower bound on ΔR, and it strictly holds only for two-body decays with massless decay products and $p_T \gg M$.

a jet with a distance parameter of at least 0.8, and the higher the p_T of the W boson, the more collimated the decay products. For top quarks, the value of p_T for which all decay products are captured by a jet with $R = 0.8$ is at least 400 GeV.

A. Quark/gluon discrimination

Since the first algorithmic definitions of jets, jet substructure observables have been widely used for quark-initiated (quark) versus gluon-initiated (gluon) jet tagging. Most measurements and searches at the LHC target a final state with a particular partonic structure and the dominant backgrounds may have a different flavor composition. Therefore, tagging jets as quark or gluon could increase the analysis sensitivity. For example, jets produced in vector-boson scattering or fusion are quark jets, while many of the background jets are gluon jets. There are many other applications, ranging from high multiplicity supersymmetry searches, initial-state jet tagging, etc.

The probability for a gluon to radiate a gluon is enhanced by a factor of $C_A/C_F = 9/4 \sim 2$ over the probability for a quark to radiate a gluon of the same energy fraction and opening angle (Altarelli and Parisi, 1977). As a result, gluon jets tend to have more constituents and a broader radiation pattern than quark jets. There are also more subtle differences due to quark and gluon electric charges and spins.

There are three key challenges of quark versus gluon jet (q/g) tagging: (1) quark and gluon labeling schemes are not unique; (2) for a given labeling scheme, quark and gluon jets are not that different; and (3) the differences that do exist are sensitive to both perturbative and nonperturbative modeling choices. Since quarks and gluons carry color charge and only colorless hadrons are observed, there is not a unique way to label a jet in simulation as originating from a quark or a gluon. Many labeling conventions exist, ranging in simplicity and model dependence from matching to outgoing matrix-element partons to parsing an entire jet clustering history (Banfi, Salam, and Zanderighi, 2006; Buckley and Pollard, 2016) to using entirely observable phase-space regions (Komiske, Metodiev, and Thaler, 2018; Metodiev and Thaler, 2018); however, no treatment escapes the problem that the notion of a quark and a gluon jet is not universal[8]: quark and gluon jet radiation depends on the production mechanism. This means that the calibration and application of q/g taggers must be treated with additional care compared with more universal classification tasks such as b tagging.

There is a plethora of jet substructure observables that can be used for q/g tagging; see, e.g., Gallicchio and Schwartz (2011) for a large survey. Many of these observables exhibit *Casimir scaling* which results in nearly the same, limited discrimination power for all the observables (Larkoski, Salam, and Thaler, 2013; Larkoski, Thaler, and Waalewijn, 2014). The most powerful single q/g observable is the particle multiplicity inside a jet (shown in Fig. 17), which does not exhibit Casimir scaling and recent theoretical advances (Frye *et al.*, 2017) have shown that its discrimination power can be largely understood from perturbative theory. There is further
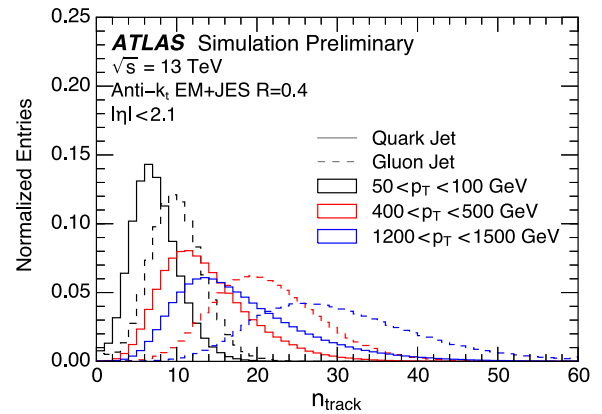

FIG. 17. The distribution of the number of tracks inside jets for quark and gluon jets in multiple jet p_T ranges. From ATLAS Collaboration, 2017g.

q/g separation possible when using the full radiation pattern inside a jet, although the combination of multiplicity and a Casimir scaling observable carries a significant fraction of the total discrimination power (Komiske, Metodiev, and Schwartz, 2017). The modeling of q/g tagging observables has a long history; see Gras *et al.* (2017) for a recent and detailed study.

Despite the challenges previously listed, both ATLAS and CMS extensively use explicit or implicit quark versus gluon tagging. Explicit taggers are algorithms designed to directly isolate quark and gluon jets while implicit techniques are designed for another purpose that also happens to perform some quark versus gluon jet tagging. The explicit taggers developed by ATLAS (Aad *et al.*, 2014a; ATLAS Collaboration, 2016f, 2017g, 2017i) and CMS (CMS Collaboration, 2013b, 2016b, 2017a, 2017c) include a variety of observables and data-driven calibration and validation techniques. These and related techniques have been successfully deployed in a variety of physics analyses (Chatrchyan *et al.*, 2012c, 2013c; CMS Collaboration, 2014b; Khachatryan *et al.*, 2015c; Aad *et al.*, 2015f; Aaboud *et al.*, 2016g; Sirunyan *et al.*, 2017f). Additionally, it has been shown that an improved W tagger can be constructed by utilizing q/g discrimination on subjets (CMS Collaboration, 2014b).

Both ATLAS and CMS have developed likelihood-based discriminants for explicit q/g tagging. The discriminants are constructed from variables sensitive to the radiation pattern of quark and gluon jets, also taking into account differences between light (uds) and heavy flavor (cb) quark jets, where the latter are more similar to gluon jets. ATLAS uses the number of tracks n_{trk} as an approximation for the number of jet constituents and the jet width (ATLAS Collaboration, 2017i) while CMS utilizes the number of particle flow constituents n_{const}, the jet axes, and fragmentation functions (CMS Collaboration, 2017a). Since the distributions of these variables depend on η, p_T, and ρ, the likelihood discriminators are constructed differentially with respect to these variables. In run 2, ATLAS also introduced a simple and robust tagger using solely n_{track} (ATLAS Collaboration, 2017g), which has the advantage of a much-simplified uncertainty derivation.
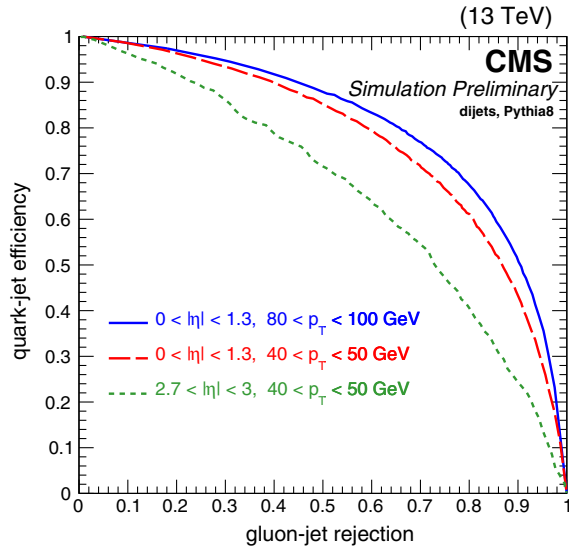
---

[8]This can be mitigated by jet grooming; see, e.g., Frye *et al.* (2016). Also, the nonuniversality may be "small" in practice (Bright-Thonney and Nachman, 2019).

FIG. 18.   The CMS q/g tagging performance in simulation for two bins in jet p_T and two bins in jet $|\eta|$. From CMS Collaboration, 2017a.

Figure 18 shows the CMS q/g tagging performance in simulation. The q/g label is obtained through a matching of jets on the detector level to outgoing partons from the matrix-element calculation. For a 50% gluon/quark efficiency, the misidentification rate (quark or gluon) is about 10%. This performance depends slightly on the jet p_T, in part because the particle multiplicity increases with p_T (and therefore the performance improves). Outside the tracking acceptance ($|\eta| \gtrsim 2.5$), q/g tagging significantly degrades due to the coarse calorimeter granularity and increased pileup sensitivity.

ATLAS (ATLAS Collaboration, 2017i) and CMS (CMS Collaboration, 2017c) are also actively studying sophisticated approaches based on modern machine learning. While these methods hold great promise for their power and flexibility, simple combinations of a small number of features often achieve a similar performance. Machine learning architecture design and input optimization are still an active area of research and development.

The modeling of q/g discriminating observables is a key concern for tagging applications. Typically, PYTHIA (Sjostrand, Mrenna, and Skands, 2006, 2008) tends to describe quarks better than HERWIG (Bahr *et al.*, 2008; Bellm *et al.*, 2016), whereas the opposite is observed for gluons. PYTHIA tends to overestimate the q/g tagging performance with respect to data, as illustrated quite strikingly in Fig. 19. This figure shows that gluon jets tend to have more tracks and have a broader radiation pattern relative to quark jets.[9] The fact that the hot spot in the bottom left of Fig. 19 is much more pronounced for Monte Carlo (MC) than for data indicates that the simulation over-predicts the difference between quark and gluon jets. In contrast, HERWIG (not shown) tends to underestimate the performance observed in data.

---

[9]The jet flavor is obtained as the type of the highest energy parton from the event record inside the jet cone. This gives nearly the same result as the CMS definition previously discussed for the two leading jets in a $2 \to 2$ calculation, but also works well for additional jets in the event.
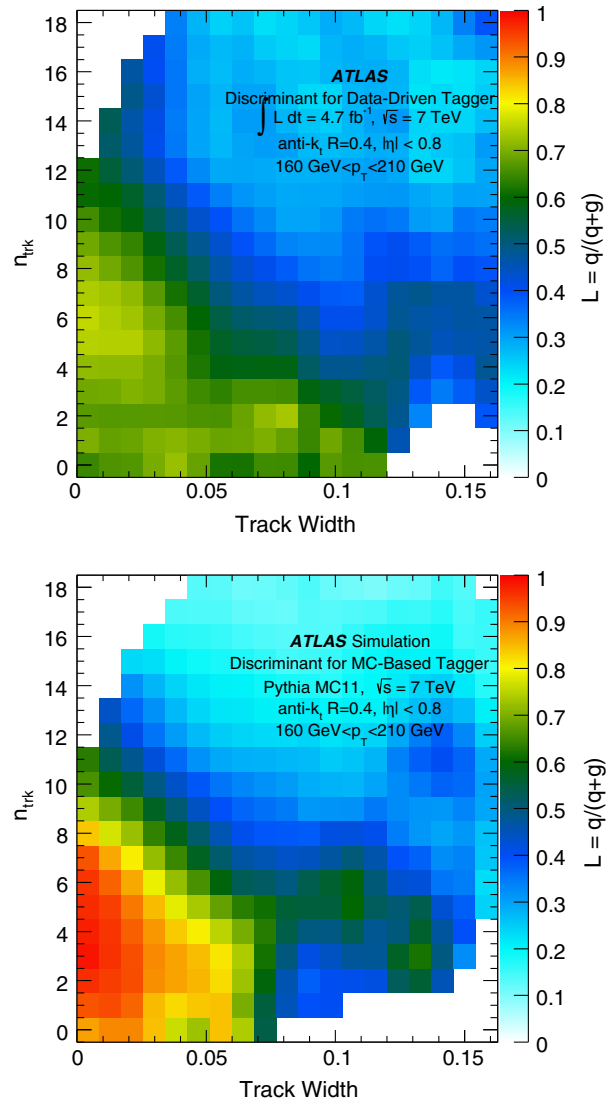

FIG. 19.   The two-dimensional q/g likelihood with ATLAS data (top) and simulation (bottom). From Aad *et al.*, 2014a.

Multiple samples with a different (but known) q/g composition can be used to extract the distribution of q/g tagging observables. ATLAS and CMS have both used Z/γ + jets and dijet samples, which are enriched in quark and gluon jets, respectively. The extracted average n_{track} from data is shown using this method in Fig. 20. As expected, gluon jets have more particles on average than quark jets and the multiplicity distribution increases with jet p_T.

The run 2 ATLAS tagger is based entirely on dijets, exploiting the rapidity dependence of the q/g fraction to extract the track multiplicity separately for quarks and gluons. A run 1 measurement is used to constrain the particle-level modeling, and dedicated track reconstruction uncertainties are used to complement the particle-level uncertainty with a run 2 detector-level uncertainty. The uncertainties on q/g tagging are 2%–5% over a wide range of 200 GeV $\lesssim p_T \lesssim 1$ TeV at a working point of 60% quark jet efficiency (ATLAS Collaboration, 2017g). The template-based calibration can also be used to directly construct the q/g tagger in data; however, when more than two observables are used to
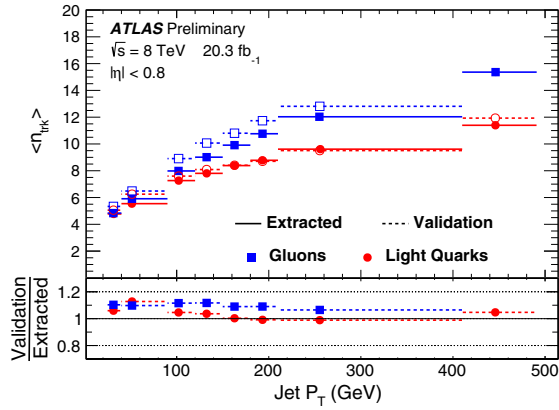
FIG. 20. The average track multiplicity in ATLAS for $Z/\gamma +$ jets (quark-enriched) and dijets (gluon-enriched). The dashed lines indicate the measurement on the validation samples: $Z/\gamma +$ 2-jets (quark-enriched) and trijets (gluon-enriched). From ATLAS Collaboration, 2016f.

construct the tagger, it becomes impractical to extract the high-dimensional templates.

The likelihood-based discriminant used for q/g tagging in CMS in run 2 is calibrated with a template-based fit using two discriminant distributions obtained from a $Z +$ jets and a dijet sample. The different quark and gluon fractions in each bin of the discriminant distributions are determined simultaneously and fitted by polynomial functions in order to obtain smooth interpolations (CMS Collaboration, 2017a).

Despite its power, the template technique has some residual nonclosure because the resulting calibrated tagger applied to another final state may not have the same performance. This is illustrated in Fig. 20, which shows how the average track multiplicities extracted for quark and gluon jets (using high-purity $Z/\gamma +$ jets and dijets data, respectively) differ from the values obtained in the $\gamma +$ 2-jet and trijet samples used for validation.

Explicit tagging is often the focus of modern q/g discrimination, but there is a broad program of implicit tagging as well. One ubiquitous example of this is the ATLAS jet calibration procedure (see Sec. III.B). Since the calorimeter response is nonlinear, a jet with a higher particle multiplicity will have a lower response for the same energy. After applying a simulation-based correction to eliminate this inclusive bias in the JES, a residual calibration is applied to correct for the dependence of the bias on the number of tracks associated with the jet and the jet width (ATLAS Collaboration, 2015b). After applying this residual GSC, the difference in response between quark and gluon jets is reduced. Implicit q/g tagging also appears in pileup jet identification (CMS Collaboration, 2013a; Aaboud *et al.*, 2017f), boson and top tagging (CMS Collaboration, 2014b; Aad *et al.*, 2015f; Sirunyan *et al.*, 2017f), and elsewhere.

Despite its long history, quark versus gluon jet tagging is still an active topic of research. Since most analyses at the LHC target processes with a known and asymmetric q/g jet composition, q/g tagging holds great promise for improving searches and measurements in the future. Further studies are required to understand the limits of q/g tagging performance and to mitigate the sample dependence for universal

definitions and calibrations. Interestingly, recent studies have shown how modern machine learning classifiers can be directly trained on data even though there are no per-jet labels (Dery *et al.*, 2017; Metodiev, Nachman, and Thaler, 2017).

B. Vector boson tagging

The hadronic, two-prong decays of weak vector bosons V have a distinct radiation pattern compared to individual high-p_T quarks or gluons. In particular, boosted bosons tend to have two distinct subjets with relatively equal momentum sharing. In contrast, most generic quark and gluon jets will have one prong and if they have two, the second one tends to be soft. Furthermore, the mass of quark and gluon jets scales with their p_T and is lower than the electroweak boson masses for low jet p_T and higher for ultrahigh p_T jets. For jets around 200 GeV, the decay products of a boosted W and a Z boson are typically captured only by a jet of radius $R \sim 1$, while smaller radii can be used at higher jet p_T. Good separation power between W and Z bosons is also desirable in a number of analyses, most notably searches for diboson resonances (see Sec. VIII.A).

ATLAS and CMS performed a broad range of studies during run 1 and the beginning of run 2, systematically identifying the influence of pileup reduction and grooming techniques on jet substructure observables used for V tagging (Khachatryan *et al.*, 2014a; Aad *et al.*, 2016e). Simulated samples containing W jets (rather than Z jets) are primarily used for these studies, as W jets are abundant in data thanks to the large quantity of $t\bar{t}$ events produced at the LHC.

The optimization of the V tagging algorithm is generally based on various factors concerning the tagged jet mass: (i) a sensible JMS (i.e., tagged jet mass close to the W mass), (ii) a narrow jet mass response with an approximate Gaussian line shape, (iii) stability with respect to pileup and jet p_T, and (iv) good background rejection at a given signal efficiency. Considering all of these factors, ATLAS decided on using the trimming algorithm (Krohn, Thaler, and Wang, 2010) with $f_{cut} = 0.05$ and $R_{sub} = 0.2$ on anti-k_T, $R = 1.0$ jets in run 2, while CMS opted for using anti-k_T, $R = 0.8$ jets, treating the pileup first with PUPPI and then applying soft drop grooming with $z_{cut} = 0.1$ and $\beta = 0$.

In addition to the comprehensive studies of grooming options (CMS Collaboration, 2014b, 2014e; ATLAS Collaboration, 2015c, 2017b; Aad *et al.*, 2016e), ATLAS and CMS both investigated the discrimination powers for a plethora of jet substructure variables, including N subjettiness (Thaler and Van Tilburg, 2011, 2012), Qjet volatility (Ellis *et al.*, 2012), ratios of energy correlation functions C_2^β (Larkoski, Salam, and Thaler, 2013), D_2^β (Larkoski, Moult, and Neill, 2014, 2016), and N_2^β (Moult, Necib, and Thaler, 2016), angularities and planar flow (Almeida *et al.*, 2009), splitting scales (Butterworth, Cox, and Forshaw, 2002; Thaler and Wang, 2008), the jet and subjet quark/gluon likelihood (QGL), and the jet pull angle (Gallicchio and Schwartz, 2010).

Both ATLAS and CMS developed simple taggers that rely on the combination of the jet mass with one other variable that improves the discriminating power between the signal and the background. The standard ATLAS V tagger for run 2 was
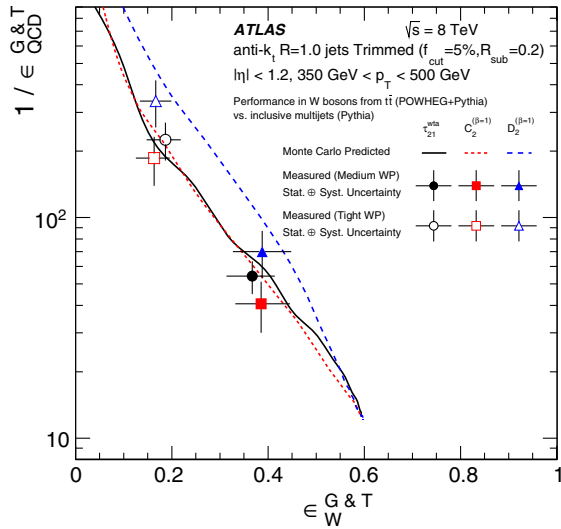
FIG. 21.   Signal efficiency vs background rejection power compared with measurements from ATLAS for $350 < p_T < 500$ GeV. From Aad *et al.*, 2016e.

chosen to be the trimmed jet mass and $D_2^{\beta=1}$ (Aad *et al.*, 2016e), known as "R2D2," while CMS decided to use the soft drop jet mass and the N-subjettiness ratio $\tau_{21} = \tau_2/\tau_1$. Despite the different choices of tagging observables and detector design, ATLAS and CMS reach a similar background rejection at a given tagging efficiency. An active field of developments is the usage of multivariate techniques for boosted V identification which have shown to be able to significantly improve the background rejection (Khachatryan *et al.*, 2014a; ATLAS Collaboration, 2017j).

In the ATLAS studies the variable $C_2^{\beta=1}$ in combination with the trimmed jet mass has been shown to be as good a discriminator[10] as τ_{21} as shown in Fig. 21. This is in contradiction to the study by CMS, where C_2^{β} is one of the weaker observables; however, a direct comparison is difficult, since in ATLAS *groomed* substructure variables are used, calculated for trimmed jets, while in CMS ungroomed variables are used. Also the particulars of particle reconstruction have a large impact on the performance of individual observables. While a study of the performance of D_2^{β} at CMS is still pending, the soft drop N_2^{β} observable was found to give similar performance to τ_{21} in CMS (Sirunyan *et al.*, 2018p).

CMS studied the QGL discriminator for its potential in V tagging applications in run 1 (CMS Collaboration, 2014b), finding that a combination of the groomed jet mass and the QGL achieved a similar discrimination power as the groomed jet mass and τ_{21}. When adding the QGL to the run 1 V tagger (pruned jet mass and τ_{21}), the misidentification rate was reduced slightly from 2.6% to 2.3% at a constant signal efficiency of 50%. A similar reduction of the misidentification

rate was observed when adding $C_2^{\beta=2}$, showing that C_2^{β} carries additional information with respect to the groomed jet mass and τ_{21}. However, the QGL and C_2^{β} exhibit a considerable pileup dependence, resulting in a degradation of their discrimination power with increasing activity. This pileup dependence is expected to be reduced when using PUPPI in place of particle flow plus CHS.

In Fig. 21 the ATLAS measurements of signal efficiencies versus background rejection power are shown for τ_{21}, C_2^{β}, and D_2^{β}, together with a selection on the trimmed jet mass [in this p_T range, the smallest mass window that captured 68% of the signal jets was found to be 71–91 GeV—see Aad *et al.* (2016e), Table 7]. The measurements are shown with statistical and systematic uncertainties. It is reassuring that the points for all three observables lie on the predicted performance curves for the two different working points studied.

In the ATLAS study, the most important systematic uncertainty is the jet substructure scale, which has been derived by comparing calorimeter jets with track jets. Once again the distributions in data lie between the ones derived with PYTHIA and HERWIG, leading to large modeling uncertainties (ATLAS Collaboration, 2015c; Aad *et al.*, 2016e). A similar observation was made by CMS (Khachatryan *et al.*, 2014a; CMS Collaboration, 2017a). Improving the modeling of jet properties and thereby reducing the differences between different event generators is a major task, but crucial for future precision studies using jet substructure.

A crucial aspect of V tagging is the derivation of background rates from multijet production in real collision data when performing measurements. A commonly used method is the extrapolation from one or more control regions, which are defined orthogonally to the signal region. Usually, these control regions are defined by inverting the jet mass window selection (Khachatryan *et al.*, 2014b, 2016f; Sirunyan *et al.*, 2017g; Aaboud *et al.*, 2017g, 2018g; ATLAS Collaboration, 2017k). Transfer functions are derived from simulation, extrapolating the rates and shapes from the control to the signal regions. Even though these transfer functions are ratios of distributions, which results in a reduction of the impact of modeling uncertainties, a residual dependence on the simulation cannot be eliminated. However, additional uncertainties in the high-p_T tails of the transfer functions can be eliminated by ensuring a constant behavior as a function of p_T. The requirement is thus a flat signal or background efficiency (depending on the needs of the analysis). In order to achieve a flat signal efficiency, ATLAS developed a p_T-dependent selection on the value of $D_2^{\beta=1}$, as this distribution shows a strong dependence on p_T (ATLAS Collaboration, 2015c). In contrast to the run 1 studies previously described, no p_T-dependent selection is made on the trimmed jet mass, as the calibrated jet mass is used to define the V tagging working point. While the jet mass resolution still increases with p_T, a constant window of ±15 GeV around the mean reconstructed W or Z boson mass is used. This results in a p_T-dependent signal and background efficiency, which can also be countered with the p_T-dependent cut on $D_2^{\beta=1}$. This leads to a constant signal efficiency, while the background efficiency shows a residual p_T dependence, as shown in Fig. 22.

---

[10]A different axis definition for the subjet axes is used in ATLAS when calculating τ_N, known as the-winner-takes-all axis (Larkoski, Neill, and Thaler, 2014), which is consistently found to perform slightly better than the standard subjet axis definition in tagging bosons.
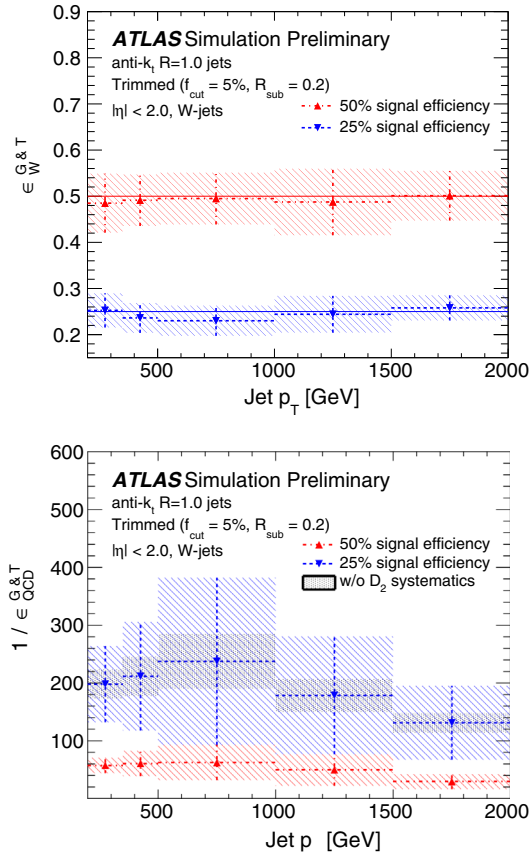
FIG. 22. Efficiency (top) and misidentification rate (bottom) for tagging boosted *W* bosons in ATLAS. Adapted from ATLAS Collaboration, 2015c.

FIG. 23. Efficiency and misidentification rate of various identification techniques for boosted *W* tagging. From CMS Collaboration, 2017a.

Another possibility has been explored by CMS. Instead of introducing p_T-dependent selection criteria, a linear transformation of the ratio τ_{21} has been studied (CMS Collaboration, 2017a), given by $\tau_{21}^{\mathrm{DDT}} = \tau_{21} - M \log[m^2/p_T/(1\,\mathrm{GeV})]$ (Dolen *et al.*, 2016), where M is a constant determined from simulation. The replacement of τ_{21} with the designed decorrelated tagger (DDT) τ_{21}^{DDT} does not affect the overall performance of the tagger, but results in an approximately flat misidentification rate as a function of p_T, as shown in Fig. 23 (bottom). The effect of the DDT method on the *V* tagging efficiency is shown in Fig. 23 (top). The efficiency increases as a function of p_T with a slope somewhat smaller than the slope for the decreasing efficiency obtained with plain τ_{21}. The development of decorrelated jet substructure taggers is an active field with new techniques, e.g., described by Aguilar-Saavedra, Collins, and Mishra (2017), Shimmin *et al.* (2017), and Moult, Nachman, and Neill (2018).

A less-studied possibility to lift the p_T dependence of substructure observables is the application of variable-*R* jets (Krohn, Thaler, and Wang, 2009). By shifting the p_T dependence to the jet clustering level with a distance parameter proportional to p_T^{-1}, a stable position of the jet mass and jet substructure variables with respect to changes in p_T can be achieved (ATLAS Collaboration, 2016g). This can lead to a stable tagging performance without the necessity of p_T-dependent optimization steps, but further experimental studies are needed to commission this strategy for use in analyses.
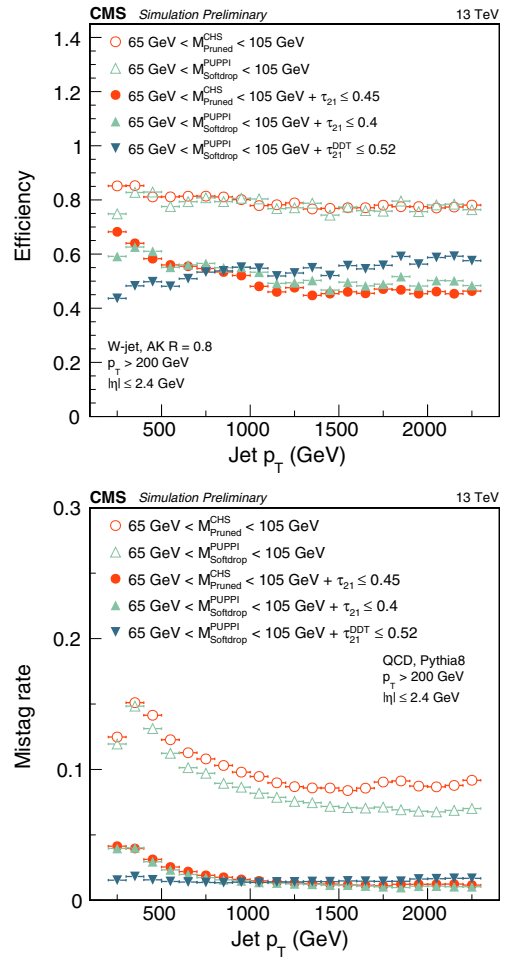
For some analyses the requirement of $p_T \gtrsim 200$ GeV is too restrictive, and hadronically decaying *V* bosons with lower p_T need to be selected. This poses a particular challenge due to the abundance of light-flavor jets at the LHC and their indistinguishability from jets from *W/Z* decays. An attempt was made by CMS to discriminate "resolved" (nonmerged) hadronic *W* decays from multijet background using the QGL, the sum of the jet charges of the dijet pair, and the jet pull angle. Combining these variables into a boosted decision tree, a misidentification rate of about 25% is achieved for a signal efficiency of 50% (CMS Collaboration, 2014b). While this is a first success, the performance is about an order of magnitude worse than *V* tagging for fully merged decays, showing the power of substructure techniques in this field.

In addition to developing tools for distinguishing boosted hadronically decaying *W* and *Z* bosons from generic quark and gluon jets, ATLAS has also built a tagger to further classify a boson jet as originating from either a *W* boson or a *Z* boson (Aad *et al.*, 2016f). While theoretically clean due to the color singlet nature of the *W* and *Z* bosons, this task is particularly challenging because the jet mass resolution is comparable to the difference $m_Z - m_W$. In order to improve the sensitivity of the tagger, jet charge and *b* tagging information are combined with the jet mass. The jet mass
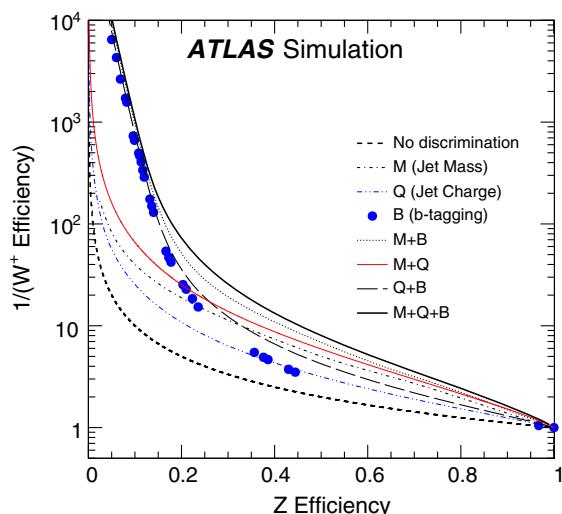
FIG. 24. Background rejection vs efficiency for discriminating Z boson jets from W boson jets for various jet observables and their combinations. From Aad *et al.*, 2016f.

distribution depends on the type of W or Z decay due to semileptonic B and D decays, so a full likelihood tagger is constructed by summing over the conditional likelihoods for each flavor type. To maximize the discrimination power from b tagging, multiple efficiency working points are used simultaneously in the tagger. Figure 24 illustrates the performance of the boson type tagger in simulation. A W^+ rejection near 8 (corresponding to a misidentification rate of 12.5%) is achieved at a Z boson efficiency of 50%. At this moderate Z boson efficiency, all of the inputs offer useful discrimination information. At low efficiencies, below the $b\bar{b}$ branching ratio for Z bosons, b tagging dominates over the jet mass and jet charge.

The boson type tagger was optimized for a relatively low boson boost $200 < p_T < 400$ GeV. The discrimination power of all of the input variables degrades with p_T due to the worsening jet mass resolution, tracking efficiency, and momentum resolution, as well as b tagging efficiency. However, there are recent developments to address each of these challenges, such as the track-assisted jet mass (see Sec. V.B), pixel-cluster splitting (ATLAS Collaboration, 2014a), and track-jet b tagging (ATLAS Collaboration, 2014b).

C. Top tagging

The three-prong decays of highly boosted top quarks in the fully hadronic decay channel offer richer phenomenology for their identification than the two-prong decays of W and Z bosons. This has been exploited in a number of algorithms, which usually aim at an optimal performance in a particular kinematic regime. Flavor tagging also plays a key role for top tagging, which offers its own challenges because the b jet from the b quark may not be isolated from the radiation resulting from the associated W boson decay. Because of the heavier mass of the top quark compared with the electroweak bosons, top tagging must also operate in a moderate boost regime where the decay products may not all be contained inside a single jet with $R \lesssim 1.0$.

The techniques for tagging boosted top quarks have evolved as fairly complex methods in comparison to the V taggers; these techniques include the following:

(a) The Johns Hopkins/CMS top tagger (CMSTT) (Kaplan *et al.*, 2008) was designed for tagging top quarks with $p_T > 1$ TeV. The algorithm is based on a decomposition of the primary jet into up to four subjets by reversing the CA clustering sequence. It was adapted by the CMS Collaboration (CMS Collaboration, 2009b, 2011a) and was adopted as the standard top-tagging algorithm in CMS in run 1, where it was typically used in the region of $p_T > 400$ GeV, with an average identification efficiency of 38% at 3% misidentification rate (CMS Collaboration, 2014f).

(b) The HEPTopTagger (HTT) (Plehn, Salam, and Spannowsky, 2010; Plehn *et al.*, 2010) was designed to target $t\bar{t}H$ production in the $H \rightarrow b\bar{b}$ decay channel. In $t\bar{t}H$ production the top quark p_T distribution peaks around 150 GeV and is steeply falling toward increasing p_T, where it is already an order of magnitude smaller at $p_T \sim 400$ GeV. This results in a requirement of nonzero signal efficiency already at $p_T \approx 200$ GeV, where the top quark decay is only moderately boosted. The HTT achieves this with a large jet distance parameter of 1.5 and a sequence of declustering, filtering, and reclustering of the original CA jet. The performance of the HTT was studied by the ATLAS and CMS Collaborations on data with a center-of-mass energy $\sqrt{s} = 7$ and 8 TeV (Aad *et al.*, 2013e, 2016k; CMS Collaboration, 2014f). Efficiencies of 10% with misidentification rates of 0.5% for jets with $200 < p_T < 250$ GeV were observed. The efficiency increases with increasing jet p_T, where a plateau is reached for $p_T > 400$ GeV, with efficiencies of approximately 40% at 3% misidentification rate, similar to the performance achieved with the CMSTT.

(c) Shower deconstruction (Soper and Spannowsky, 2011, 2013) was designed to be analogous to running a parton shower Monte Carlo generator in reverse, where emission and decay probabilities at each vertex, color connections, and kinematic requirements are considered. Small-radius (generally $R = 0.2$) subjets are reconstructed with the CA algorithm and all possible *shower histories* that can lead to the observed leading final state anti-k_T, $R = 1.0$ jet are calculated. Each shower history is assigned a probability weight factor based on the aforementioned considerations (to be signal-like or backgroundlike), then a likelihood ratio $\chi(p_N)$ is constructed, and the $\log \chi(p_N)$ is used as the discriminating substructure variable. For top quark tagging, efficiencies of 80% with misidentification rates of 50% for jets with $500 < p_T < 1000$ GeV were observed. The efficiency increases with increasing jet p_T, where a plateau is reached for $p_T > 2000$ GeV, with efficiencies of ∼80% at 10% misidentification rate. Recently, the shower deconstruction algorithm was optimized for top quarks with $p_T > 800$ GeV in context of the W' to tb hadronic search (Aaboud *et al.*, 2018d) by using exclusive k_T subjets.
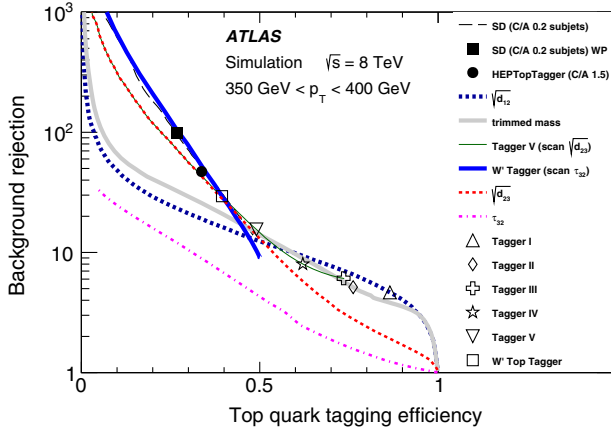
FIG. 25. Top quark tagging efficiency vs background rejection for various substructure variables and combinations in ATLAS. From Aad *et al.*, 2016k.
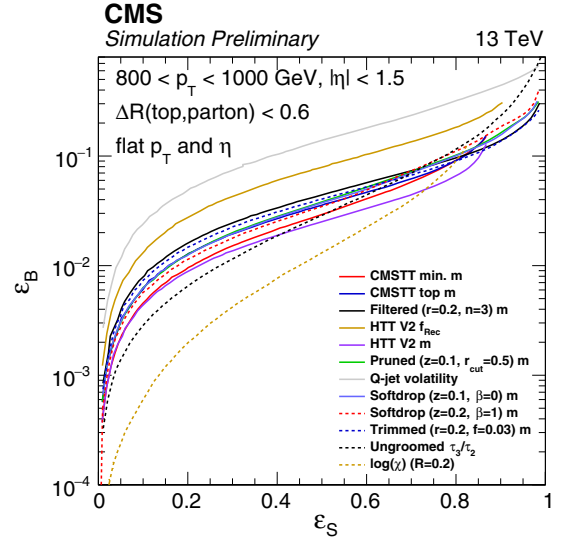

FIG. 26. Background vs signal efficiency for the single variables studied in the optimization of top tagging for CMS run 2 analyses. From CMS Collaboration, 2016a.

In addition to the dedicated techniques previously described, simpler algorithms using grooming and substructure similar to *V* tagging methods have been investigated by ATLAS. A performance study at 7 TeV (Aad *et al.*, 2013e) investigated a variety of performance metrics relating to the usage of groomed jets. Different grooming algorithms were investigated for their resilience to pileup and mass resolution. It was concluded that trimmed anti-k_T jets with a distance parameter of 1.0 and trimming parameters of $R_{sub} = 0.3$ and $f_{cut} = 0.05$ were a good candidate for a one-fits-all large-R jet definition. This jet definition became standard in ATLAS for W, Z, or H and top quark tagging in run 1. A later ATLAS study (Aad *et al.*, 2016k) investigated the various methods available for tagging hadronic, highly boosted top quarks. The so-called tagger V has $M_{jet} > 100$ GeV, $\sqrt{d_{12}} > 40$ GeV, and $\sqrt{d_{23}} > 20$ GeV, where $\sqrt{d_{ij}}$ is the k_T-splitting scale (Butterworth, Cox, and Forshaw, 2002). The efficiency versus rejection is shown for various taggers in Fig. 25. The difference between taggers III and V is the additional requirement on $\sqrt{d_{23}}$ in tagger V. At efficiencies smaller than 45%, the W' tagger, based on $\sqrt{d_{12}}$ and the *N*-subjettiness ratios τ_{21} and τ_{32}, has better background rejection than taggers III and V. ATLAS also tested the HTT and shower deconstruction (ATLAS Collaboration, 2017l), which have been found to have good background rejection (larger than 50) for efficiency values smaller than about 35%. However, similar to the CMS experiment, the background efficiencies of the two taggers show a significant rise with increasing p_T.

CMS has focused on enhancing the performance of CMSTT and HTT by identifying observables which carry discriminatory power, but have only small or moderate correlations with the observables used in the main algorithm. Typically, correlation coefficients of about 0.3 or less are required for noticeable improvement when augmenting an algorithm with additional variables. Examples for discriminating variables which fulfill this are *N*-subjettiness ratios, energy correlation functions and their ratios, and *b* tagging. A study by the CMS Collaboration showed that at 20% signal efficiency, the background rejection of the CMSTT can be improved by a factor of 5 when adding information from τ_{32} and subjet *b* tagging

information (CMS Collaboration, 2014f). At higher efficiencies, the improvements become smaller. For the HTT, improvements of similar size are observed for $p_T > 200$ GeV, becoming less significant at higher p_T.

The ATLAS choice of $R = 1.0$ jets compared to CMS ($R = 0.8$) results in an earlier rise of the tagging efficiency with increasing jet p_T.

The large difference in performance of the single variable τ_{32} between ATLAS (Fig. 25) and CMS (Fig. 26) is due to jet grooming. Although the CMS study shows only the receiver operating characteristic (ROC) curves for $800 < p_T < 1000$ GeV, the overall picture does not change when studying top quarks in the region of $p_T \approx 400$ GeV. Instead, in ATLAS τ_{32} is calculated from trimmed jets, which results in less discrimination power when used as the sole tagging variable compared to ungroomed τ_{32}. However, groomed τ_{32} can still lead to considerable improvements when combined with other variables.

As with *V* tagging previously discussed, ATLAS and CMS took advantage of the LHC shutdown between runs 1 and 2 to perform broad studies of the different top taggers available, with emphasis on their stability with respect to pileup and other detector effects, instead of the utmost gain in performance (ATLAS Collaboration, 2015d; CMS Collaboration, 2016a). Single variables and their combinations are studied and compared with shower deconstruction, CMSTT, HTT, and an improved version of the HTT with shrinking cone size (HTTv2) (Kasieczka *et al.*, 2015).

Figure 26 shows a comparison based on simulation of the single variable performance in CMS, where signal jets are generated through a heavy resonance decaying to $t\bar{t}$ and background jets are taken from QCD multijet production. Note that for this study reconstructed jets are matched to a generated parton, and the distance between the top quark and its decay products must be less than 0.6 (0.8) for a reconstructed $R = 0.8$ (1.5) jet, to ensure that the top quark decay products are fully merged and reconstructed in a single jet. The best single variable in terms of efficiency versus background rejection is the discriminator $\log \chi$, calculated with
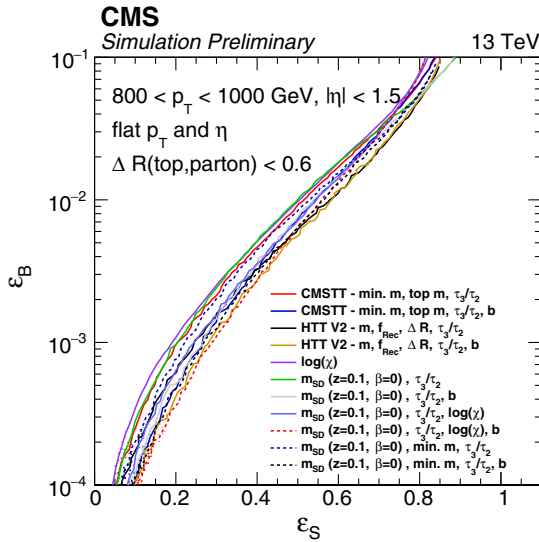
FIG. 27. Background efficiency vs signal efficiency for combined variables studied in the optimization of top tagging for CMS run 2 analyses. From CMS Collaboration, 2016a.
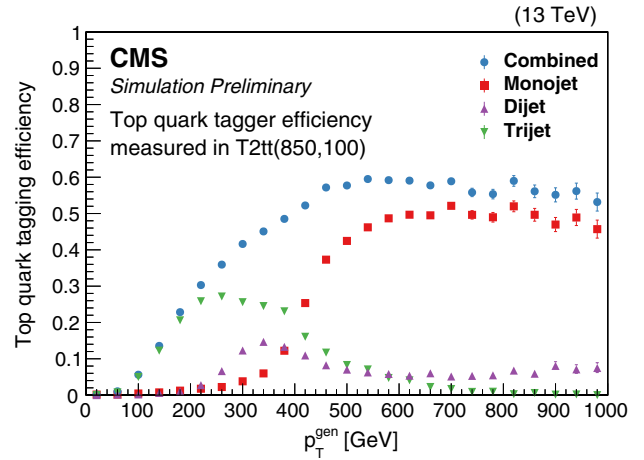

FIG. 28. Top-tagging efficiency of three different top-tagging methods and the combined efficiency, as a function of the generated top quark p_T. From CMS Collaboration, 2017d.

shower deconstruction. The second best variables are the *N*-subjettiness ratio τ_{32} at low efficiency and the jet mass calculated with the HTTv2 at high efficiency values. The individual groomed jet masses show similar performance, and the CMS Collaboration moved to using the soft drop mass due to its beneficial theoretical properties (Larkoski, Moult, and Nachman, 2017). The default for CMS run 2 analyses was chosen to be the soft drop jet mass combined with τ_{32} for top tagging at high p_T. Generally, at high boost, the combination of a groomed mass with τ_{32} leads to a large gain in background rejection.

The CMS study also investigated combining single variables with more complex taggers. Combining shower deconstruction with the soft drop mass τ_{32} and subjet *b* tagging can lead to improvements as shown in Fig. 27; however, the efficiency and misidentification rate for this combination were found to not be stable as a function of jet p_T (the combined algorithms were studied using working points corresponding to a background efficiency of 0.3). At low boosts, the dedicated HTTv2 shows the best performance. In this kinematic region, using groomed τ_{32}, obtained by using the set of particles from the soft drop jet instead of the original jet, helps to improve the performance.

In the shutdown between runs 1 and 2, ATLAS commissioned a single top tagger for use by physics analyses. The rationale behind this approach was the potential benefit of having an efficient top tagger with well-understood efficiency and associated systematic uncertainties validated in the run 1 dataset. Similarly as for run 1, the supported top tagger makes use of anti-k_T, $R = 1.0$ trimmed jets, but with a parameter of $R_{sub} = 0.2$ instead of 0.3 as used in run 1. Candidate top jets are required to satisfy a calibrated mass window requirement $122.5 < M_{jet} < 222.5$ GeV and a p_T-dependent, one-sided cut on τ_{32} (ATLAS Collaboration, 2015d). The variable τ_{32} has been chosen since it shows the best background rejection in combination with a small correlation with M_{jet}, a reduced p_T dependence, and good performance across a large range in p_T.

A common problem of top-tagging algorithms is the rise of the misidentification rate with increasing p_T, which is due to the peak of the mass distribution for quark- and gluon-initiated background jets shifting to higher values. For some taggers, for example the CMSTT, this shift also results in a decrease of the efficiency once a high p_T threshold is crossed (larger than 1 TeV) (CMS Collaboration, 2011a). A possible solution to this is offered by the variable-*R* (VR) algorithm, introduced in Sec. VI.B. The ATLAS Collaboration studied the performance of the VR algorithm for top tagging and reported a stabilization of the position of the jet mass peak for a large range of p_T (ATLAS Collaboration, 2016g). The VR jets are shown to improve the performance of the jet mass, $\sqrt{d_{12}}$ and τ_{32} for top tagging, when compared to trimmed jets. An interesting development using VR jets is the heavy object tagger with variable *R* (Lapsien, Kogler, and Haller, 2016), which combines the VR algorithm with a clustering veto, resulting in a single jet clustering sequence producing groomed jets with subjets.

Most top taggers target either the region of low to intermediate boosts or the highly boosted regime. However, in typical searches for new physics at the LHC nonvanishing efficiency for the full kinematic reach is crucial. Several attempts of combining different reconstruction and identification algorithms have been made. A search for resonances decaying to $t\bar{t}$ by the ATLAS Collaboration uses a cascading selection from boosted to resolved (Aad *et al.*, 2015g), where the resolved topology is reconstructed and identified using a χ^2-sorting algorithm. To efficiently identify top quarks over a broad p_T range in the search for top squark pair production, reclustered variable-*R* jets are used with $R = 0.4$ jets as inputs to the jet reclustering algorithm (Aaboud *et al.*, 2016c, 2018j).

A search for supersymmetry in CMS (CMS Collaboration, 2017d) uses three distinct topologies: fully merged top quark decays (monojet), merged *W* boson decays (dijet), and resolved decays (trijet). The efficiency of the three categories is shown in Fig. 28, where the turn-on of the combined efficiency starts at values as low as $p_T \approx 100$ GeV. The resolved trijet category is identified using three anti-k_T jets

with a distance parameter of 0.4, where the large combinatorial background is suppressed through a multivariate analysis, which achieves a misidentification rate of approximately 20%. There exist other approaches to cover the transition from low to high Lorentz boosts, using a single algorithm. In the HTTv2 algorithm, the jet size is reduced until an optimal size R_{opt} is found, defined by the fractional jet mass contained in the smaller jet. This results in better performance at high p_{T}, while keeping a low misidentification rate at low p_{T}.

An important step toward the commissioning of top taggers within an experiment is measurements of the efficiency and misidentification rate in real collision data. Generally, high-purity samples of top jets in data are obtained using a tight signal selection (an electron or muon, well separated from a high-p_{T} large-R jet, and an additional b-tagged jet) to ensure that events contain a fully merged top quark decay in a single large-R jet. This can never be fully achieved, as no requirements on the substructure of the large-R jet can be imposed without biasing the efficiency measurement. This results in an efficiency measurement that will be based on a sample also containing partially merged or even nonmerged top quark decays. These can be subtracted from the efficiency measurement by using simulated events, as done in a study by the ATLAS Collaboration (Aad *et al.*, 2016k), with the drawback of relying on a specific simulation and the ambiguous definition of a fully merged top quark decay. By not correcting for nonmerged top quark decays, efficiency values are obtained smaller than the ones suggested by ROC curve studies; see, for example, CMS Collaboration (2016a). Instead of subtracting the top backgrounds, the CMS Collaboration performed a simultaneous extraction of the efficiencies for fully and partially merged categories (CMS Collaboration, 2017b).

Measurements of the misidentification rate can be carried out by selecting a dijet sample, which is dominated by light-flavor jets. The disadvantage of this approach is the high p_{T} threshold of unprescaled jet triggers, which results in measurements starting from $p_{\mathrm{T}} > 400$ GeV or higher. A solution to this is the tag-and-probe method, in which the tagged jet can be required to fail top-tagging selection criteria, resulting in a sample with negligible contamination of $t\bar{t}$ production, even after requiring the probe jet to be top tagged (CMS Collaboration, 2016a). Another approach is to use a nonisolated electron trigger, where the electron fails off-line identification criteria. This yields events mainly from light-flavor multijet production, where a jet is misidentified as an electron at the trigger level. While the top-tag misidentification rate can be measured starting from smaller values of p_{T} with this strategy, a non-negligible amount of $t\bar{t}$ contamination has to be subtracted after requiring a top-tagged jet (Aad *et al.*, 2016k).

As an example, the efficiency and misidentification rate of shower deconstruction with the requirement $\log(\chi) > 2.5$, as measured in ATLAS, are shown in Fig. 29. The efficiency of 30% with a misidentification rate of 1% for $350 < p_{\mathrm{T}} < 400$ GeV agrees well with the values obtained from Fig. 25. Note that the largest uncertainty of the efficiency measurement stems from the choice of the MC event generator used to simulate $t\bar{t}$ production. The uncertainty of the misidentification
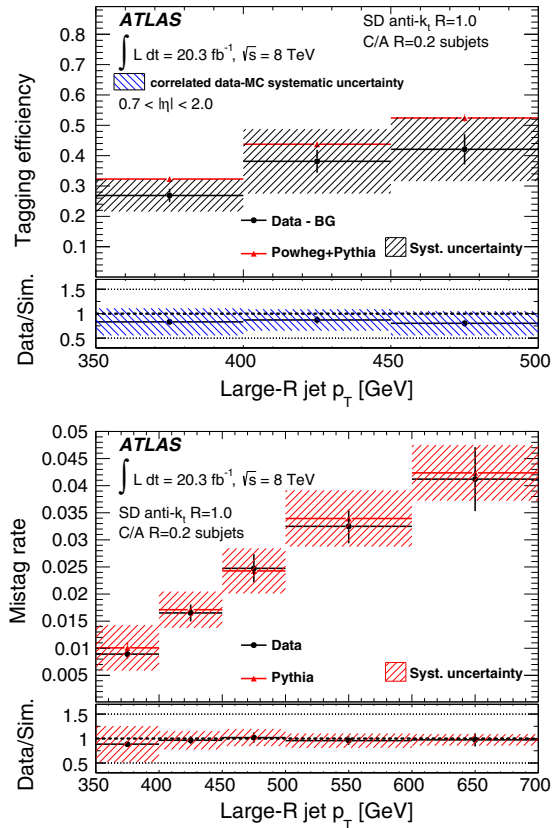

FIG. 29. ATLAS measurements of the efficiency (top) and misidentification rate (bottom) for trimmed jets with a distance parameter of 1.0 tagged with shower deconstruction. From Aad *et al.*, 2016k.

rate measurement is dominated by the energy scales and resolutions of the subjets and large-R jets.

D. $H \to b\bar{b}$ tagging

The identification of jets originating from the fragmentation of b quarks (b tagging) is a crucial task in many areas of particle physics. Algorithms used for b tagging usually rely on the distinct signature of B hadron decays, for example, the presence of a secondary vertex due to the long B hadron lifetime of about 1.5 ps.

ATLAS and CMS both use dedicated b tagging algorithms that have been developed and optimized over more than a decade. Both experiments use multivariate techniques with various input parameters related to the secondary vertex or charged-particle tracks originating from the B hadron decay. For run 2 analyses, CMS uses the CSVv2 algorithm (Sirunyan *et al.*, 2018c) and ATLAS uses the MV2c10 algorithm (ATLAS Collaboration, 2016h). Typically, efficiencies of around 70% with misidentification rates of 1% for light quark and gluon jets and 20% for charm jets are achieved with these algorithms.

While b tagging in busy hadronic environments plays an important role for top tagging, it is the key challenge for tagging boosted $H \to b\bar{b}$ signatures. Other jet substructure observables can improve performance, but are often less powerful once two b tagged jets or subjets are required

(as this necessarily forces the jet to have two prongs). The lighter mass of the Higgs boson compared with the top quark also means that the b jets from the H decay become merged at a lower parent particle boost.

The boosted $H \to b\bar{b}$ signature is present in many models of physics beyond the standard model: resonant HH and VH production, searches for boosted mono-H, or vectorlike quark searches in the tH and bH final states. Because of the large predicted branching fraction for the $H \to b\bar{b}$ decay of about 58%, its coupling to b quarks is one of the most interesting to study. For a large fraction of Higgs bosons with $p_T > 300$ GeV, the two b quark jets merge into a single jet for a jet distance parameter of $R = 0.8$ or 1.0, as used in CMS and ATLAS, respectively. Several phenomeno-logical studies have explored $H \to b\bar{b}$ tagging algorithms using jet substructure, although ultimately the optimal per-formance comes from using a combination of substructure information and the track and vertex information related to the B hadron lifetime.

The approaches to identify boosted $H \to b\bar{b}$ candidates that have been explored (and used) at CMS and ATLAS include the following:

(a) Subjet b tagging (CMS Collaboration, 2013c, 2013d; ATLAS Collaboration, 2014b, 2016i, 2016j, 2016k), where standard b tagging is applied to each of the subjets [the standard for CMS is the CSVv2 algorithm (CMS Collaboration, 2016d), and for ATLAS is MV2c20 (ATLAS Collaboration, 2016h)]. Tagging b jets in dense environments is of particular impor-tance here and was studied by ATLAS (ATLAS Collaboration, 2014c). In CMS subjets with $R = 0.4$ are clustered with the k_T algorithm using the constituents of the large-R jet, while for ATLAS track jets with a radius of 0.2 are matched to the large-R jet using the ghost-association technique. At high p_T the subjets start to overlap causing the standard b tagging techniques to break down due to double counting of tracks and secondary vertices when computing the subjet b tag discriminants.

(b) Double-b tagging (CMS Collaboration, 2016e; AT-LAS Collaboration, 2016k; Sirunyan *et al.*, 2018c), where in ATLAS the term double-b tagging means that the two leading p_T track jets must pass the same b tagging requirement. In CMS, the double-b tagger (CMS Collaboration, 2016e; Sirunyan *et al.*, 2018c) uses the N-subjettiness axes and the pruned anti-k_T, $R = 0.8$ jet mass with a window of $50 < M < 200$ GeV to reduce the multijet background.

The Higgs-jet efficiency versus the inclusive multijet rejection is shown in Fig. 30 for ATLAS subjet b tagging, where the performance curves are shown for double-b tag-ging, leading subjet b tagging, and asymmetric b tagging[11] requirements. None of the curves reach a Higgs-jet efficiency
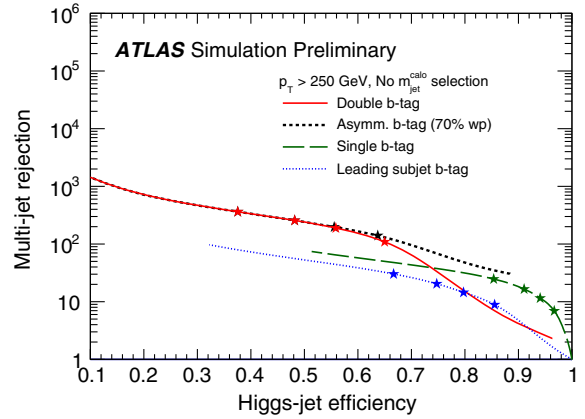

FIG. 30. The rejection of inclusive multijets vs Higgs-jet efficiency using all large-R jets with $p_T > 250$ GeV for single, double, asymmetric, and leading subjet b tagging requirements. From ATLAS Collaboration, 2016k.

of 100% due to the imperfect efficiency to reconstruct the track jets needed for b tagging and, in the case of asymmetric b tagging, also due to the 70% b tagging working point requirement on one of the track jets.

The CMS double-b tagging algorithm (CMS Collaboration, 2016e; Sirunyan *et al.*, 2018c) attempts to fully exploit the strong correlations between the b hadron flight directions and the energy flows of the two subjets, while adapting the variables used in the CSVv2 algorithm. The flexibility of the double-b tagger is ensured by avoiding a strong perfor-mance dependence on the jet p_T and mass.

With the double-b tagger, at the same signal efficiency, the misidentification rate is uniformly lower by about a factor of 2 compared to the subjet b tagging approach. Given the different kinematic properties expected for a $b\bar{b}$ pair origi-nating from the decay of a massive resonance compared to gluon splitting, the misidentification rate for the gluon splitting background reduces from 60% to 50% at 80% signal efficiency and from 20% to 10% at 35% signal efficiency. At high p_T, even larger performance improve-ments are observed, which is an important gain for searches for heavy resonances, where very high p_T jets are expected. In Fig. 31 the signal efficiencies and misidentification rates for the double-b tagger are shown as a function of jet p_T for three operating points: loose, medium, and tight, which correspond to 80%, 70%, and 35% signal efficiency, respec-tively, for a jet p_T of about 1000 GeV. The misidentification rate is mostly flat across the p_T range considered while the signal efficiency decreases with increasing p_T, as expected from the degradation of the tracking performance inside high p_T jets.

Because of the small cross section of producing events with boosted $H \to b\bar{b}$ or $Z \to b\bar{b}$ jets, the efficiency of the ATLAS and CMS Higgs identification algorithms is measured using QCD multijet events enriched in jets from gluon splitting, $g \to b\bar{b}$ with a topology similar to that of boosted $H \to b\bar{b}$ jets.

CMS selects topologies as similar as possible to a signal jet by requiring the jet $p_T > 300$ GeV and pruned mass >50 GeV (CMS Collaboration, 2016e; Sirunyan *et al.*,

---

[11]Asymmetric b tagging means that, among the two leading p_T track jets, the track jet with the largest b tagging weight must pass the fixed 70% b tagging working point threshold, while the b tagging requirement of the other jet is varied.
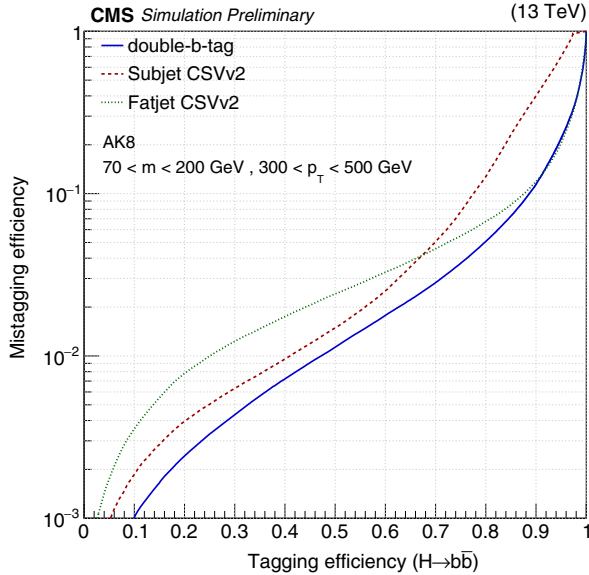
FIG. 31. The misidentification rate for inclusive multijets vs Higgs-jet efficiency using jets with $300 < p_T < 500$ GeV and pruned jet mass $70 < m < 200$ GeV for three different b tagging requirements. From CMS Collaboration, 2016e.

2018c). Each jet has to contain at least two muons, each with $p_T > 7$ GeV and $|\eta| < 2.4$. Each pruned subjet is required to have at least one muon among its constituents and within $\Delta R < 0.4$ from the subjet axis ("double-muon tagged"). The double-muon tag enriches events with gluons splitting into $b\bar{b}$ where both b quarks give rise to a semileptonic B hadron decay. Such $g \to b\bar{b}$ events are proxies for the signal topology. An alternative selection that requires at least one muon is also examined as a cross-check for the measurement ("single-muon tagged"). While this single-muon selection allows for a larger dataset in which to perform the tagger efficiency measurement, the gluon splitting topology in this inclusive phase space is less signal-like relative to the double-muon selection. Thus, to maximize the similarity between the $g \to b\bar{b}$ and the $H \to b\bar{b}$ topologies, the measurement is performed requiring double-muon tagged jets. It is worth noting however that the jet mass depends on the number of muons and a large fraction of the signal will not contain two muons.

ATLAS performed a similar measurement selecting events with at least one anti-k_T, $R = 1.0$ jet with $p_T > 250$ GeV that has two ghost-associated $R = 0.2$ track jets (ATLAS Collaboration, 2016k). As opposed to the measurement from CMS, only one of the subjets is required to have a muon associated with it. Kinematic and substructure variables are compared in data and MC after correcting for flavor composition differences of the large-R jet observed between data and MC simulation and are found to be in good agreement.

One of the major backgrounds for analyses selecting boosted H or Z bosons decaying to $b\bar{b}$ is $t\bar{t}$ production. The misidentification rate for boosted top quark jets faking H jets was measured in data by CMS (CMS Collaboration, 2016e; Sirunyan *et al.*, 2018c) in enriched data samples of lepton + jets $t\bar{t}$ events.

As previously discussed, for high p_T of the Higgs boson, the two subjets from b quarks start overlapping and the performance of identifying the subjets as fixed-radius track jets decreases significantly. To improve the performance of the ATLAS standard $H \to b\bar{b}$ identification algorithm for searches that require the presence of high-p_T Higgs bosons, the ATLAS Collaboration studied alternative methods like the use of variable-radius track jets, exclusive k_T subjets, calorimeter subjets reconstructed in the center-of-mass frame of the Higgs jet candidate (ATLAS Collaboration, 2017m), and the combination of three jet shape and jet substructure variables into a multivariate discriminator (ATLAS Collaboration, 2012). For highly boosted Higgs bosons, these reconstruction techniques significantly outperform the usage of fixed-radius track jets.

VII. STANDARD MODEL CROSS SECTION MEASUREMENTS

The measurement of jet properties is crucial to constrain the standard model in new energy regimes and constitutes an important test of perturbative calculations of jet structure over a wide region of phase space. Moreover jet cross section measurements provide constraints on the parton distribution functions (PDFs) and the strong coupling constant α_s. The precise knowledge of jet properties also improves the precision of other measurements and searches by constraining the modeling of important background processes. Jet substructure observable measurements are challenging as they require a precise measurement of the radiation pattern within the jet and thus a detailed understanding of the jet constituent properties. Section VII.A describes measurements of various jet substructure properties, starting from the most widely used and well understood: the jet mass.

Jet substructure properties can also be used to extend measurements of SM cross sections to higher energy, where access to the hadronic branching ratios of W, Z, and H bosons and top quarks is important. Section VII.B introduces cross section measurements for SM objects at high p_T. The use of jet substructure in these cases is similar to the application for the searches described in Sec. VIII.

A. Measurements of jet substructure

1. Jet mass

The first measurement of the normalized dijet differential cross section as a function of the jet mass was performed by the ATLAS Collaboration with a dataset corresponding to 35 pb^{-1} of 7 TeV pp collisions (Aad *et al.*, 2012a). The cross section for both groomed and ungroomed CA $R = 1.2$ jets was measured separately to gain sensitivity to both the hard and soft jet physics and to gain a deeper understanding of the various effects involved in QCD radiation. For the ungroomed jet mass, large discrepancies were observed in the tails of the mass distribution between the predictions from the MC event generators PYTHIA and HERWIG++ and the data, whereas the core of the mass distribution agreed within approximately 20% over the considered p_T range. The largest discrepancies occur at low jet masses which are sensitive to the underlying event description, hadronization model, and pileup effects.
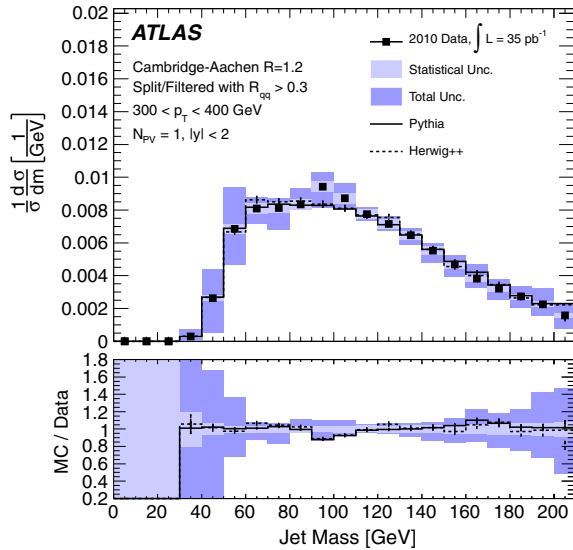
FIG. 32. Normalized differential cross section as a function of the jet mass for CA jets with $R = 1.2$ after splitting and filtering. From Aad *et al.*, 2012a.
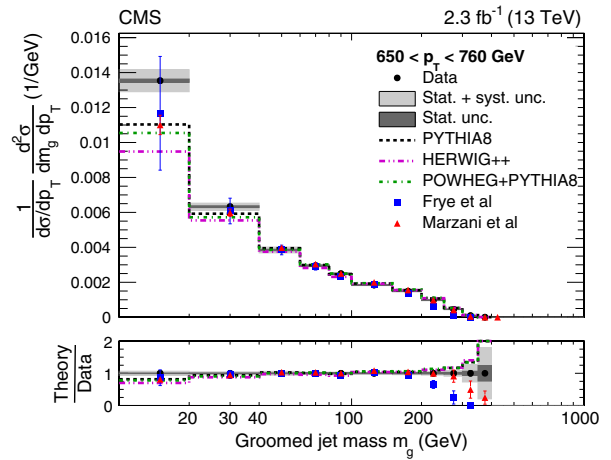

FIG. 33. Normalized differential cross section as a function of the mass for jets groomed with the soft drop algorithm in data and for two theoretical calculations. From Sirunyan *et al.*, 2018o.

The normalized cross section after applying the split filtering algorithm (Butterworth *et al.*, 2008) is shown in Fig. 32 with the mass drop parameters $\mu_{\rm frac} = 0.67$ and $y_{\rm filt} = 0.09$, and a filtering parameter of $R_{\rm filt} = \min(0.3, \Delta R/2)$. After removing soft radiation from the jet which is difficult to model, the MC prediction is in excellent agreement with the data within statistical precision. The CMS Collaboration performed a similar measurement with anti-$k_{\rm T}$ $R = 0.7$ jets using various grooming techniques in selected dijet events using 5 fb^{-1} of $\sqrt{s} = 7$ TeV data and found as well that the agreement between data and the MC prediction improves significantly after grooming techniques are applied (Chatrchyan *et al.*, 2013b). Furthermore, a measurement of the cross section was performed in $V +$ jet final states which overall show a slightly better data or MC agreement than that observed in dijet events suggesting that the simulation of quark jets is better than for gluon jets.

The CMS (ATLAS) Collaboration measured the double-differential jet cross section in balanced dijet events at $\sqrt{s} = 13$ TeV for groomed anti-$k_{\rm T}$ $R = 0.8$ jets with the soft drop algorithm with $z_{\rm cut} = 0.1$ and $\beta = 0$ ($\beta = 0, 1, 2$) (Aaboud *et al.*, 2018c; Sirunyan *et al.*, 2018o). The soft drop algorithm was chosen as it allows one to compare the unfolded measurement directly to theoretical calculations which exceed the precision of parton shower MC simulations. The jet energies of the ungroomed jets used in the ATLAS measurement are corrected for pileup effects and calibrated to the generator level while no explicit mass calibration is applied to the groomed jets as the unfolding procedure accounts for differences between the reconstructed and generator-level masses. The CMS Collaboration applied calibration factors derived from simulation and using *in situ* techniques (from boosted W bosons) to correct the jet energy and mass scale. Furthermore, the jet energy and mass are smeared in MC simulation to match the resolution measurements in data. Various sources of systematic uncertainties, categorized as experimental and theoretical uncertainties, that impact the jet

mass measurement are taken into account. While CMS evaluated the effect of the jet energy and mass scale uncertainties on the measurement by varying the energy and mass by their respective uncertainties, ATLAS evaluated the experimental uncertainties based on the accuracy of the modeling of the topological cluster energies and positions as well as their reconstruction efficiency. Theoretical uncertainties on the physics model are taken into account by comparing the response matrix for various MC generators.

The comparison of the normalized cross section with two analytical calculations as measured by CMS is shown in Fig. 33. ATLAS measured instead the $\log_{10}\rho^2$ distribution, shown in Fig. 34, where ρ is the ratio of the soft drop jet mass to the ungroomed jet $p_{\rm T}$. Both measurements are compared to calculations at next-to-leading order (NLO) with next-to-leading-logarithm (NLL) and leading order (LO) with next-to-next-to-leading-logarithm (NNLL) accuracy. Good
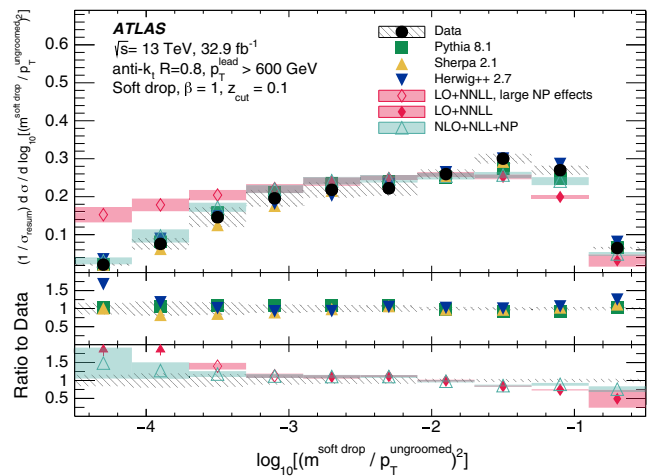

FIG. 34. Comparison of the unfolded $\log_{10}\rho^2$ distribution for $z_{\rm cut} = 0.1$, $\beta = 1$ in data to various Monte Carlo particle-level predictions and theory predictions, normalized to the integrated cross section measured in the resummation regime $-3.7 < \log_{10}\rho^2 < -1.7$. From (Aaboud *et al.*, 2018c.
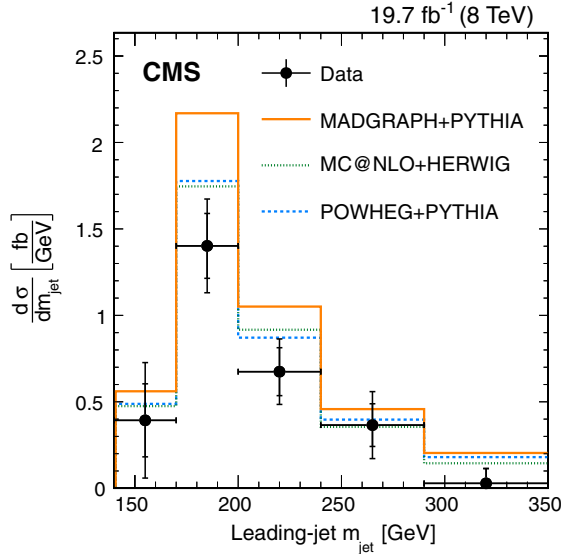
FIG. 35. Particle-level differential $t\bar{t}$ cross section measurement as a function of the leading jet mass compared to the predictions for three different Monte Carlo event generators. From Sirunyan *et al.*, 2017e.
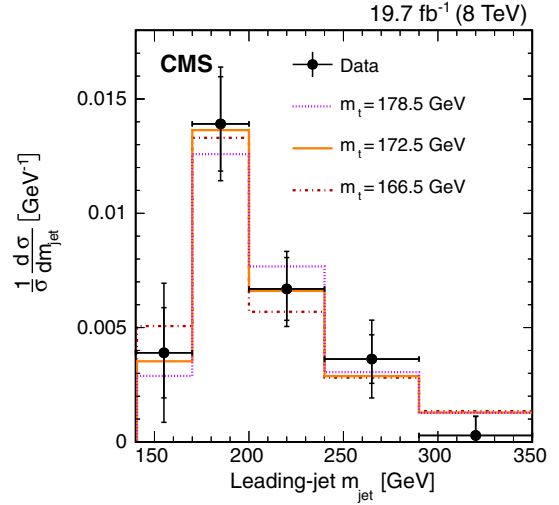

FIG. 36. Normalized particle-level differential $t\bar{t}$ cross section measurement as a function of the leading jet mass compared to predictions using three different top quark mass values. From Sirunyan *et al.*, 2017e.

agreement between the data and the predictions is observed in resummation regime $-3.7 < \log_{10} \rho^2 < -1.7$. For higher jet masses, where fixed-order effects play an important role, the NLO + NLL calculation provides a better description than the LO + NNLL calculation.

In addition to generic QCD jets, the jet mass has also been measured for boosted top quarks in lepton + jets $t\bar{t}$ events collected by the CMS Collaboration at 8 TeV (Sirunyan *et al.*, 2017e). This measurement is the first jet mass distribution unfolded at the particle level probing three prong decays. Large-R jets are reconstructed with the CA algorithm using a distance parameter of 1.2. The larger value of R in this measurement compared to the default $R = 0.8$ applied for top-tagging applications in CMS is due to an optimization of statistical precision versus the width of the jet mass distribution at the particle level and the JMR. The number of fully merged top quarks grows with increasing R, but so does the width of the jet mass distribution and the susceptibility to pileup and the underlying event. The leading jet p_{T} is required to be above 400 GeV to ensure the hadronic top quark decay to be fully captured within the large-R jet. No substructure selection is applied on the high-p_{T} large-R jet in order not to bias the jet mass measurement. A requirement of $p_{\mathrm{T}} >$ 150 GeV is imposed on the subleading jet to select the b quark from the leptonically decaying top quark. A veto on additional jets with $p_{\mathrm{T}} > 150$ GeV is applied, which results in a fraction of 65% of fully merged top quark decays within the large-R jet. The particle-level differential $t\bar{t}$ cross section as a function of the leading jet mass is shown in Fig. 35. The simulations shown predict a larger cross section than observed in the measurement, consistent with the $t\bar{t}$ cross section measurements from the ATLAS and CMS Collaborations at high p_{T}. The shape of the jet mass distribution is well described by the simulations. The experimental systematic uncertainties are dominated by the uncertainties on the jet mass and energy scale, but are smaller than the uncertainties

due to the signal modeling, coming from the choice of the top quark mass, the parton showering, and the choice of the factorization and renormalization scales.

The normalized mass distribution from boosted top quarks, shown in Fig. 36, can be used to extract the top quark mass. The normalized distribution is used since only the shape can be reliably calculated, and it has the additional benefit that systematic uncertainties partially cancel. The top quark mass is measured to be

$$m_t = 170.8 \pm 6.0(\text{stat}) \pm 2.8(\text{syst})$$
$$\pm 4.6(\text{model}) \pm 4.0(\text{theo}) \text{ GeV}$$

in agreement with top quark mass measurement in resolved $t\bar{t}$ events (CDF, D0 Collaborations, Tevatron Electroweak Working Group, 2014; Aad *et al.*, 2015c; CMS Collaboration, 2013d; Aaboud *et al.*, 2016d), albeit with a much larger uncertainty. This constitutes a proof of principle, presenting the possibility to extract a fundamental SM parameter from a jet mass distribution. This is of particular interest as ambiguities arise in the interpretation of traditional m_t measurements (Hoang, Plätzer, and Samitz, 2018), which can be circumvented by measurements and analytical calculations in the highly boosted regime (Butenschoen *et al.*, 2016; Hoang *et al.*, 2019). Future measurements at $\sqrt{s} = 13$ TeV will allow for a higher statistical precision and, in combination with jet grooming and pileup mitigation techniques, lead to a large improvement in the total precision of the measurement. Measurements at higher jet p_{T} will facilitate comparisons with analytical calculations.

2. Jet charge

The jet charge (Aad *et al.*, 2016h; Sirunyan *et al.*, 2017h) is defined as the energy weighted sum of the electric charges of the jet constituents
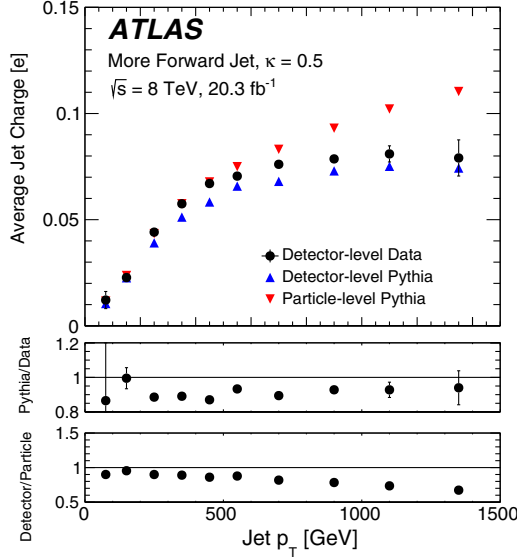
FIG. 37. The detector- and particle-level average jet charges as functions of jet p_T. From Aad *et al.*, 2016h.

FIG. 38. Unfolded jet charge distribution for $\kappa = 0.6$ in data and MC prediction. From Sirunyan *et al.*, 2017h.

$$Q_\kappa = \sum_{i \in J} \left(\frac{p_{T,i}}{p_{T,J}} \right)^\kappa q_i, \qquad (9)$$

where q_i is the electric charge of particle i and the free parameter κ that controls the sensitivity to soft particles within the jet. The ATLAS (CMS) Collaboration measured the jet charge for different values of κ using anti-k_T jets with a radius parameter of $R = 0.4$ ($R = 0.5$) in a sample of dijet events. The ATLAS Collaboration distinguishes between the two leading jets using the pseudorapidity instead of the p_T to avoid cases where the leading particle-level jet is reconstructed as the subleading detector-level jet due to the jet energy resolution and to gain sensitivity to different jet flavors. The average jet charge at detector and particle levels for the more forward of the leading jets and for $\kappa = 0.5$ is shown in Fig. 37. Because of the increasing fraction of scattering valence up quark jets (up quark charge > 0), the average jet charge increases with p_T. The difference of the average jet charge distribution at the detector level and the particle level in Fig. 37 shows that the unfolding corrections are large and growing at high p_T, due to the loss of charged-particle tracks inside jets as a result of track merging. The average jet charge as predicted by PYTHIA8 (Sjostrand, Mrenna, and Skands, 2008) using the Perugia tunes (Skands, 2010) is smaller than that observed in data due to a well-known overestimation of the multiplicity inside jets. The dominating systematic uncertainties are the track p_T resolution and the choice of MC generator used to construct the response matrix (PYTHIA6 versus HERWIG++) for the CMS Collaboration whereas the uncertainties on the unfolding procedure, the jet energy resolution at low p_T, and uncertainties on the tracking at high p_T dominate the measurement of the ATLAS Collaboration. The unfolded jet charge distribution ($\kappa = 0.6$) of the leading jet in data is compared to the prediction from POWHEG + PYTHIA8 (PH + P8) and POWHEG + HERWIG++ (PH + HPP) in Fig. 38. The different hadronization and fragmentation models used by PYTHIA8 and HERWIG++ have the largest impact on the jet
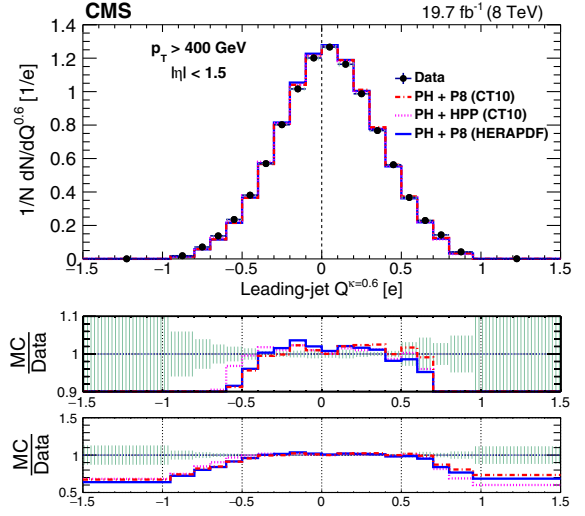
charge distribution. Variations of the jet charge can also be observed for different PDF sets; however, the effect of the relative flavor fraction in the dijet samples is significantly smaller than the choice of the showering and fragmentation models. It was further found that the predicted jet charge distribution has a significant dependence on the chosen value of α_s that describes final state radiation whereas it is insensitive to the NLO QCD effect in the matrix element calculation, color-reconnection, and multiple parton interactions. These findings are consistent between the ATLAS and CMS Collaborations.

In addition to studying the sensitivity to various nonperturbative aspects of hadronization and parton distribution functions, the jet charge measurement by ATLAS includes the first direct comparison of a jet substructure quantity with a perturbative calculation at the LHC. As it is not collinear safe, the average jet charge is not calculable. However, the p_T dependence for a particular jet type has been calculated (Waalewijn, 2012; Krohn *et al.*, 2013). A new technique was introduced by Aad *et al.* (2016h) to separately extract the average up and down quark jet charges. For a fixed p_T, the more forward of the two dijets has a higher energy and is therefore more likely to be the scattering parton with a higher momentum fraction of the proton. In turn, the higher momentum fraction parton is most likely to be a valence quark. Therefore, the fraction of up quark jets is higher for the more forward dijet than the more central dijet. Assuming further that the jet charge is entirely determined by the jet p_T and parton origin, one can then solve a system of equations to extract the average up and down quark jet charges in each bin of jet p_T:

$$\langle Q_J^f \rangle = f_u^f \langle Q_J^u \rangle + f_d^f \langle Q_J^d \rangle,$$
$$\langle Q_J^c \rangle = f_u^c \langle Q_J^u \rangle + f_d^c \langle Q_J^d \rangle, \qquad (10)$$

where f = forward, c = central, u = up, and d = down. As expected (although not an input), the average up quark charge is positive and the average down quark charge is negative; furthermore, the latter is roughly half the former in absolute value. The p_T dependence of $\langle Q_J^{u,d} \rangle$ is fit with a logarithmic scale violating term c: $\langle Q \rangle_i = \langle Q \rangle_0 [1 + c_\kappa \ln(p_{T,i}/p_{T,0})]$,
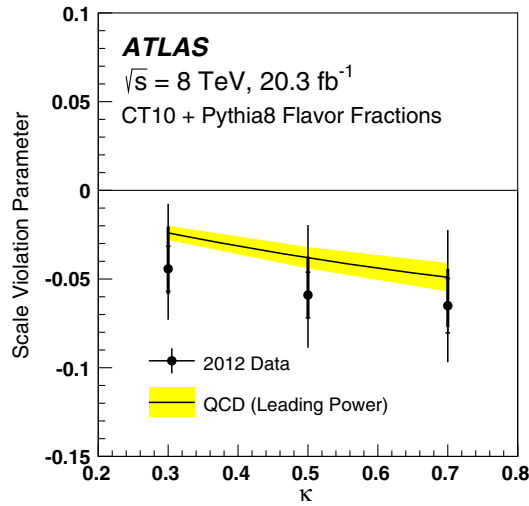
FIG. 39. The measured and predicted values of the average jet charge scale violation parameter c_κ. From Aad *et al.*, 2016h.

where i represents the p_T bin. Figure 39 shows the measured and predicted values of c_κ. The uncertainties are large, but there is an indication that $c < 0$ and $\partial c/\partial \kappa < 0$ as predicted.

3. Other jet substructure observables

The ATLAS and CMS Collaborations have performed further precision measurements of hadronic jet substructure in pp collisions, correcting for acceptance and resolution such as jet and event shapes (Aad *et al.*, 2011a, 2012b, 2013a; Chatrchyan *et al.*, 2012b; Sirunyan *et al.*, 2018e; Aaboud *et al.*, 2019c), charged-particle multiplicities (Aad *et al.*, 2011b, 2016l; Chatrchyan *et al.*, 2012b), the jet fragmentation functions (Aad *et al.*, 2011c; Aaboud *et al.*, 2019a), color flow (Aad *et al.*, 2015h) and k_T splitting scales, N-subjettiness ratios as well as further substructure variables such as planar flow and angularity (Aad *et al.*, 2012a, 2013d).

B. Measurements with jet substructure

While measurements of jet substructure observables such as jet mass, jet charge, and event shape variables have been discussed in Sec. V, the following sections present measurements of other quantities through the exploitation of jet substructure techniques such as top tagging.

1. Differential $t\bar{t}$ cross section measurements

The selection cuts applied in traditional $t\bar{t}$ cross section measurements (Chatrchyan *et al.*, 2013d; Aad *et al.*, 2015e, 2016c; Khachatryan *et al.*, 2015d, 2017c; Aaboud *et al.*, 2017k, 2017i) are chosen to maximize the acceptance and minimize the associated uncertainties on the fiducial and total cross section measurements. The fiducial region is such that events with top p_T below 100 GeV and above 600 GeV are underrepresented, with the former caused by trigger and reconstruction efficiencies and the latter by collimated decays from large Lorentz boosts. This is evident from Fig. 40, where a drop in selection efficiency below 100 GeV and above 600 GeV is apparent. This results in a small number of events
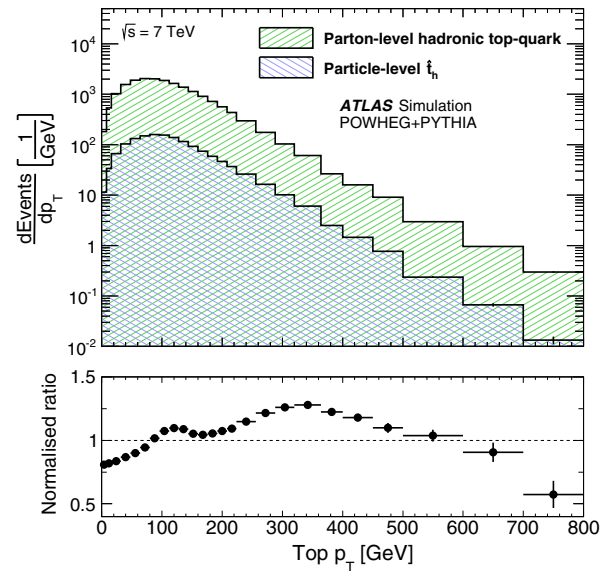

FIG. 40. The drop in fiducial efficiency at top $p_T > 600$ GeV when reconstructing top quarks with individual anti-k_T, $R = 0.4$ jets (resolved reconstruction). Adapted from Aad *et al.*, 2015e.

being selected with high top quark p_T, as seen in the ATLAS run 1 (7 TeV) measurement shown in Fig. 41. This means that an interesting region in terms of new physics is the least well measured. Despite often having similar signal efficiencies to resolved reconstructed techniques, boosted top-tagging techniques allow for more precise measurements at high p_T due to their higher background rejection.

The ATLAS Collaboration performed a measurement of the boosted $t\bar{t}$ differential cross section as a function
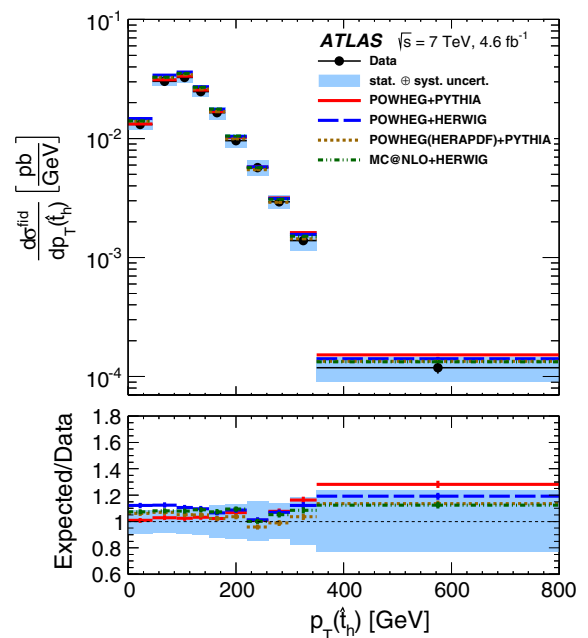

FIG. 41. The small number of top jets identified at high-p_T results in very coarse cross section measurement when using the resolved reconstruction technique. Adapted from Aad *et al.*, 2015e.
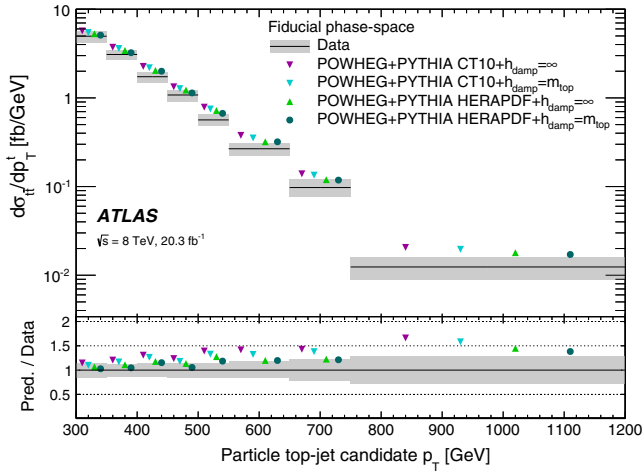
FIG. 42. Particle-level differential $t\bar{t}$ cross section measurement for two different PDF sets and choices of the h_{damp} parameters. From Aad *et al.*, 2016i.
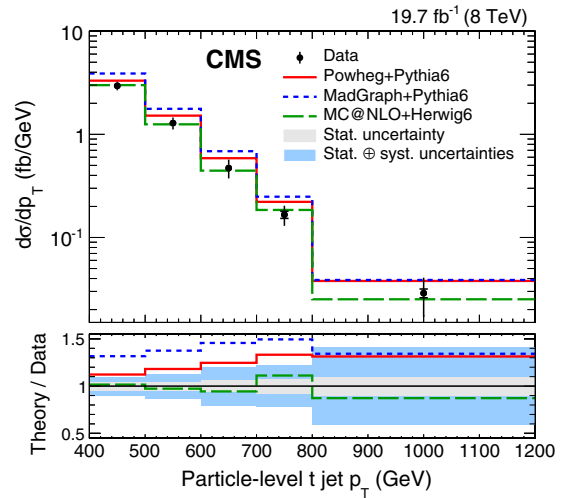

FIG. 43. Comparison of the particle-level differential $t\bar{t}$ cross section as a function of the jet p_T to three different MC generators. From Khachatryan *et al.*, 2016g.

of the top quark p_T in the lepton + jets channel (Aad *et al.*, 2016i). A least one anti-k_T jet, trimmed with $R_{\mathrm{sub}} = 0.3$ and $f_{\mathrm{cut}} = 0.05$, is required with $|\eta| < 2$ and $p_T > 300$ GeV. To select events with boosted top quarks, the large-R jet is required to have a mass larger than 100 GeV and $\sqrt{d_{12}} > 40$ GeV (tagger III, see Sec. VI.C). The reconstructed p_T distribution of the anti-k_T $R = 1.0$ trimmed jet is unfolded to the parton and particle levels. The measured particle-level differential cross section is compared in Fig. 42 to the predictions of several MC generators normalized to the NNLO + NNLL inclusive cross section. Overall good agreement is observed, but a harder p_T spectrum is predicted by the simulation than observed in data with larger discrepancies at high p_T. The differential cross section measurement is also compared to predictions from POWHEG + PYTHIA using either the HERAPDF (Aaron *et al.*, 2010) or CT10 (Lai *et al.*, 2010) PDF set and two different values for the resummation damping factors h_{damp}, $h_{\mathrm{damp}} = m_{\mathrm{top}}$ and $h_{\mathrm{damp}} = \infty$. The best data or MC agreement is observed when using the HERAPDF set and $h_{\mathrm{damp}} = m_{\mathrm{top}}$. For each of the settings, the trend of a harder p_T spectrum in simulation compared to data persists.

A similar measurement by the CMS Collaboration based on 8 TeV data (Khachatryan *et al.*, 2016g) uses the CMSTT algorithm to reconstruct boosted top quarks. The unfolded results are in agreement with the ATLAS measurement and show a similar trend between data and simulation as shown in Fig. 43.

These measurements extend up to a top quark p_T of 1.2 TeV, allowing for higher precision thanks to the usage of jet substructure techniques. The largest uncertainties at the highest values of p_T in ATLAS and CMS come from the large-R jet energy scale and the extrapolation of the b-jet calibration to high p_T.

The parton-level differential cross section in top quark p_T has also been measured in the all-hadronic final state by the CMS Collaboration using 8 TeV data (CMS Collaboration, 2017e). This measurement relies on pruned jets with an N subjettiness and subjet-b tagging requirement to suppress the

large amount of background from QCD dijet production. The cross section is determined from a maximum likelihood fit to the jet mass distributions for signal enriched and signal depleted regions. This allows for a simultaneous extraction of the $t\bar{t}$ cross section and the QCD background. The measurement is in agreement with the results from the lepton + jets final states, but has somewhat larger statistical uncertainties of up to about 40% in the highest p_T bin with $0.8 < p_T < 1.2$ TeV.

The increased $\sqrt{s}$ at run 2 of the LHC offers the possibility for more precise differential $t\bar{t}$ cross section measurements in the highly boosted regime. The $t\bar{t}$ production cross section increased by more than a factor of 10 for top quark $p_T > 400$ GeV when going from $\sqrt{s} = 8$ to 13 TeV.

The first measurement based on 3.2 fb^{-1} of 13 TeV data in the lepton + jets channel was performed by ATLAS (Aaboud *et al.*, 2017k). The measurement extends to p_T of 1.5 TeV and a similar trend as at 8 TeV is observed between the data and the simulation at high p_T. A newer measurement of the $t\bar{t}$ differential cross section in the all-hadronic channel was performed by the ATLAS Collaboration with 36.1 fb^{-1} of 13 TeV data (Aaboud *et al.*, 2018m). The measurement used trimmed anti-k_T $R = 1.0$ jets with $R_{\mathrm{sub}} = 0.2$ and $f_{\mathrm{cut}} = 0.05$. To obtain a flat signal efficiency of 50% and a quark/gluon rejection of approximately 17 (10) for $p_T = 500$ (1000) GeV, p_T dependent criteria are applied on the jet mass and τ_{32}. Furthermore the two top-tagged large-R jets are required to have a b tagged small-R jet within $\Delta R < 1.0$. The event selection results in a signal-to-background ratio of approximately 3:1. The measured fiducial phase-space cross section is $\sigma = 292 \pm 7(\mathrm{stat}) \pm 76(\mathrm{syst})$ compared to the POWHEG + PYTHIA8 prediction of 384 ± 36 fb at NNLO + NNLL. The measured normalized differential cross section as a function of the top jet p_T and rapidity is in good agreement with the different MC predictions. Larger discrepancies are observed for the p_T of the $t\bar{t}$ system as shown in Fig. 44. The measurement is dominated by the systematic uncertainties on the jet energy, mass, and substructure scale of the large-R
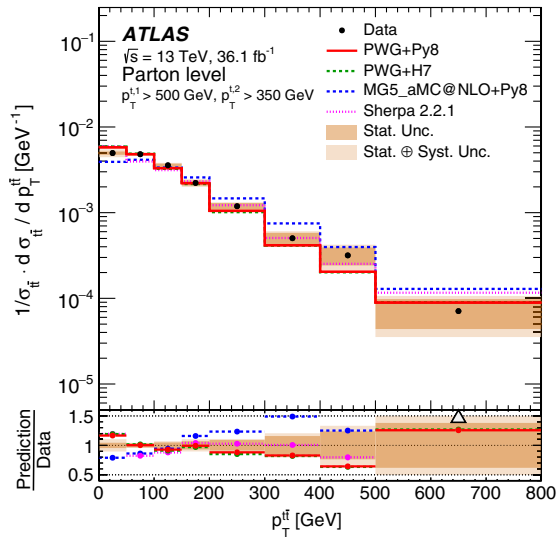
FIG. 44. The normalized differential cross section as a function of the $t\bar{t}$ p_T as measured by ATLAS in the all-hadronic channel at 13 TeV. From Aaboud *et al.*, 2018m.
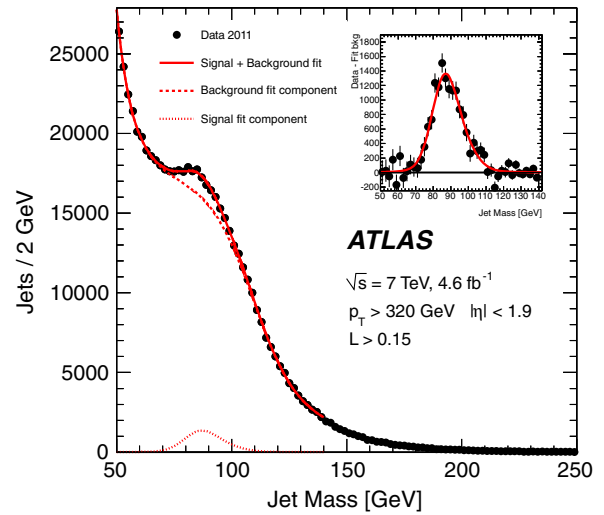

FIG. 45. Binned maximum likelihood fit to the jet mass distribution in data for selected W and Z events reconstructed as one single ungroomed anti-k_T $R = 0.6$ jet. From Aad *et al.*, 2014d.

jets, alternative parton shower model, and the uncertainties on the b jet identification.

2. W, Z, and H cross sections

The cross section of boosted W and Z boson production was measured by ATLAS in 4.6 fb^{-1} of 7 TeV pp collisions (Aad *et al.*, 2014d). The hadronically decaying W and Z bosons are reconstructed as one single ungroomed anti-k_T $R = 0.6$ jet with $p_T > 320$ GeV, $|\eta| < 1.9$ and masses ranging between 50 and 140 GeV. The W and Z signals are enhanced over the dominating QCD background by constructing a likelihood discriminant from three substructure variables, thrust minor (Brandt *et al.*, 1964; Farhi, 1977), sphericity (Bjorken and Brodsky, 1970), and aplanarity (Bjorken and Brodsky, 1970), resulting in a signal efficiency of 56% and a background rejection of 89%. The jet mass distribution after subtracting the expected background from $t\bar{t}$ events is shown in Fig. 45. A binned maximum likelihood fit to the jet mass distribution is used to extract the W and Z jet signal yield and to calculate the inclusive cross section. Only the combined $W + Z$ cross section measurement is performed in this analysis due to the limited jet mass resolution. The combined $W + Z$ cross section is measured to be $\sigma_{W+Z} = 8.5 \pm 0.8(\text{stat}) \pm 1.5(\text{syst})$ pb and is in agreement with the standard model prediction of $\sigma_{W+Z} = 5.1 \pm 0.5$ pb within 2 standard deviations. The dominating systematic uncertainties are the jet mass resolution and the choice of the QCD background PDF. The signal significance was furthermore studied when using groomed jets instead of ungroomed jets. Without an optimization of the analysis for groomed jets, similar significances were observed for groomed and ungroomed jets as expected due to the low number of pileup vertices in the 7 TeV dataset.

As discussed in Sec. VI.D the SM Higgs boson decays with approximately 58% into $b\bar{b}$. However, the $H \to b\bar{b}$ decay in the resolved channel can be studied only in associated production with either a vector boson (W or Z) (Aaboud *et al.*, 2017l; Sirunyan *et al.*, 2018k), top quarks, or via the

vector-boson-fusion production mechanism due to the overwhelming multijet background. To search for $H \to b\bar{b}$ in the gluon-gluon fusion production mode with an additional high-p_T jet, jet substructure techniques can be employed to suppress the enormous multijet background. The CMS Collaboration performed a search for the SM Higgs boson using a dijet topology with 35.9 fb^{-1} of 13 TeV pp collisions (Sirunyan *et al.*, 2018l). The analysis used anti-k_T $R = 0.8$ jets corrected with the PUPPI algorithm to reduce the effects from pileup, and modified with the soft drop algorithm ($\beta = 0$, $z_{\text{cut}} = 0.1$) to mitigate the effects from the underlying event and soft or wide-angle radiation. At least one large-R jet with $p_T > 450$ GeV and $|\eta| < 2.5$ is required. To distinguish the two prong structure of a jet containing the full $H \to b\bar{b}$ decay from quark- or gluon-initiated jets, the N_2^1 variable, calculated from the generalized energy correlation functions, is exploited. To ensure a flat QCD background rejection of 26% over the considered mass and p_T range, a decorrelation procedure (Dolen *et al.*, 2016) is applied to N_2^1. The multijet background is further suppressed by utilizing the double-b tagger. The $W/Z + $ jets background is estimated from MC simulation and the shape of the multijet background is determined in a validation region in data with lower values of the double-b tagger discriminator. The soft drop mass distribution of the leading jet is shown in Fig. 46 with a clear resonant structure at the mass of the W and Z bosons. The SM background processes and the potential signal from SM $H \to b\bar{b}$ production are estimated simultaneously. The observed (expected) significance for the $H \to b\bar{b}$ process is 1.5 (0.7)σ. The measured cross section for the $Z + $ jets process is $0.85 \pm 0.16(\text{stat}) {}^{+1.0}_{-0.4}(\text{syst})$ pb which is in agreement with the SM prediction of 1.09 ± 0.11 pb. This is the first observation of $Z \to b\bar{b}$ in the single jet topology.

The ATLAS Collaboration also measured the high p_T $Z \to b\bar{b}$ cross section using two nearby b tagged anti-k_T $R = 0.4$ jets (instead of one large-radius jet) in 19.5 fb^{-1} of 8 TeV pp
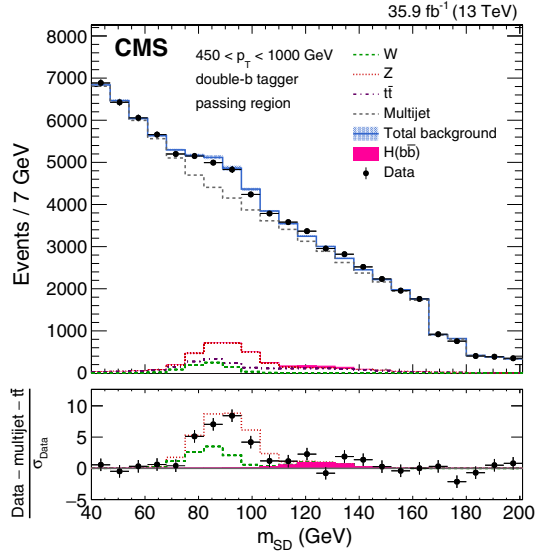
FIG. 46. Soft drop jet mass m_{SD} of anti-k_T $R = 0.8$ jets in data and for the dominating background processes; multijet production and W and $Z + $ jets events. Jets are required to pass criteria on N_2^1 and to be identified as double-b jets by the double-b tagger introduced in Sec. VI.D. From Sirunyan *et al.*, 2018l.

collisions (Aad *et al.*, 2014b). The measured fiducial cross section was determined to be $\sigma_{Z \to b\bar{b}} = 2.02 \pm 0.33$ pb which is in excellent agreement with the next-to-leading-order theoretical predictions.

VIII. SEARCHES FOR NEW PHYSICS

Jet substructure methods have been successfully applied in a large variety of searches for physics beyond the SM. The respective exclusion limits are substantially improved through the application of these methods. In some cases the decay signature of heavy beyond the standard model (BSM) particles would not be accessible without the application of jet substructure methods.

As the number of such BSM searches is very large, only a small subset of the published results can be discussed here. The following sections give an overview of a selection of searches for $t\bar{t}$ resonances (Chatrchyan *et al.*, 2012a; Aad *et al.*, 2013b, 2013c, 2015g; Khachatryan *et al.*, 2016k; ATLAS Collaboration, 2016a; Sirunyan *et al.*, 2017i), diboson resonances (Chatrchyan *et al.*, 2013a; Khachatryan *et al.*, 2014b, 2014c, 2015e, 2016a, 2016e, 2016f, 2017d; Aad *et al.*, 2015a, 2016a; Aaboud *et al.*, 2016a, 2016e, 2017g, 2018e, 2018f, 2018g, 2018l; Sirunyan *et al.*, 2017b, 2017c, 2017g, 2018j; CMS Collaboration, 2017f), vectorlike quarks (Chatrchyan *et al.*, 2014; Khachatryan *et al.*, 2015b, 2016h, 2016i, 2017e; Aad *et al.*, 2016b, 2016j; Sirunyan *et al.*, 2017j, 2017k, 2017l, 2017m, 2018d, 2018m, 2018n; Aaboud *et al.*, 2017m, 2017n), and leptophobic Z' (Sirunyan *et al.*, 2018p; Aaboud *et al.*, 2019b). Further searches using jet substructure techniques can be found (Aad *et al.*, 2014c, 2015d, 2016m; Khachatryan *et al.*, 2015a, 2016b, 2016c, 2016d, 2016j, 2016l, 2017b; Aaboud *et al.*, 2016c, 2016f, 2017j, 2017o, 2018d, 2018h, 2018i, 2018j, 2018k; Sirunyan

et al., 2017d, 2017f, 2017n, 2017o, 2017p, 2018f, 2018g, 2018h, 2018i, 2018q, 2018r).

A. Diboson resonances

Several new physics models predict resonances coupling strongly to vector bosons to play a role in the cancellation of large corrections to the Higgs mass. These models include extensions of the SM Higgs doublet, where the simplest realizations are two-Higgs-doublet models (Branco *et al.*, 2012) with heavy, neutral Higgs bosons, which can have large branching fractions to top quarks and W, Z, or H bosons. Alternatives are composite Higgs models (Banks, 1984; Georgi, Kaplan, and Galison, 1984; Georgi and Kaplan, 1984; Kaplan and Georgi, 1984; Kaplan, Georgi, and Dimopoulos, 1984; Dugan, Georgi, and Kaplan, 1985; Georgi, 1986; Bellazzini, Csáki, and Serra, 2014) or Randall-Sundrum Kaluza-Klein models (Randall and Sundrum, 1999; Davoudiasl, Hewett, and Rizzo, 2000; Pomarol, 2000; Agashe *et al.*, 2003).

Searches for new resonances generally focus at high masses with $m > 1$ TeV such that the SM bosons receive high Lorentz boosts. In more than 60% of the cases, W, Z, and H bosons decay into a quark-antiquark pair, which makes the reconstruction of such decays with jet substructure techniques an essential ingredient for these searches. In the following, the analysis strategies and results from CMS and ATLAS using pp collision data with $\sqrt{s} = 13$ TeV are discussed.

The searches for diboson resonances are performed in semileptonic (Aaboud *et al.*, 2016a; Sirunyan *et al.*, 2017b) and fully hadronic final states (Aaboud *et al.*, 2017g, 2018g; Sirunyan *et al.*, 2017g, 2018j). As the methods of jet substructure analyses exhibit their full strength in hadronic final states, the following discussion gives a summary and comparison of the ATLAS and CMS results in the search for W and Z resonances in hadronic final states only.

In an analysis performed by the CMS Collaboration (Sirunyan *et al.*, 2018j) events with two anti-k_T jets with $R = 0.8$, corrected with the PUPPI algorithm, and $65 < m_{\text{soft drop}} < 105$ GeV are selected. The jet is considered to be a W boson candidate if the mass is in the range 65–85 GeV, while it is a Z boson candidate if the mass is in the range 85–105 GeV. This leads to the three signal categories WW, ZZ, and WZ. The jets are further categorized according to τ_{21} into high purity (HP, $\tau_{21} < 0.35$) and low purity (LP, $0.35 < \tau_{21} < 0.75$). Events are always required to have one HP V jet, and are divided into HP and LP events, depending on whether the other V jet is of high or low purity. To further suppress the large QCD multijet background a requirement on the dijet kinematics $|\eta_1 - \eta_2| < 1.3$ is applied.

The background is estimated from a signal + background fit with the function

$$\frac{dN}{dm_{jj}} = \frac{P_0}{(m_{jj}/\sqrt{s})^{P_1}},$$

where P_0 is a normalization parameter and P_1 is a parameter describing the shape. This parametrization has been tested and validated on simulated events and on data in a control region. As shown in Fig. 47 the data in the signal region are well
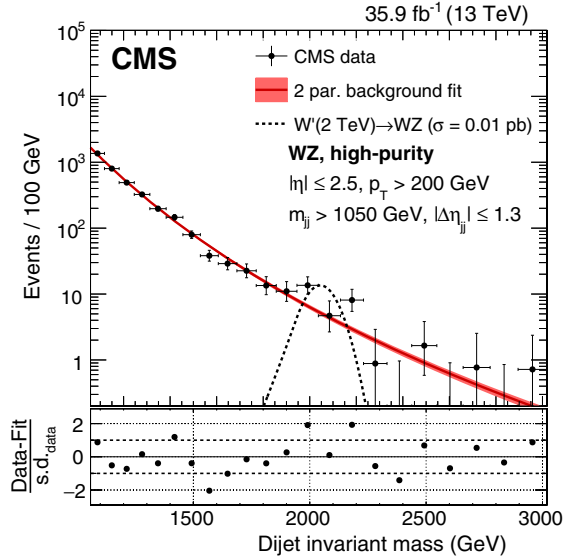
FIG. 47. Dijet invariant mass distribution in the high purity *WZ* category of the fully hadronic *WW*, *WZ*, and *ZZ* resonance search. The fit under the background-only hypothesis is overlaid. From Sirunyan *et al.*, 2018j.
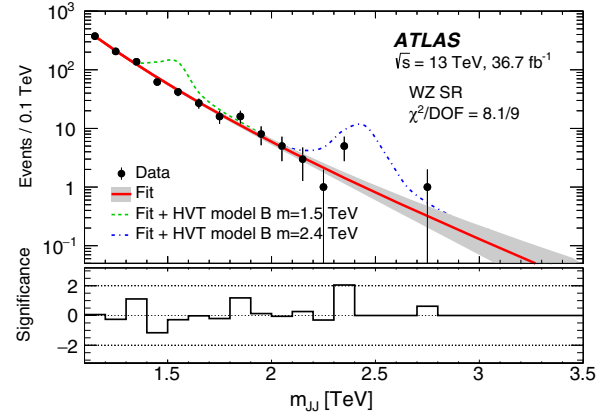

FIG. 48. The observed data in the signal region of the *WZ* category. Also shown is the fitted background prediction. The gray region represents the uncertainty in the background estimate. From Aaboud *et al.*, 2018g.

described by the fit function. Figure 47 also shows that no excess over the background-only hypothesis is observed.

A similar analysis was performed by the ATLAS Collaboration (Aaboud *et al.*, 2018g). In this analysis events are required to have at least two large-*R* jets with $p_T >$ 200 GeV in the pseudorapidity range $|\eta| < 2.0$. These jets are reconstructed with the anti-k_T algorithm with a radius parameter $R = 1.0$. The trimming algorithm is applied using k_T subjets with $R = 0.2$. The rapidity separation between the two leading jets has to satisfy $|\Delta y_{12}| < 1.2$.

The large-*R* jet mass is computed from the combined mass (see Sec. V.B) and is required to be within a window of the expected *W* or *Z* mass value. The window width varies from 22 to 40 GeV depending on the jet p_T. In addition, the $D_2^{\beta=1}$ variable is used to select jets with a two-prong structure.

Similar to the CMS analysis, the background is estimated by fitting the dijet invariant mass distribution with the parametric form

$$\frac{dn}{dx} = p_1(1-x)^{p_2+\xi p_3} x^{p_3},$$

where *n* is the number of events, *x* is a dimensionless variable related to the dijet mass m_{JJ}, $x = m_{JJ}/\sqrt{s}$, p_1 is a normalization factor, p_2 and p_3 are dimensionless shape parameters, and ξ is a constant chosen to remove the correlation between p_2 and p_3 in the fit.

The dijet invariant mass distributions for these events are shown in Fig. 48, where good agreement is found between data and the expectations from the background fit.

In the case of boosted *H* bosons, different reconstruction methods have to be used to benefit from the presence of *b* quarks in $H \to b\bar{b}$ decays (see Sec. VI.D). Results have been published on the search for *WH* and *ZH* final states (Sirunyan *et al.*, 2017c; Aaboud *et al.*, 2017g, 2018l) as well as for *HH*

final states (Aad *et al.*, 2015a; Aaboud *et al.*, 2016e; CMS Collaboration, 2017f).

B. $t\bar{t}$ resonances

The models of new physics mentioned in the previous section also predict resonances decaying to pairs of top quarks. An example for an alternative model is the top color model which contains a *Z'* boson (Hill, 1995), with exclusive decays to top quarks.

In case of boosted $t \to bW$ events with leptonic *W* boson decays, the lepton may overlap with the associated *b* quark jet. Therefore, the usual lepton-isolation criteria, which are used to mitigate the contamination with QCD multijet background, are relaxed. The CMS and ATLAS Collaborations follow different strategies for this purpose. In CMS (Khachatryan *et al.*, 2016k; Sirunyan *et al.*, 2017i), the lepton must have a large angular separation from the associated *b* jet candidate of $\Delta R(\text{lepton}, \text{jet}) > 0.5$ or it must have a transverse momentum relative to the jet axis p_T^{rel} above 25 GeV. This requirement removes background contributions from semileptonic *B* hadron decays. In ATLAS (Aad *et al.*, 2015g; Aaboud *et al.*, 2018n), the lepton isolation is achieved by a variable isolation cone that changes as a function of the transverse momentum (Rehermann and Tweedie, 2011). Interestingly, studies performed in CMS for 13 TeV show that the CMS implementation of such a variable isolation criterion is not as powerful as the selection based on $\Delta R(\text{lepton}, \text{jet})$ and p_T^{rel} (CMS Collaboration, 2016c).

To reconstruct the boosted hadronic top decay, the presence of a single high-momentum, large-*R*, top-tagged jet is required. In CMS (ATLAS) the large-*R* jet is reconstructed with the CA (anti-k_T) algorithm with a size parameter of $R = 0.8$ (1.0). The selection requirement on the transverse momentum is $p_T > 400$ (300) GeV. ATLAS applies trimming to the large-*R* jets with the parameters $f_{\text{cut}} = 0.05$ and $R_{\text{sub}} = 0.3$ and the jets are required to have a mass $m_{\text{jet}} > 100$ GeV and $\sqrt{d_{12}} > 40$ GeV. The strategy followed by CMS is to apply the CMSTT algorithm (as defined in Sec. VI.C), where the mass of the jet has to satisfy $140 < m_{\text{jet}} < 250$ GeV. In addition, the *N*-subjettiness ratio τ_{32} must be smaller than 0.7.

The variable of interest is the invariant mass $m_{t\bar{t}}$ of the $t\bar{t}$ system. It is reconstructed from the top-tagged large-R jet, a b tagged small-R jet, as well as the lepton and the missing energy. Once the top-pair system is reconstructed, events are further divided into categories based on the lepton flavor and the number of b-tagged and top-tagged jets. This gives several analysis categories with different background compositions: the top-tagged and b-tagged events are dominated by the SM $t\bar{t}$ background, while events without top tags and b tags are mostly composed of W + jets events.

Similar methods are applied in case both W bosons decay hadronically (Khachatryan *et al.*, 2016k). To access the region with jets of lower momenta with $200 < p_\mathrm{T} < 400$ GeV a dedicated algorithm with a larger jet size parameter of $R = 1.5$ (CA15 jets) is applied in CMS. The larger jet size extends the analysis coverage to the case of intermediate or smaller Lorentz boosts. These low-p_T jets are required to be identified by the HEPTopTagger algorithm (as described in Sec. VI.C). This approach improves the sensitivity for smaller masses of the hypothetical $t\bar{t}$ resonance.

Even with the requirement of two top-tagged jets, the event sample is dominated by QCD dijet events. This background is estimated using a data-driven technique, where an antitag and probe method is used. The τ_{32} requirement is reversed on one jet to select a sample dominated by QCD events. The opposite jet is then used to measure the misidentification rate for the top-tagging requirements. The measured misidentification rate ranges from 5% to 10%, depending on the jet momentum, τ_{32}, and the b tagging requirements applied. This differential rate is used in a sample of single top-tagged events to predict the double top-tagged event contribution from QCD processes in each individual event category. Closure tests performed in data and simulation are performed to validate the background estimation for each of the signal regions.

No significant excess above the predicted background is observed in the measured $t\bar{t}$ invariant mass spectrum. Figure 49 shows the $m_{t\bar{t}}$ spectrum in the analysis category with the highest S/B fraction.

Depending on the model, narrow $t\bar{t}$ resonances are excluded for masses less than approximately 4 TeV. The exclusion limits are weaker for scenarios with large width of the resonance.

C. Vectorlike quarks

Vectorlike quarks (VLQs) are predicted by a variety of theories introducing a mechanism that stabilizes the mass of the Higgs particle. Such theories include little Higgs models (Arkani-Hamed, Cohen, and Georgi, 2001; Schmaltz and Tucker-Smith, 2005), models with extra dimensions (Antoniadis, Benakli, and Quiros, 2001; Hosotani, Noda, and Takenaga, 2005), and composite Higgs models (Antoniadis, Benakli, and Quiros, 2001; Agashe, Contino, and Pomarol, 2005; Hosotani, Noda, and Takenaga, 2005). As VLQs are expected to have large masses and have top quarks and vector bosons as decay products, jet substructure analyses have been applied in many searches for VLQs.

The first search for VLQs using jet substructure methods was an inclusive search for pair-produced T quarks
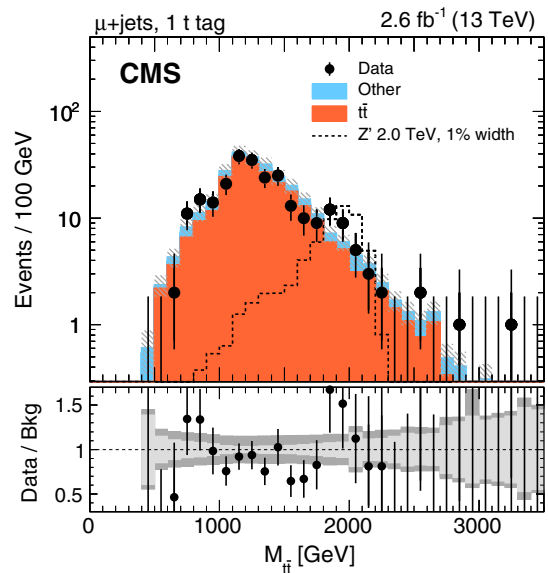

FIG. 49. Invariant mass of the reconstructed $t\bar{t}$ pair in data and simulation for the lepton + jets channel in the category with one top-tagged jet. From Sirunyan *et al.*, 2017i.

(Chatrchyan *et al.*, 2014). As VLQs may have many decay modes ($T \to bW$, $T \to tZ$, $T \to tH$, $B \to tW$, $B \to bZ$, $B \to bH$), a large variety of final states needs to be explored. For this reason, an inclusive search has been performed without the attempt to reconstruct a specific decay chain. The CA algorithm was used with a distance parameter $R = 0.8$ (CA8 jets). Boosted W jets are identified based on the mass of the CA8 jet while boosted top jets are identified with the CMSTT, described in Sec. VIII.B.

The first search for VLQs in the all-hadronic final state (Khachatryan *et al.*, 2015b) targeted the $T \to tH$ decay mode. The CA algorithm with a large size parameter of $R = 1.5$ was applied to cluster top quarks and Higgs bosons in single large jets. To identify the origin of the large CA jets a top-tagging algorithm (HEPTopTagger) and a Higgs tagging algorithm based on subjet-b tagging (see Sec. VI.D) were used. This was the first time these two algorithms have been applied in a data analysis by the CMS Collaboration. Two subjets must be b tagged and their invariant mass must be greater than 60 GeV to fulfill the Higgs tagging requirement. The multiplicity of these Higgs tags is shown in Fig. 50 which demonstrates that both the QCD multijet and the $t\bar{t}$ backgrounds can be suppressed by several orders of magnitudes.

Extensive use of substructure methods has also been made by the ATLAS Collaboration, in particular, for the search for single production of VLQs. The single production modes may have higher cross sections than pair production depending on the VLQ mass and the coupling parameters (Aguilar-Saavedra *et al.*, 2013). ATLAS performed an analysis (Aad *et al.*, 2016j) where the VLQ is searched for in the decay mode with a W boson and a top quark ($B \to tW$). Final states with at least one lepton are considered, where either the W boson or the top quark appear in a boosted configuration. They are identified by the application of a jet mass requirement ($m > 50$ GeV) on a trimmed large-R anti-k_T jet with a distance parameter $R = 1.0$.
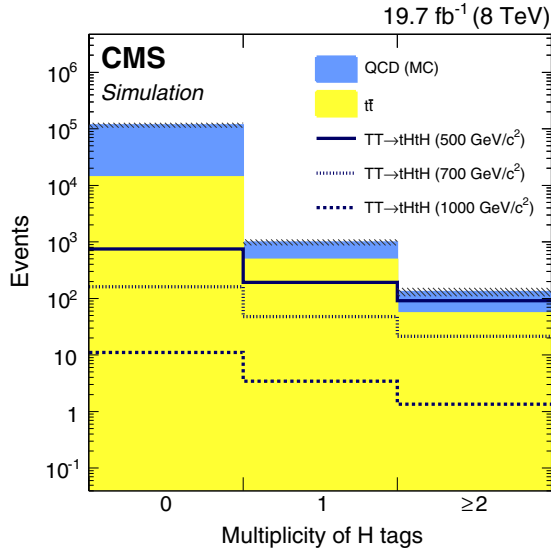
FIG. 50. Multiplicity of CA15 jets which fulfill the Higgs tagging criteria. The solid histograms represent the simulated background processes ($t\bar{t}$ and QCD multijet). The hatched error bands show the statistical uncertainty of the simulated events. From Khachatryan *et al.*, 2015b.

A different strategy is followed in another ATLAS search (Aad *et al.*, 2016b), where the decay into the bW final state is investigated ($T/Y \rightarrow bW$). As the W boson is assumed to decay leptonically, no boosted hadronic W or top quark decays are present. Therefore, the analysis uses a veto on the presence of massive ($m > 70$ GeV), trimmed large-R anti-k_T jets with $R = 1.0$, to suppress the dominant $t\bar{t}$ background.

Today, jet substructure methods are widely employed in almost all VLQ searches published by the LHC Collaborations (Khachatryan *et al.*, 2017e; Sirunyan *et al.*, 2017j, 2017k, 2017l, 2017m, 2018m; Aaboud *et al.*, 2017m). The excluded VLQ masses are exceeding 1 TeV for all branching fractions, thanks to jet substructure techniques.

D. Leptophobic Z'

Besides resonances coupling to heavy SM particles, there exist predictions for resonances that couple to quarks and gluons (Baur, Hinchliffe, and Zeppenfeld, 1987; Hewett and Rizzo, 1989; Baur, Spira, and Zerwas, 1990; Langacker, 2009), including simplified dark matter (DM) models in which resonances couple only to quarks and DM particles (Goodman *et al.*, 2010; Rajaraman *et al.*, 2011; An, Huo, and Wang, 2013). When the new particle (such as a Z') is sufficiently light ($m_{Z'} \ll 1$ TeV), it can be boosted when produced in association with initial-state radiation and thus entirely captured by a single large-radius jet (Sirunyan *et al.*, 2018p; Aaboud *et al.*, 2019b). Searching in this mode can significantly extend the sensitivity of the existing search program, where resolved low-mass resonance searches typically degrade due to high trigger thresholds and the enormous QCD multijet background.

Both ATLAS and CMS have used this strategy to look for boosted Z' jets. Jets in the CMS analysis are reconstructed
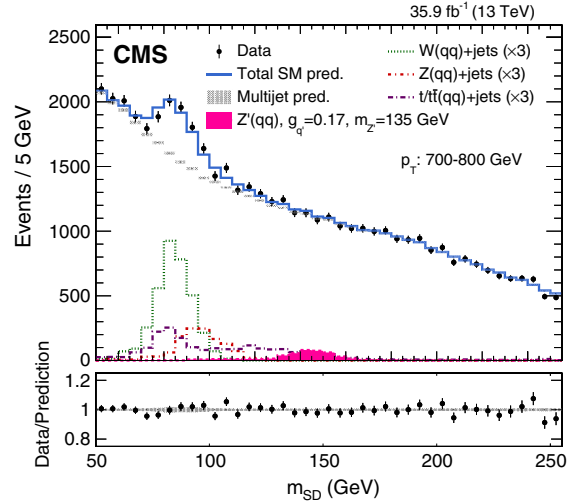

FIG. 51. Soft drop jet mass of anti-k_t $R = 0.8$ jets in data and for the dominating background processes, multijet production, and W and $Z +$ jets events. From Sirunyan *et al.*, 2018p.

with the anti-k_T algorithm with $R = 0.8$ and corrected for effects from pileup and the underlying event with PUPPI and the soft drop algorithm ($\beta = 0$, $z_{cut} = 0.1$), whereas anti-k_T $R = 1.0$ jets, trimmed with $R_{sub} = 0.2$ and $f_{cut} = 5\%$, are used in ATLAS. To suppress the dominating QCD multijet background, CMS applies criteria on N_2^1 (Moult, Necib, and Thaler, 2016) and ATLAS chooses τ_{21} as a discriminator. To avoid distortions of the jet mass spectrum due to a large correlation between the jet mass and substructure variables, a decorrelation with the DDT method is applied. Data-driven techniques are used to determine the dominating background
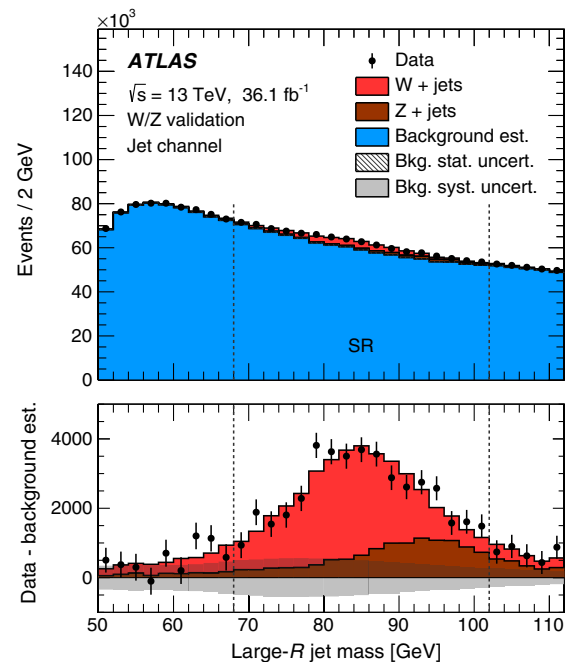

FIG. 52. Trimmed jet mass distribution anti-k_T $R = 1.0$ jets in data and for the dominating background processes. From Aaboud *et al.*, 2019b.

from QCD multijet production. Subdominant processes such as W and Z + jets events are estimated from MC simulation. The jet mass distributions of the large-R jet are shown in Figs. 51 and 52 for the CMS and ATLAS analyses, respectively. No evidence for a resonant structure on top of the SM background is observed.

IX. CONCLUSIONS

Jet substructure is the term used to describe the calculations, algorithms, and analysis techniques developed over the last decade and reviewed in this article. These methods are used to exploit the details of hadronic activity detectable by modern particle detectors such as ATLAS and CMS, and precision standard model measurements and searches for physics beyond the standard model at both these experiments increasingly rely on one or more of the tools developed by the jet substructure community. With increasingly sophisticated hardware and software capabilities, jet substructure techniques of the future will grow in complexity and utility, further empowering the exploration of the subnuclear properties of nature.

ACKNOWLEDGMENTS

---

[12]Boost 2016 Participants, "Boost Zurich 2016," https://indico.cern.ch/event/439039/.

[13]Boost 2017 Participants, "Boost Buffalo 2017," https://indico.cern.ch/event/579660/.

REFERENCES

Aaboud, M., *et al.* (ATLAS Collaboration), 2016a, "Searches for heavy diboson resonances in pp collisions at $\sqrt{s} = 13$ TeV with the ATLAS detector," J. High Energy Phys. 09, 173.

Aaboud, M., *et al.* (ATLAS Collaboration), 2016b, "Charged-particle distributions at low transverse momentum in $\sqrt{s} = 13$ TeV pp interactions measured with the ATLAS detector at the LHC," Eur. Phys. J. C 76, 502.

Aaboud, M., *et al.* (ATLAS Collaboration), 2016c, "Search for top squarks in final states with one isolated lepton, jets, and missing transverse momentum in $\sqrt{s} = 13$ TeV pp collisions with the ATLAS detector," Phys. Rev. D 94, 052009.

Aaboud, M., *et al.* (ATLAS Collaboration), 2016d, "Measurement of the top quark mass in the $t\bar{t} \rightarrow$ dilepton channel from $\sqrt{s} = 8$ TeV ATLAS data," Phys. Lett. B 761, 350–371.

Aaboud, M., *et al.* (ATLAS Collaboration), 2016e, "Search for pair production of Higgs bosons in the $b\bar{b}b\bar{b}$ final state using proton–proton collisions at $\sqrt{s} = 13$ TeV with the ATLAS detector," Phys. Rev. D 94, 052002.

Aaboud, M., *et al.* (ATLAS Collaboration), 2016f, "Search for dark matter produced in association with a hadronically decaying vector boson in pp collisions at $\sqrt{s} = 13$ TeV with the ATLAS detector," Phys. Lett. B 763, 251.

Aaboud, M., *et al.* (ATLAS Collaboration), 2016g, "Search for the Standard Model Higgs boson produced by vector-boson fusion and decaying to bottom quarks in $\sqrt{s} = 8$ TeV pp collisions with the ATLAS detector," J. High Energy Phys. 11, 112.

Aaboud, M., *et al.* (ATLAS Collaboration), 2017a, "Jet reconstruction and performance using particle flow with the ATLAS Detector," Eur. Phys. J. C 77, 466.

Aaboud, M., *et al.* (ATLAS Collaboration), 2017b, "A measurement of the calorimeter response to single hadrons and determination of the jet energy scale uncertainty using LHC Run-1 pp-collision data with the ATLAS detector," Eur. Phys. J. C 77, 26.

Aaboud, M., *et al.* (ATLAS Collaboration), 2017c, "Jet energy scale measurements and their systematic uncertainties in proton-proton collisions at $\sqrt{s} = 13$ TeV with the ATLAS detector," Phys. Rev. D 96, 072002.

Aaboud, M., *et al.* (ATLAS Collaboration), 2017d, "Performance of the ATLAS Transition Radiation Tracker in Run 1 of the LHC: tracker properties," J. Instrum. 12, P05002.

Aaboud, M., *et al.* (ATLAS Collaboration), 2017e, "Performance of the ATLAS Track Reconstruction Algorithms in Dense Environments in LHC Run 2," Eur. Phys. J. C 77, 673.

Aaboud, M., *et al.* (ATLAS Collaboration), 2017f, "Identification and rejection of pile-up jets at high pseudorapidity with the ATLAS detector," Eur. Phys. J. C 77, 580; 77, 712(E) (2017).

Aaboud, M., *et al.* (ATLAS Collaboration), 2017g, "Search for heavy resonances decaying to a W or Z boson and a Higgs boson in the $q\bar{q}^{(\prime)}b\bar{b}$ final state in pp collisions at $\sqrt{s} = 13$ TeV with the ATLAS detector," Phys. Lett. B 774, 494–515.

Aaboud, M., *et al.* (ATLAS Collaboration), 2017h, "Search for new phenomena with large jet multiplicities and missing transverse momentum using large-radius jets and flavour-tagging at ATLAS in 13 TeV pp collisions," J. High Energy Phys. 12, 034.

Aaboud, M., *et al.* (ATLAS Collaboration), 2017i, "Measurements of top-quark pair differential cross-sections in the $e\mu$ channel in pp collisions at $\sqrt{s} = 13$ TeV using the ATLAS detector," Eur. Phys. J. C 77, 292.

Aaboud, M., *et al.* (ATLAS Collaboration), 2017j, "Search for heavy resonances decaying to a Z boson and a photon in pp collisions at $\sqrt{s} = 13$ TeV with the ATLAS detector," Phys. Lett. B 764, 11–30.

Aaboud, M., *et al.* (ATLAS Collaboration), 2017k, "Measurements of top-quark pair differential cross-sections in the lepton+jets channel in pp collisions at $\sqrt{s} = 13$ TeV using the ATLAS detector," J. High Energy Phys. 11, 191.

Aaboud, M., *et al.* (ATLAS Collaboration), 2017l, "Evidence for the $H \rightarrow b\bar{b}$ decay with the ATLAS detector," J. High Energy Phys. 12, 024.

Aaboud, M., *et al.* (ATLAS Collaboration), 2017m, "Search for pair production of heavy vector-like quarks decaying to high-p_T W bosons and b quarks in the lepton-plus-jets final state in pp collisions at $\sqrt{s} = 13$ TeV with the ATLAS detector," J. High Energy Phys. 10, 141.

Aaboud, M., *et al.* (ATLAS Collaboration), 2017n, "Search for pair production of vector-like top quarks in events with one lepton, jets, and missing transverse momentum in $\sqrt{s} = 13$ TeV pp collisions with the ATLAS detector," J. High Energy Phys. 08, 052.

Aaboud, M., *et al.* (ATLAS Collaboration), 2017o, "Search for a scalar partner of the top quark in the jets plus missing transverse momentum final state at $\sqrt{s} = 13$ TeV with the ATLAS detector," J. High Energy Phys. 12, 085.

Aaboud, M., *et al.* (ATLAS Collaboration), 2018a, "Observation of Higgs boson production in association with a top quark pair at the LHC with the ATLAS detector," Phys. Lett. B **784**, 173.

Aaboud, M., *et al.* (ATLAS Collaboration), 2018b, "Observation of $H \to b\bar{b}$ decays and VH production with the ATLAS detector," Phys. Lett. B **786**, 59–86.

Aaboud, M., *et al.* (ATLAS Collaboration), 2018c, "Measurement of the soft-drop jet mass in pp collisions at $\sqrt{s} = 13$ TeV with the ATLAS detector," Phys. Rev. Lett. **121**, 092001.

Aaboud, M., *et al.* (ATLAS Collaboration), 2018d, "Search for $W' \to tb$ decays in the hadronic final state using pp collisions at $\sqrt{s} = 13$ TeV with the ATLAS detector," Phys. Lett. B **781**, 327.

Aaboud, M., *et al.* (ATLAS Collaboration), 2018e, "Search for WW/WZ resonance production in $\ell\nu qq$ final states in pp collisions at $\sqrt{s} = 13$ TeV with the ATLAS detector," J. High Energy Phys. 03, 042.

Aaboud, M., *et al.* (ATLAS Collaboration), 2018f, "Searches for heavy ZZ and ZW resonances in the $\ell\ell qq$ and $\nu\nu qq$ final states in pp collisions at $\sqrt{s} = 13$ TeV with the ATLAS detector," J. High Energy Phys. 03, 009.

Aaboud, M., *et al.* (ATLAS Collaboration), 2018g, "Search for diboson resonances with boson-tagged jets in pp collisions at $\sqrt{s} = 13$ TeV with the ATLAS detector," Phys. Lett. B **777**, 91–113.

Aaboud, M., *et al.* (ATLAS Collaboration), 2018h, "A search for resonances decaying into a Higgs boson and a new particle X in the $XH \to qqbb$ final state with the ATLAS detector," Phys. Lett. B **779**, 24.

Aaboud, M., *et al.* (ATLAS Collaboration), 2018i, "Search for squarks and gluinos in final states with jets and missing transverse momentum using 36 fb^{-1} of $\sqrt{s} = 13$ TeV pp collision data with the ATLAS detector," Phys. Rev. D **97**, 112001.

Aaboud, M., *et al.* (ATLAS Collaboration), 2018j, "Search for top-squark pair production in final states with one lepton, jets, and missing transverse momentum using 36 fb^{-1} of $\sqrt{s} = 13$ TeV pp collision data with the ATLAS detector," J. High Energy Phys. 06, 108.

Aaboud, M., *et al.* (ATLAS Collaboration), 2018k, "Search for supersymmetry in final states with missing transverse momentum and multiple b-jets in proton-proton collisions at $\sqrt{s} = 13$ TeV with the ATLAS detector," J. High Energy Phys. 06, 107.

Aaboud, M., *et al.* (ATLAS Collaboration), 2018l, "Search for heavy resonances decaying into a W or Z boson and a Higgs boson in final states with leptons and b-jets in 36 fb^{-1} of $\sqrt{s} = 13$ TeV pp collisions with the ATLAS detector," J. High Energy Phys. 03, 174; 2018, 11, 051(E).

Aaboud, M., *et al.* (ATLAS Collaboration), 2018m, "Measurements of $t\bar{t}$ differential cross-sections of highly boosted top quarks decaying to all-hadronic final states in pp collisions at $\sqrt{s} = 13$ TeV using the ATLAS detector," Phys. Rev. D **98**, 012003.

Aaboud, M., *et al.* (ATLAS Collaboration), 2018n, "Search for heavy particles decaying into top-quark pairs using lepton-plus-jets events in proton proton collisions at $\sqrt{s} = 13$ TeV with the ATLAS detector," Eur. Phys. J. C **78**, 565.

Aaboud, M., *et al.* (ATLAS Collaboration), 2019a, "Properties of $g \to b\bar{b}$ at small opening angles in pp collisions with the ATLAS detector at $\sqrt{s} = 13$ TeV," Phys. Rev. D **99**, 052004.

Aaboud, M., *et al.* (ATLAS Collaboration), 2019b, "Search for light resonances decaying to boosted quark pairs and produced in association with a photon or a jet in proton-proton collisions at $\sqrt{s} = 13$ TeV with the ATLAS detector," Phys. Lett. B **788**, 316–335.

Aaboud, M., *et al.* (ATLAS Collaboration), 2019c, "Measurement of jet-substructure observables in top quark, W boson and light jet production in proton-proton collisions at $\sqrt{s} = 13$ TeV with the ATLAS detector," J. High Energy Phys. 08, 033.

Aad, G., *et al.* (ATLAS Collaboration), 2008, "The ATLAS Experiment at the CERN Large Hadron Collider," J. Instrum. **3**, S08003.

Aad, G., *et al.* (ATLAS Collaboration), 2010, "The ATLAS Inner Detector commissioning and calibration," Eur. Phys. J. C **70**, 787–821.

Aad, G., *et al.* (ATLAS Collaboration), 2011a, "Study of jet shapes in inclusive jet production in pp collisions at $\sqrt{s} = 7$ TeV using the ATLAS detector," Phys. Rev. D **83**, 052003.

Aad, G., *et al.* (ATLAS Collaboration), 2011b, "Properties of jets measured from tracks in proton-proton collisions at center-of-mass energy $\sqrt{s} = 7$ TeV with the ATLAS detector," Phys. Rev. D **84**, 054001.

Aad, G., *et al.* (ATLAS Collaboration), 2011c, "Measurement of the jet fragmentation function and transverse profile in proton-proton collisions at a center-of-mass energy of 7 TeV with the ATLAS detector," Eur. Phys. J. C **71**, 1795.

Aad, G., *et al.* (ATLAS Collaboration), 2012a, "Jet mass and substructure of inclusive jets in $\sqrt{s} = 7$ TeV pp collisions with the ATLAS experiment," J. High Energy Phys. 05, 128.

Aad, G., *et al.* (ATLAS Collaboration), 2012b, "Measurement of event shapes at large momentum transfer with the ATLAS detector in pp collisions at $\sqrt{s} = 7$ TeV," Eur. Phys. J. C **72**, 2211.

Aad, G., *et al.* (ATLAS Collaboration), 2013a, "Measurement of jet shapes in top-quark pair events at $\sqrt{s} = 7$ TeV using the ATLAS detector," Eur. Phys. J. C **73**, 2676.

Aad, G., *et al.* (ATLAS Collaboration), 2013b, "Search for $t\bar{t}$ resonances in the lepton plus jets final state with ATLAS using 4.7 fb^{-1} of pp collisions at $\sqrt{s} = 7$ TeV," Phys. Rev. D **88**, 012004.

Aad, G., *et al.* (ATLAS Collaboration), 2013c, "Search for resonances decaying into top-quark pairs using fully hadronic decays in pp collisions with ATLAS at $\sqrt{s} = 7$ TeV," J. High Energy Phys. 01, 116.

Aad, G., *et al.* (ATLAS Collaboration), 2013d, "Measurement of k_T splitting scales in $W \to \ell\nu$ events at $\sqrt{s} = 7$ TeV with the ATLAS detector," Eur. Phys. J. C **73**, 2432.

Aad, G., *et al.* (ATLAS Collaboration), 2013e, "Performance of jet substructure techniques for large-R jets in proton-proton collisions at $\sqrt{s} = 7$ TeV using the ATLAS detector," J. High Energy Phys. 09, 076.

Aad, G., *et al.* (ATLAS Collaboration), 2014a, "Light-quark and gluon jet discrimination in pp collisions at $\sqrt{s} = 7$ TeV with the ATLAS Detector," Eur. Phys. J. C **74**, 3023.

Aad, G., *et al.* (ATLAS Collaboration), 2014b, "Measurement of the cross section of high transverse momentum $Z \to b\bar{b}$ production in proton–proton collisions at $\sqrt{s} = 8$ TeV with the ATLAS Detector," Phys. Lett. B **738**, 25–43.

Aad, G., *et al.* (ATLAS Collaboration), 2014c, "Search for dark matter in events with a hadronically decaying W or Z boson and missing transverse momentum in pp collisions at $\sqrt{s} = 8$ TeV with the ATLAS detector," Phys. Rev. Lett. **112**, 041802.

Aad, G., *et al.* (ATLAS Collaboration), 2014d, "Measurement of the cross-section of high transverse momentum vector bosons reconstructed as single jets and studies of jet substructure in pp collisions at $\sqrt{s} = 7$ TeV with the ATLAS detector," New J. Phys. **16**, 113013.

Aad, G., *et al.* (ATLAS Collaboration), 2015a, "Search for Higgs boson pair production in the $b\bar{b}b\bar{b}$ final state from pp collisions at $\sqrt{s} = 8$ TeV with the ATLAS detector," Eur. Phys. J. C **75**, 412.

Aad, G., *et al.* (ATLAS Collaboration), 2015b, "Jet energy measurement and its systematic uncertainty in proton-proton collisions at $\sqrt{s} = 7$ TeV with the ATLAS detector," Eur. Phys. J. C **75**, 17.

Aad, G., *et al.* (ATLAS Collaboration), 2015c, "Measurement of the top quark mass in the $t\bar{t} \rightarrow$ lepton + jets and $t\bar{t} \rightarrow$ dilepton channels using $\sqrt{s} = 7$ TeV ATLAS data," Eur. Phys. J. C **75**, 330.

Aad, G., *et al.* (ATLAS Collaboration), 2015d, "Search for $W' \rightarrow tb \rightarrow qqbb$ decays in pp collisions at $\sqrt{s} = 8$ TeV with the ATLAS detector," Eur. Phys. J. C **75**, 165.

Aad, G., *et al.* (ATLAS Collaboration), 2015e, "Differential top-antitop cross-section measurements as a function of observables constructed from final-state particles using pp collisions at $\sqrt{s} = 7$ TeV in the ATLAS detector," J. High Energy Phys. 06, 100.

Aad, G., *et al.* (ATLAS Collaboration), 2015f, "Search for high-mass diboson resonances with boson-tagged jets in proton-proton collisions at $\sqrt{s} = 8$ TeV with the ATLAS detector," J. High Energy Phys. 12, 055.

Aad, G., *et al.* (ATLAS Collaboration), 2015g, "A search for $t\bar{t}$ resonances using lepton-plus-jets events in proton-proton collisions at $\sqrt{s} = 8$ TeV with the ATLAS detector," J. High Energy Phys. 08, 148.

Aad, G., *et al.* (ATLAS Collaboration), 2015h, "Measurement of colour flow with the jet pull angle in $t\bar{t}$ events using the ATLAS detector at $\sqrt{s} = 8$ TeV," Phys. Lett. B **750**, 475–493.

Aad, G., *et al.* (ATLAS Collaboration), 2016a, "Combination of searches for WW, WZ, and ZZ resonances in pp collisions at $\sqrt{s} = 8$ TeV with the ATLAS detector," Phys. Lett. B **755**, 285–305.

Aad, G., *et al.* (ATLAS Collaboration), 2016b, "Search for single production of vector-like quarks decaying into Wb in pp collisions at $\sqrt{s} = 8$ TeV with the ATLAS detector," Eur. Phys. J. C **76**, 442.

Aad, G., *et al.* (ATLAS Collaboration), 2016c, "Measurements of top-quark pair differential cross-sections in the lepton+jets channel in pp collisions at $\sqrt{s} = 8$ TeV using the ATLAS detector," Eur. Phys. J. C **76**, 538.

Aad, G., *et al.* (ATLAS Collaboration), 2016d, "Performance of pile-up mitigation techniques for jets in pp collisions at $\sqrt{s} = 8$ TeV using the ATLAS detector," Eur. Phys. J. C **76**, 581.

Aad, G., *et al.* (ATLAS Collaboration), 2016e, "Identification of boosted, hadronically decaying W bosons and comparisons with ATLAS data taken at $\sqrt{s} = 8$ TeV," Eur. Phys. J. C **76**, 154.

Aad, G., *et al.* (ATLAS Collaboration), 2016f, "A new method to distinguish hadronically decaying boosted Z bosons from W bosons using the ATLAS detector," Eur. Phys. J. C **76**, 238.

Aad, G., *et al.* (ATLAS Collaboration), 2016g, "Search for pair production of gluinos decaying via stop and sbottom in events with b-jets and large missing transverse momentum in pp collisions at $\sqrt{s} = 13$ TeV with the ATLAS detector," Phys. Rev. D **94**, 032003.

Aad, G., *et al.* (ATLAS Collaboration), 2016h, "Measurement of jet charge in dijet events from $\sqrt{s} = 8$ TeV pp collisions with the ATLAS detector," Phys. Rev. D **93**, 052003.

Aad, G., *et al.* (ATLAS Collaboration), 2016i, "Measurement of the differential cross-section of highly boosted top quarks as a function of their transverse momentum in $\sqrt{s} = 8$ TeV proton-proton collisions using the ATLAS detector," Phys. Rev. D **93**, 032009.

Aad, G., *et al.* (ATLAS Collaboration), 2016j, "Search for the production of single vector-like and excited quarks in the Wt final state in pp collisions at $\sqrt{s} = 8$ TeV with the ATLAS detector," J. High Energy Phys. 02, 110.

Aad, G., *et al.* (ATLAS Collaboration), 2016k, "Identification of high transverse momentum top quarks in pp collisions at $\sqrt{s} = 8$ TeV with the ATLAS detector," J. High Energy Phys. 06, 093.

Aad, G., *et al.* (ATLAS Collaboration), 2016l, "Measurement of the charged-particle multiplicity inside jets from $\sqrt{s} = 8$ TeV pp collisions with the ATLAS detector," Eur. Phys. J. C **76**, 322.

Aad, G., *et al.* (ATLAS Collaboration), 2016m, "Search for dark matter produced in association with a Higgs boson decaying to two bottom quarks in pp collisions at $\sqrt{s} = 8$ TeV with the ATLAS detector," Phys. Rev. D **93**, 072007.

Aad, G., *et al.* (ATLAS Collaboration), 2017, "Topological cell clustering in the ATLAS calorimeters and its performance in LHC Run 1," Eur. Phys. J. C **77**, 490.

Aaron, F. D., *et al.* (H1, and ZEUS Collaborations), 2010, "Combined Measurement and QCD Analysis of the Inclusive e+- p Scattering Cross Sections at HERA," J. High Energy Phys. 01, 109.

Abachi, S., *et al.* (D0 Collaboration), 1995a, "Observation of the top quark," Phys. Rev. Lett. **74**, 2632.

Abachi, S., *et al.* (D0 Collaboration), 1995b, "Transverse energy distributions within jets in $p\bar{p}$ collisions at $\sqrt{s} = 1.8$ TeV," Phys. Lett. B **357**, 500.

Abbott, B., *et al.* (ATLAS IBL Collaboration), 2018, "Production and Integration of the ATLAS Insertable B-Layer," J. Instrum. **13**, T05008.

Abe, F., *et al.* (CDF Collaboration), 1993, "A Measurement of jet shapes in $p\bar{p}$ collisions at $\sqrt{s} = 1.8$ TeV," Phys. Rev. Lett. **70**, 713.

Abe, F., *et al.* (CDF Collaboration), 1995, "Observation of top quark production in $\bar{p}p$ collisions with the Collider Detector at Fermilab," Phys. Rev. Lett. **74**, 2626.

Abreu, P., *et al.* (DELPHI Collaboration), 1996, "Energy dependence of the differences between the quark and gluon jet fragmentation," Z. Phys. C **70**, 179.

Acciarri, M., *et al.* (L3 Collaboration), 1997, "K_s^0 and Λ production in quark and gluon jets at LEP," Phys. Lett. B **407**, 389; 427, 409(E) (1998).

Adams, D., *et al.*, 2015, "Towards an Understanding of the Correlations in Jet Substructure," Eur. Phys. J. C **75**, 409.

Adloff, C., *et al.* (H1 Collaboration), 1999, "Measurement of internal jet structure in dijet production in deep inelastic scattering at HERA," Nucl. Phys. B **545**, 3.

Agashe, K., A. Belyaev, T. Krupovnickas, G. Perez, and J. Virzi, 2008, "LHC Signals from Warped Extra Dimensions," Phys. Rev. D **77**, 015003.

Agashe, K., R. Contino, and A. Pomarol, 2005, "The minimal composite Higgs model," Nucl. Phys. B **719**, 165.

Agashe, K., A. Delgado, M. J. May, and R. Sundrum, 2003, "RS1, custodial isospin and precision tests," J. High Energy Phys. 08, 050.

Aguilar-Saavedra, J. A., R. Benbrik, S. Heinemeyer, and M. Pérez-Victoria, 2013, "Handbook of vectorlike quarks: Mixing and single production," Phys. Rev. D **88**, 094010.

Aguilar-Saavedra, J. A., J. H. Collins, and R. K. Mishra, 2017, "A generic anti-QCD jet tagger," J. High Energy Phys. 11, 163.

Alexander, G., *et al.* (OPAL Collaboration), 1991, "A direct observation of quark-gluon jet differences at LEP," Phys. Lett. B **265**, 462.

Almeida, L. G., S. J. Lee, G. Perez, G. F. Sterman, I. Sung, and J. Virzi, 2009, "Substructure of high-p_T jets at the LHC," Phys. Rev. D **79**, 074017.

Altarelli, G., and G. Parisi, 1977, "Asymptotic freedom in parton language," Nucl. Phys. B **126**, 298.

Altheimer, A., *et al.*, 2012, "Jet Substructure at the Tevatron and LHC: New results, new tools, new benchmarks," J. Phys. G **39**, 063001.

Altheimer, A., *et al.*, 2014, "Boosted objects and jet substructure at the LHC. Report of BOOST2012, held at IFIC Valencia, 23rd–27th of July 2012," Eur. Phys. J. C **74**, 2792.

An, H., R. Huo, and L.-T. Wang, 2013, "Searching for low mass dark portal at the LHC," Phys. Dark Univ. **2**, 50–57.

Antoniadis, I., K. Benakli, and M. Quiros, 2001, "Finite Higgs mass without supersymmetry," New J. Phys. **3**, 20.

Arkani-Hamed, N., A. G. Cohen, and H. Georgi, 2001, "Electroweak symmetry breaking from dimensional deconstruction," Phys. Lett. B **513**, 232.

ATLAS Collaboration, 2012, "Identification and tagging of double b-hadron jets with the ATLAS detector," ATLAS CONF Note ATLAS-CONF-2012-100.

ATLAS Collaboration, 2014a, "A neural network clustering algorithm for the ATLAS silicon pixel detector," J. Instrum. **9**, P09009.

ATLAS Collaboration, 2014b, "Flavor tagging with track jets in boosted topologies with the ATLAS detector," ATLAS PUB Note ATL-PHYS-PUB-2014-013.

ATLAS Collaboration, 2014c, "b-tagging in dense environments," ATLAS PUB Note ATL-PHYS-PUB-2014-014.

ATLAS Collaboration, 2015a, "Measurement of performance of the pixel neural network clustering algorithm of the ATLAS experiment at $\sqrt{s} = 13$ TeV," ATLAS PUB Note ATL-PHYS-PUB-2015-044.

ATLAS Collaboration, 2015b, "Jet global sequential corrections with the ATLAS detector in proton-proton collisions at $\sqrt{s} = 8$ TeV," ATLAS CONF Note ATLAS-CONF-2015-002.

ATLAS Collaboration, 2015c, "Identification of boosted, hadronically-decaying W and Z bosons in $\sqrt{s} = 13$ TeV Monte Carlo Simulations for ATLAS," ATLAS PUB Note ATL-PHYS-PUB-2015-033.

ATLAS Collaboration, 2015d, "Boosted hadronic top identification at ATLAS for early 13 TeV data," ATLAS PUB Note ATL-PHYS-PUB-2015-053.

ATLAS Collaboration, 2016a, "Search for heavy particles decaying to pairs of highly-boosted top quarks using lepton-plus-jets events in proton–proton collisions at $\sqrt{s} = 13$ TeV with the ATLAS detector," ATLAS CONF Note ATLAS-CONF-2016-014.

ATLAS Collaboration, 2016b, "Measurement of track reconstruction inefficiencies in the core of jets via pixel dE/dx with the ATLAS experiment using $\sqrt{s} = 13$ TeV pp collision data," ATLAS PUB Note ATL-PHYS-PUB-2016-007.

ATLAS Collaboration, "Event displays from run 2 physics analyses," 2016c, https://twiki.cern.ch/twiki/bin/view/AtlasPublic/EventDisplayRun2Physics.

ATLAS Collaboration, 2016d, "Jet mass reconstruction with the ATLAS detector in early Run 2 data," ATLAS CONF Note ATLAS-CONF-2016-035.

ATLAS Collaboration, 2016e, "Measurement of large radius jet mass reconstruction performance at $\sqrt{s} = 8$ TeV using the ATLAS detector," ATLAS CONF Note ATLAS-CONF-2016-008.

ATLAS Collaboration, 2016f, "Discrimination of light quark and gluon jets in pp collisions at $\sqrt{s} = 8$ TeV with the ATLAS detector," ATLAS CONF Note ATLAS-CONF-2016-034.

ATLAS Collaboration, 2016g, "Boosted object tagging with variable-R jets in the ATLAS detector," ATLAS PUB Note ATL-PHYS-PUB-2016-013.

ATLAS Collaboration, 2016h, "Optimisation of the ATLAS b-tagging performance for the 2016 LHC Run," ATLAS PUB Note ATL-PHYS-PUB-2016-012.

ATLAS Collaboration, 2016i, "Studies of b-tagging performance and jet substructure in a high p_T $g \rightarrow b\bar{b}$ rich sample of large-R jets from pp collisions at $\sqrt{s} = 8$ TeV with the ATLAS detector," ATLAS CONF Note ATLAS-CONF-2016-002.

ATLAS Collaboration, 2016j, "Performance of b-jet identification in the ATLAS experiment," J. Instrum. **11**, P04008.

ATLAS Collaboration, 2016k, "Boosted Higgs ($\rightarrow b\bar{b}$) boson identification with the ATLAS detector at $\sqrt{s} = 13$ TeV," ATLAS CONF Note ATLAS-CONF-2016-039.

ATLAS Collaboration, 2017a, "Modelling of Track Reconstruction Inside Jets with the 2016 ATLAS $\sqrt{s} = 13$ TeV pp Dataset," ATLAS PUB Note ATL-PHYS-PUB-2017-016.

ATLAS Collaboration, 2017b, "Impact of Alternative Inputs and Grooming Methods on Large-R Jet Reconstruction in ATLAS," ATLAS PUB Note ATL-PHYS-PUB-2017-020.

ATLAS Collaboration, 2017c, "Constituent-level pileup mitigation performance using 2015 data," ATLAS CONF Note ATLAS-CONF-2017-065.

ATLAS Collaboration, 2017d, "Jet reclustering and close-by effects in ATLAS Run 2," ATLAS CONF Note ATLAS-CONF-2017-062.

ATLAS Collaboration, 2017e, "In-situ measurements of large-radius jet reconstruction performance," ATLAS CONF Note ATLAS-CONF-2017-063.

ATLAS Collaboration, 2017f, "Top and boson tagger background performance - Moriond 2017," Technical Report ATL-JETM-2017-005.

ATLAS Collaboration, 2017g, "Quark versus gluon jet tagging using charged particle multiplicity with the ATLAS detector," ATLAS PUB Note ATL-PHYS-PUB-2017-009.

ATLAS Collaboration, 2017h, "Improving jet substructure performance in atlas using track-caloclusters," ATLAS PUB Note ATL-PHYS-PUB-2017-015.

ATLAS Collaboration, 2017i, "Quark versus gluon jet tagging using jet images with the ATLAS detector," ATLAS PUB Note ATL-PHYS-PUB-2017-017.

ATLAS Collaboration, 2017j, "Identification of hadronically-decaying W bosons and top quarks using high-level features as input to boosted decision trees and deep neural networks in ATLAS at $\sqrt{s} = 13$ TeV," ATLAS PUB Note ATL-PHYS-PUB-2017-004.

ATLAS Collaboration, 2017k, "Search for WW/WZ resonance production in $\ell\nu qq$ final states in pp collisions at $\sqrt{s} = 13$ TeV with the ATLAS detector," ATLAS CONF Note ATLAS-CONF-2017-051.

ATLAS Collaboration, 2017l, "Performance of top quark and W boson tagging in Run 2 with ATLAS," ATLAS CONF Note ATLAS-CONF-2017-064.

ATLAS Collaboration, 2017m, "Variable radius, exclusive-k_T, and center-of-mass subjet reconstruction for Higgs($\rightarrow b\bar{b}$) tagging in ATLAS," ATLAS PUB Note ATL-PHYS-PUB-2017-010.

Bahr, M., *et al.*, 2008, "Herwig++ Physics and Manual," Eur. Phys. J. C **58**, 639–707.

Banfi, A., G. P. Salam, and G. Zanderighi, 2006, "Infrared safe definition of jet flavor," Eur. Phys. J. C **47**, 113.

Banks, T., 1984, "Constraints on SU(2) x U(1) breaking by vacuum misalignment," Nucl. Phys. B **243**, 125–130.

Barber, D. P., *et al.*, 1979, "Discovery of Three Jet Events and a Test of Quantum Chromodynamics at PETRA Energies," Phys. Rev. Lett. **43**, 830.

Bartel, W., *et al.* (JADE Collaboration), 1980, "Observation of planar three jet events in e^+e^- annihilation and evidence for gluon bremsstrahlung," Phys. Lett. B **91**, 142.

Bartel, W., *et al.* (JADE Collaboration), 1986, "Experimental studies on multijet production in e^+e^- annihilation at PETRA energies," Z. Phys. C **33**, 23.

Baur, U., I. Hinchliffe, and D. Zeppenfeld, 1987, "Excited quark production at hadron colliders," Int. J. Mod. Phys. A **02**, 1285.

Baur, U., M. Spira, and P. M. Zerwas, 1990, "Excited quark and lepton production at hadron colliders," Phys. Rev. D **42**, 815.

Bellazzini, B., C. Csáki, and J. Serra, 2014, "Composite Higgses," Eur. Phys. J. C **74**, 2766.

Bellm, J., *et al.*, 2016, "Herwig 7.0/Herwig++ 3.0 release note," Eur. Phys. J. C **76**, 196.

Berger, Ch., *et al.* (PLUTO Collaboration), 1979, "Evidence for gluon bremsstrahlung in e^+e^- annihilations at high energies," Phys. Lett. B **86**, 418.

Berta, P., M. Spousta, D. W. Miller, and R. Leitner, 2014, "Particle-level pileup subtraction for jets and jet shapes," J. High Energy Phys. 06, 092.

Bertolini, D., T. Chan, and J. Thaler, 2014, "Jet Observables Without Jet Algorithms," J. High Energy Phys. 04, 013.

Bertolini, D., P. Harris, M. Low, and N. Tran, 2014, "Pileup per particle identification," J. High Energy Phys. 10, 059.

Bethke, S., *et al.* (JADE Collaboration), 1988, "Experimental investigation of the energy dependence of the strong coupling strength," Phys. Lett. B **213**, 235.

Bjorken, J. D., and S. J. Brodsky, 1970, "Statistical model for electron-positron annihilation into hadrons," Phys. Rev. D **1**, 1416.

Branco, G. C., P. M. Ferreira, L. Lavoura, M. N. Rebelo, M. Sher, and J. P. Silva, 2012, "Theory and phenomenology of two-Higgs-doublet models," Phys. Rep. **516**, 1–102.

Brandelik, R., *et al.* (TASSO Collaboration), 1979, "Evidence for planar events in e^+e^- annihilation at high energies," Phys. Lett. B **86**, 243.

Brandt, S., C. Peyrou, R. Sosnowski, and A. Wroblewski, 1964, "The principal axis of jets—an attempt to analyse high-energy collisions as two-body processes," Phys. Lett. **12**, 57.

Breitweg, J., *et al.* (ZEUS Collaboration), 1998, "Measurement of jet shapes in photoproduction at HERA," Eur. Phys. J. C **2**, 61.

Breitweg, J., *et al.* (ZEUS Collaboration), 1999, "Measurement of jet shapes in high-Q^2 deep inelastic scattering at HERA," Eur. Phys. J. C **8**, 367–380.

Bright-Thonney, S., and B. Nachman, 2019, "Investigating the Topology Dependence of Quark and Gluon Jets," J. High Energy Phys. 03, 098.

Buckley, A., and C. Pollard, 2016, "QCD-aware partonic jet clustering for truth-jet flavour labelling," Eur. Phys. J. C **76**, 71.

Buskulic, D., *et al.* (ALEPH Collaboration), 1995, "Study of the subjet structure of quark and gluon jets," Phys. Lett. B **346**, 389.

Butenschoen, M., B. Dehnadi, A. H. Hoang, V. Mateu, M. Preisser, and I. W. Stewart, 2016, "Top quark mass calibration for Monte Carlo event generators," Phys. Rev. Lett. **117**, 232001.

Butterworth, J. M., B. E. Cox, and J. R. Forshaw, 2002, "WW scattering at the CERN LHC," Phys. Rev. D **65**, 096014.

Butterworth, J. M., A. R. Davison, M. Rubin, and G. P. Salam, 2008, "Jet substructure as a new Higgs search channel at the LHC," Phys. Rev. Lett. **100**, 242001.

Cacciari, M., G. P. Salam, and G. Soyez, 2008a, "The anti-k_t jet clustering algorithm," J. High Energy Phys. 04, 063.

Cacciari, M., G. P. Salam, and G. Soyez, 2008b, "The catchment area of jets," J. High Energy Phys. 04, 005.

Cacciari, M., G. P. Salam, and G. Soyez, 2015, "SoftKiller, a particle-level pileup removal method," Eur. Phys. J. C **75**, 59.

Catani, S., Y. Dokshitzer, M. Olsson, G. Turnock, and B. Webber, 1991, "New clustering algorithm for multijet cross sections in e^+e^- annihilation," Phys. Lett. B **269**, 432.

Catani, S., Y. Dokshitzer, M. Seymour, and B. Webber, 1993, "Longitudinally-invariant $k_\perp$-clustering algorithms for hadron-hadron collisions," Nucl. Phys. B **406**, 187.

Catani, S., Y. Dokshitzer, and B. Webber, 1992, "The $k_\perp$-clustering algorithm for jets in deep inelastic scattering and hadron collisions," Phys. Lett. B **285**, 291.

CDF, D0 Collaborations, and Tevatron Electroweak Working Group, 2014, "Combination of CDF and D0 results on the mass of the top quark using up to 9.7 fb^{-1} at the Tevatron" [https://arxiv.org/abs/1608.01881].

Chatrchyan, S., *et al.* (CMS Collaboration), 2008, "The CMS experiment at the CERN LHC," J. Instrum. **3**, S08004.

Chatrchyan, S., *et al.* (CMS Collaboration), 2012a, "Search for anomalous $t\bar{t}$ production in the highly-boosted all-hadronic final state," J. High Energy Phys. 09, 029; 2014, 03, 132(E).

Chatrchyan, S., *et al.* (CMS Collaboration), 2012b, "Shape, transverse size, and charged hadron multiplicity of jets in pp collisions at 7 TeV," J. High Energy Phys. 06, 160.

Chatrchyan, S., *et al.* (CMS Collaboration), 2012c, "Search for a Higgs boson in the decay channel $H \to ZZ^{(*)} \to q\bar{q}\ell^-l^+$ in pp collisions at $\sqrt{s} = 7$ TeV," J. High Energy Phys. 04, 036.

Chatrchyan, S., *et al.* (CMS Collaboration), 2013a, "Search for heavy resonances in the W/Z-tagged dijet mass spectrum in pp collisions at 7 TeV," Phys. Lett. B **723**, 280.

Chatrchyan, S., *et al.* (CMS Collaboration), 2013b, "Studies of jet mass in dijet and W/Z + jet events," J. High Energy Phys. 05, 090.

Chatrchyan, S., *et al.* (CMS Collaboration), 2013c, "Measurement of the hadronic activity in events with a Z and two jets and extraction of the cross section for the electroweak production of a Z with two jets in pp collisions at $\sqrt{s} = 7$ TeV," J. High Energy Phys. 10, 062.

Chatrchyan, S., *et al.* (CMS Collaboration), 2013d, "Measurement of differential top-quark pair production cross sections in pp colisions at $\sqrt{s} = 7$ TeV," Eur. Phys. J. C **73**, 2339.

Chatrchyan, S., *et al.* (CMS Collaboration), 2014, "Inclusive search for a vector-like T quark with charge $\frac{2}{3}$ in pp collisions at $\sqrt{s} = 8$ TeV," Phys. Lett. B **729**, 149.

CMS Collaboration, 1997, "The CMS hadron calorimeter project: Technical Design Report," Technical Report CERN-LHCC-97-031, Geneva.

CMS Collaboration, 2009a, "Particle-Flow Event Reconstruction in CMS and Performance for Jets, Taus, and MET," CMS Physics Analysis Summary CMS-PAS-PFT-09-001.

CMS Collaboration, 2009b, "A Cambridge-Aachen (C-A) based jet algorithm for boosted top-jet tagging," CMS Physics Analysis Summary CMS-PAS-JME-09-001.

CMS Collaboration, 2010, "Commissioning of the Particle-Flow reconstruction in Minimum-Bias and Jet Events from pp Collisions at 7 TeV," CMS Physics Analysis Summary CMS-PAS-PFT-10-002.

CMS Collaboration, 2011a, "Jet substructure algorithms," CMS Physics Analysis Summary CMS-PAS-JME-10-013.

CMS Collaboration, 2011b, "Determination of Jet Energy Calibration and Transverse Momentum Resolution in CMS," J. Instrum. **6**, P11002.

CMS Collaboration, 2013a, "Pileup jet identification," CMS Physics Analysis Summary CMS-PAS-JME-13-005.

CMS Collaboration, 2013b, "Performance of quark/gluon discrimination in 8 TeV pp data," CMS Physics Analysis Summary CMS-PAS-JME-13-002.

CMS Collaboration, 2013c, "Identification of b-quark jets with the CMS experiment," J. Instrum. **8**, P04013.

CMS Collaboration, 2013d, "Performance of b tagging at $\sqrt{s} = 8$ TeV in multijet, $t\bar{t}$ and boosted topology events," CMS Physics Analysis Summary CMS-PAS-BTV-13-001.

CMS Collaboration, 2014a, "Description and performance of track and primary-vertex reconstruction with the CMS tracker," J. Instrum. **9**, P10009.

CMS Collaboration, 2014b, "V Tagging Observables and Correlations," CMS Physics Analysis Summary CMS-PAS-JME-14-002.

CMS Collaboration, 2014c, "High p_T jet tracking with JetCore tracking and pixel cluster splitting," CMS Detector Performance Summary.

CMS Collaboration, 2014d, "Jet energy scale uncertainty correlations between ATLAS and CMS," CMS Physics Analysis Summary CMS-PAS-JME-14-003.

CMS Collaboration, 2014e, "Pileup Removal Algorithms," CMS Physics Analysis Summary CMS-PAS-JME-14-001.

CMS Collaboration, 2014f, "Boosted top jet tagging at CMS," CMS Physics Analysis Summary CMS-PAS-JME-13-007.

CMS Collaboration, 2016a, "Top tagging with new approaches," CMS Physics Analysis Summary CMS-PAS-JME-15-002.

CMS Collaboration, 2016b, "Performance of quark/gluon discrimination in 13 TeV data," CMS Detector Performance Summary CMS-DP-2016-070.

CMS Collaboration, 2016c, "Search for $t\bar{t}$ resonances in boosted semileptonic final states in pp collisions at $\sqrt{s} = 13$ TeV," CMS Physics Analysis Summary CMS-PAS-B2G-15-002.

CMS Collaboration, 2016d, "Identification of b quark jets at the CMS experiment in the LHC Run 2," CMS Physics Analysis Summary CMS-PAS-BTV-15-001.

CMS Collaboration, 2016e, "Identification of double-b quark jets in boosted event topologies," CMS Physics Analysis Summary CMS-PAS-BTV-15-002.

CMS Collaboration, 2017a, "Jet algorithms performance in 13 TeV data," CMS Physics Analysis Summary CMS-PAS-JME-16-003.

CMS Collaboration, 2017b, "W and top tagging scale factors," CMS Detector Performance Summary CMS-DP-2017-026.

CMS Collaboration, 2017c, "New developments for jet substructure reconstruction in CMS," CMS Detector Performance Summary CMS-DP-2017-027.

CMS Collaboration, 2017d, "Search for supersymmetry using hadronic top quark tagging in 13 TeV pp collisions," CMS Physics Analysis Summary CMS-PAS-SUS-16-050.

CMS Collaboration, 2017e, "Measurement of the differential $t\bar{t}$ cross section with high-p_T top-quark jets in the all-hadronic channel at $\sqrt{s} = 8$ TeV," CMS Physics Analysis Summary CMS-PAS-TOP-16-018.

CMS Collaboration, 2017f, "Search for heavy resonances decaying to a pair of Higgs bosons in the four b quark final state in proton-proton collisions at $\sqrt{s} = 13$ TeV," CMS Physics Analysis Summary CMS-PAS-B2G-16-026.

Contardo, D., M. Klute, J. Mans, L. Silvestris, and J. Butler, 2015, "Technical Proposal for the Phase-II Upgrade of the CMS Detector," Technical Report CMS-TDR-15-02.

Cukierman, A., and B. Nachman, 2017, "Mathematical Properties of Numerical Inversion for Jet Calibrations," Nucl. Instrum. Methods Phys. Res., Sect. A **858**, 1.

Dasgupta, M., A. Fregoso, S. Marzani, and G. P. Salam, 2013, "Towards an understanding of jet substructure," J. High Energy Phys. 09, 029.

Davoudiasl, H., J. L. Hewett, and T. G. Rizzo, 2000, "Bulk gauge fields in the Randall-Sundrum model," Phys. Lett. B **473**, 43.

Dery, L. M., B. Nachman, F. Rubbo, and A. Schwartzman, 2017, "Weakly supervised classification in high energy physics," J. High Energy Phys. 05, 145.

Dokshitzer, Y. L., G. D. Leder, S. Moretti, and B. R. Webber, 1997, "Better jet clustering algorithms," J. High Energy Phys. 08, 001.

Dolen, J., P. Harris, S. Marzani, S. Rappoccio, and N. Tran, 2016, "Thinking outside the ROCs: Designing Decorrelated Taggers (DDT) for jet substructure," J. High Energy Phys. 05, 156.

Dugan, M. J., H. Georgi, and D. B. Kaplan, 1985, "Anatomy of a composite Higgs model," Nucl. Phys. B **254**, 299–326.

Ellis, R. K., W. J. Stirling, and B. R. Webber, 1996, *QCD and Collider Physics*, Cambridge Monographs on Particle Physics, Nuclear Physics and Cosmology Vol. 8, pp. 1–435 [https://www.cambridge.org/de/academic/subjects/physics/particle-physics-and-nuclear-physics/qcd-and-collider-physics?format=PB&isbn=9780521545891].

Ellis, S. D., A. Hornig, T. S. Roy, D. Krohn, and M. D. Schwartz, 2012, "Qjets: A non-deterministic approach to tree-based jet substructure," Phys. Rev. Lett. **108**, 182003.

Ellis, S. D., Z. Kunszt, and D. E. Soper, 1992, "Jets at hadron colliders at order α_s^3: A look inside," Phys. Rev. Lett. **69**, 3615.

Ellis, S. D., C. K. Vermilion, and J. R. Walsh, 2010, "Recombination algorithms and jet substructure: Pruning as a tool for heavy particle searches," Phys. Rev. D **81**, 094023.

Farhi, E., 1977, "Quantum chromodynamics test for jets," Phys. Rev. Lett. **39**, 1587.

Frye, C., A. J. Larkoski, M. D. Schwartz, and K. Yan, 2016, "Factorization for groomed jet substructure beyond the next-to-leading logarithm," J. High Energy Phys. 07, 064.

Frye, C., A. J. Larkoski, J. Thaler, and K. Zhou, 2017, "Casimir meets poisson: Improved quark/gluon discrimination with counting observables," J. High Energy Phys. 09, 083.

Gallicchio, J., and Y.-T. Chien, 2018, "Quit Using Pseudorapidity, Transverse Energy, and Massless Constituents.," arXiv:1802.05356.

Gallicchio, J., and M. D. Schwartz, 2010, "Seeing in color: Jet superstructure," Phys. Rev. Lett. **105**, 022001.

Gallicchio, J., and M. D. Schwartz, 2011, "Quark and gluon tagging at the LHC," Phys. Rev. Lett. **107**, 172001.

Georgi, H., 1986, "A tool kit for builders of composite models," Nucl. Phys. B **266**, 274.

Georgi, H., and D. B. Kaplan, 1984, "Composite Higgs and custodial SU(2)," Phys. Lett. B **145**, 216–220.

Georgi, H., D. B. Kaplan, and P. Galison, 1984, "Calculation of the composite Higgs mass," Phys. Lett. B **143**, 152–154.

Goodman, J., M. Ibe, A. Rajaraman, W. Shepherd, T. M. P. Tait, and H.-B. Yu, 2010, "Constraints on dark matter from colliders," Phys. Rev. D **82**, 116010.

Gras, P., *et al.*, 2017, "Systematics of quark/gluon tagging," J. High Energy Phys. 07, 091.

Hanson, G., *et al.*, 1975, "Evidence for jet structure in hadron production by e^+e^- annihilation," Phys. Rev. Lett. **35**, 1609.

Hewett, J. L., and T. G. Rizzo, 1989, "Low-energy phenomenology of superstring inspired E(6) models," Phys. Rep. **183**, 193.

Hill, C. T., 1995, "Topcolor assisted technicolor," Phys. Lett. B **345**, 483–489.

Hoang, A. H., S. Mantry, A. Pathak, and I. W. Stewart, 2019, "Extracting a short distance top mass with light grooming," Phys. Rev. D **100**, 074021.

Hoang, A. H., S. Plätzer, and D. Samitz, 2018, "On the cutoff dependence of the quark mass parameter in angular ordered parton showers," J. High Energy Phys. 10, 200.

Hosotani, Y., S. Noda, and K. Takenaga, 2005, "Dynamical gauge-Higgs unification in the electroweak theory," Phys. Lett. B **607**, 276.

Kaplan, D. B., and H. Georgi, 1984, "SU(2) x U(1) breaking by vacuum misalignment," Phys. Lett. B **136**, 183.

Kaplan, D. B., H. Georgi, and S. Dimopoulos, 1984, "Composite Higgs scalars," Phys. Lett. B **136**, 187–190.

Kaplan, D. E., K. Rehermann, M. D. Schwartz, and B. Tweedie, 2008, "Top Tagging: A method for identifying boosted hadronically decaying top quarks," Phys. Rev. Lett. **101**, 142001.

Kasieczka, G., T. Plehn, T. Schell, T. Strebler, and G. P. Salam, 2015, "Resonance searches with an updated top tagger," J. High Energy Phys. 06, 203.

Khachatryan, V., et al. (CMS Collaboration), 2014a, "Identification techniques for highly boosted W bosons that decay into hadrons," J. High Energy Phys. 12, 017.

Khachatryan, V., et al. (CMS Collaboration), 2014b, "Search for massive resonances decaying into pairs of boosted bosons in semi-leptonic final states at $\sqrt{s} = 8$ TeV," J. High Energy Phys. 08, 174.

Khachatryan, V., et al. (CMS Collaboration), 2014c, "Search for massive resonances in dijet systems containing jets tagged as W or Z boson decays in pp collisions at $\sqrt{s} = 8$ TeV," J. High Energy Phys. 08, 173.

Khachatryan, V., et al. (CMS Collaboration), 2015a, "Searches for third-generation squark production in fully hadronic final states in proton-proton collisions at $\sqrt{s} = 8$ TeV," J. High Energy Phys. 06, 116.

Khachatryan, V., et al. (CMS Collaboration), 2015b, "Search for vector-like T quarks decaying to top quarks and Higgs bosons in the all-hadronic channel using jet substructure," J. High Energy Phys. 06, 080.

Khachatryan, V., et al. (CMS Collaboration), 2015c, "Search for the standard model Higgs boson produced through vector boson fusion and decaying to $b\bar{b}$," Phys. Rev. D **92**, 032008.

Khachatryan, V., et al. (CMS Collaboration), 2015d, "Measurement of the differential cross section for top quark pair production in pp collisions at $\sqrt{s} = 8$ TeV," Eur. Phys. J. C **75**, 542.

Khachatryan, V., et al. (CMS Collaboration), 2015e, "Search for narrow high-mass resonances in proton proton collisions at $\sqrt{s} = 8$ TeV decaying to a Z and a Higgs boson," Phys. Lett. B **748**, 255–277.

Khachatryan, V., et al. (CMS Collaboration), 2016a, "Search for heavy resonances decaying to two Higgs bosons in final states containing four b quarks," Eur. Phys. J. C **76**, 371.

Khachatryan, V., et al. (CMS Collaboration), 2016b, "Search for dark matter in proton-proton collisions at 8 TeV with missing transverse momentum and vector boson tagged jets," J. High Energy Phys. 12, 083; 2017, 08, 035(E).

Khachatryan, V., et al. (CMS Collaboration), 2016c, "Search for $W' \to tb$ in proton-proton collisions at $\sqrt{s} = 8$ TeV," J. High Energy Phys. 02, 122.

Khachatryan, V., et al. (CMS Collaboration), 2016d, "Search for the production of an excited bottom quark decaying to tW in proton-proton collisions at $\sqrt{s} = 8$ TeV," J. High Energy Phys. 01, 166.

Khachatryan, V., et al. (CMS Collaboration), 2016e, "Search for a massive resonance decaying into a Higgs boson and a W or Z boson in hadronic final states in proton-proton collisions at $\sqrt{s} = 8$ TeV," J. High Energy Phys. 02, 145.

Khachatryan, V., et al. (CMS Collaboration), 2016f, "Search for massive WH resonances decaying into the $\ell\nu b\bar{b}$ final state at $\sqrt{s} = 8$ TeV," Eur. Phys. J. C **76**, 237.

Khachatryan, V., et al. (CMS Collaboration), 2016g, "Measurement of the integrated and differential $t\bar{t}$ production cross sections for high-p_t top quarks in pp collisions at $\sqrt{s} = 8$ TeV," Phys. Rev. D **94**, 072002.

Khachatryan, V., et al. (CMS Collaboration), 2016h, "Search for vector-like charge 2/3 T quarks in proton-proton collisions at $\sqrt{s} = 8$ TeV," Phys. Rev. D **93**, 012003.

Khachatryan, V., et al. (CMS Collaboration), 2016i, "Search for pair-produced vectorlike B quarks in proton-proton collisions at $\sqrt{s} = 8$ TeV," Phys. Rev. D **93**, 112009.

Khachatryan, V., et al. (CMS Collaboration), 2016j, "Search for supersymmetry in pp collisions at $\sqrt{s} = 8$ TeV in final states with boosted W bosons and b jets using razor variables," Phys. Rev. D **93**, 092009.

Khachatryan, V., et al. (CMS Collaboration), 2016k, "Search for resonant $t\bar{t}$ production in proton-proton collisions at $\sqrt{s} = 8$ TeV," Phys. Rev. D **93**, 012001.

Khachatryan, V., et al. (CMS Collaboration), 2016l, "Search for direct pair production of supersymmetric top quarks decaying to all-hadronic final states in pp collisions at $\sqrt{s} = 8$ TeV," Eur. Phys. J. C **76**, 460.

Khachatryan, V., et al. (CMS Collaboration), 2017a, "Jet energy scale and resolution in the CMS experiment in pp collisions at 8 TeV," J. Instrum. **12**, P02014.

Khachatryan, V., et al. (CMS Collaboration), 2017b, "Search for supersymmetry in the all-hadronic final state using top quark tagging in pp collisions at $\sqrt{s} = 13$ TeV," Phys. Rev. D **96**, 012004.

Khachatryan, V., et al. (CMS Collaboration), 2017c, "Measurement of differential cross sections for top quark pair production using the lepton+jets final state in proton-proton collisions at 13 TeV," Phys. Rev. D **95**, 092001.

Khachatryan, V., et al. (CMS Collaboration), 2017d, "Search for heavy resonances decaying into a vector boson and a Higgs boson in final states with charged leptons, neutrinos, and b quarks," Phys. Lett. B **768**, 137–162.

Khachatryan, V., et al. (CMS Collaboration), 2017e, "Search for single production of a heavy vector-like T quark decaying to a Higgs boson and a top quark with a lepton and jets in the final state," Phys. Lett. B **771**, 80.

Komiske, P. T., E. M. Metodiev, B. Nachman, and M. D. Schwartz, 2017, "Pileup Mitigation with Machine Learning (PUMML)," J. High Energy Phys. 12, 051.

Komiske, P. T., E. M. Metodiev, and M. D. Schwartz, 2017, "Deep learning in color: Towards automated quark/gluon jet discrimination," J. High Energy Phys. 01, 110.

Komiske, P. T., E. M. Metodiev, and J. Thaler, 2018, "An operational definition of quark and gluon jets," J. High Energy Phys. 11, 059.

Krohn, D., M. D. Schwartz, T. Lin, and W. J. Waalewijn, 2013, "Jet charge at the LHC," Phys. Rev. Lett. **110**, 212001.

Krohn, D., M. D. Schwartz, M. Low, and L.-T. Wang, 2014, "Jet Cleansing: Pileup Removal at High Luminosity," Phys. Rev. D **90**, 065020.

Krohn, D., J. Thaler, and L.-T. Wang, 2009, "Jets with variable R," J. High Energy Phys. 06, 059.

Krohn, D., J. Thaler, and L.-T. Wang, 2010, "Jet Trimming," J. High Energy Phys. 02, 084.

Lai, H.-L., M. Guzzi, J. Huston, Z. Li, P. M. Nadolsky, J. Pumplin, and C.-P. Yuan, 2010, "New parton distributions for collider physics," Phys. Rev. D **82**, 074024.

Langacker, P., 2009, "The physics of heavy Z' gauge bosons," Rev. Mod. Phys. **81**, 1199.

Lapsien, T., R. Kogler, and J. Haller, 2016, "A new tagger for hadronically decaying heavy particles at the LHC," Eur. Phys. J. C **76**, 600.

Larkoski, A. J., S. Marzani, G. Soyez, and J. Thaler, 2014, "Soft Drop," J. High Energy Phys. 05, 146.

Larkoski, A. J., I. Moult, and B. Nachman, 2017, "Jet substructure at the Large Hadron Collider: A review of recent advances in theory and machine learning.," arXiv:1709.04464.

Larkoski, A. J., I. Moult, and D. Neill, 2014, "Power counting to better jet observables," J. High Energy Phys. 12, 009.

Larkoski, A. J., I. Moult, and D. Neill, 2016, "Analytic boosted boson discrimination," J. High Energy Phys. 05, 117.

Larkoski, A. J., D. Neill, and J. Thaler, 2014, "Jet shapes with the broadening axis," J. High Energy Phys. 04, 017.

Larkoski, A. J., G. P. Salam, and J. Thaler, 2013, "Energy correlation functions for jet substructure," J. High Energy Phys. 06, 108.

Larkoski, A. J., J. Thaler, and W. J. Waalewijn, 2014, "Gaining (mutual) information about quark/gluon discrimination," J. High Energy Phys. 11, 129.

Metodiev, E. M., B. Nachman, and J. Thaler, 2017, "Classification without labels: Learning from mixed samples in high energy physics," J. High Energy Phys. 10, 174.

Metodiev, E. M., and J. Thaler, 2018, "Jet topics: Disentangling quarks and gluons at colliders," Phys. Rev. Lett. **120**, 241602.

Moult, I., B. Nachman, and D. Neill, 2018, "Convolved substructure: Analytically decorrelating jet substructure observables," J. High Energy Phys. 05, 002.

Moult, I., L. Necib, and J. Thaler, 2016, "New angles on energy correlation functions," J. High Energy Phys. 12, 153.

Nachman, B., P. Nef, A. Schwartzman, M. Swiatlowski, and C. Wanotayaroj, 2015, "Jets from Jets: Re-clustering as a tool for large radius jet reconstruction and grooming at the LHC," J. High Energy Phys. 02, 075.

Plehn, T., G. P. Salam, and M. Spannowsky, 2010, "Fat jets for a light Higgs," Phys. Rev. Lett. **104**, 111801.

Plehn, T., M. Spannowsky, M. Takeuchi, and D. Zerwas, 2010, "Stop reconstruction with tagged tops," J. High Energy Phys. 10, 078.

Pomarol, A., 2000, "Gauge bosons in a five-dimensional theory with localized gravity," Phys. Lett. B **486**, 153.

Rajaraman, A., W. Shepherd, T. M. P. Tait, and A. M. Wijangco, 2011, "LHC bounds on interactions of dark matter," Phys. Rev. D **84**, 095013.

Randall, L., and R. Sundrum, 1999, "A Large mass hierarchy from a small extra dimension," Phys. Rev. Lett. **83**, 3370.

Rehermann, K., and B. Tweedie, 2011, "Efficient identification of boosted semileptonic top quarks at the LHC," J. High Energy Phys. 03, 059.

Salam, G. P., 2010, "Towards Jetography," Eur. Phys. J. C **67**, 637.

Salam, G. P., and G. Soyez, 2007, "A practical seedless infrared-safe cone jet algorithm," J. High Energy Phys. 05, 086.

Schmaltz, M., and D. Tucker-Smith, 2005, "Little Higgs review," Annu. Rev. Nucl. Part. Sci. **55**, 229.

Seymour, M. H., 1994, "Searches for new particles using cone and cluster jet algorithms: A comparative study," Z. Phys. C **62**, 127.

Shimmin, C., P. Sadowski, P. Baldi, E. Weik, D. Whiteson, E. Goul, and A. Søgaard, 2017, "Decorrelated jet substructure tagging using adversarial neural networks," Phys. Rev. D **96**, 074034.

Sirunyan, A. M., *et al.* (CMS Collaboration), 2017a, "Particle-flow reconstruction and global event description with the CMS detector," J. Instrum. **12**, P10003.

Sirunyan, A. M., *et al.* (CMS Collaboration), 2017b, "Combination of searches for heavy resonances decaying to WW, WZ, ZZ, WH, and ZH boson pairs in proton-proton collisions at $\sqrt{s} = 8$ and 13 TeV," Phys. Lett. B **774**, 533.

Sirunyan, A. M., *et al.* (CMS Collaboration), 2017c, "Search for heavy resonances that decay into a vector boson and a Higgs boson in hadronic final states at $\sqrt{s} = 13$ TeV," Eur. Phys. J. C **77**, 636.

Sirunyan, A. M., *et al.* (CMS Collaboration), 2017d, "Search for high-mass $Z\gamma$ resonances in proton-proton collisions at $\sqrt{s} = 8$ and 13 TeV using jet substructure techniques," Phys. Lett. B **772**, 363–387.

Sirunyan, A. M., *et al.* (CMS Collaboration), 2017e, "Measurement of the jet mass in highly boosted $t\bar{t}$ events from pp collisions at $\sqrt{s} = 8$ TeV," Eur. Phys. J. C **77**, 467.

Sirunyan, A. M., *et al.* (CMS Collaboration), 2017f, "Search for direct production of supersymmetric partners of the top quark in the all-jets final state in proton-proton collisions at $\sqrt{s} = 13$ TeV," J. High Energy Phys. 10, 005.

Sirunyan, A. M., *et al.* (CMS Collaboration), 2017g, "Search for massive resonances decaying into WW, WZ or ZZ bosons in proton-proton collisions at $\sqrt{s} = 13$ TeV," J. High Energy Phys. 03, 162.

Sirunyan, A. M., *et al.* (CMS Collaboration), 2017h, "Measurements of jet charge with dijet events in pp collisions at $\sqrt{s} = 8$ TeV," J. High Energy Phys. 10, 131.

Sirunyan, A. M., *et al.* (CMS Collaboration), 2017i, "Search for $t\bar{t}$ resonances in highly boosted lepton+jets and fully hadronic final states in proton-proton collisions at $\sqrt{s} = 13$ TeV," J. High Energy Phys. 07, 001.

Sirunyan, A. M., *et al.* (CMS Collaboration), 2017j, "Search for electroweak production of a vector-like quark decaying to a top quark and a Higgs boson using boosted topologies in fully hadronic final states," J. High Energy Phys. 04, 136.

Sirunyan, A. M., *et al.* (CMS Collaboration), 2017k, "Search for single production of vector-like quarks decaying to a Z boson and a top or a bottom quark in proton-proton collisions at $\sqrt{s} = 13$ TeV," J. High Energy Phys. 05, 029.

Sirunyan, A. M., *et al.* (CMS Collaboration), 2017l, "Search for pair production of vector-like T and B quarks in single-lepton final states using boosted jet substructure in proton-proton collisions at $\sqrt{s} = 13$ TeV," J. High Energy Phys. 11, 085.

Sirunyan, A. M., *et al.* (CMS Collaboration), 2017m, "Search for a heavy resonance decaying to a top quark and a vector-like top quark at $\sqrt{s} = 13$ TeV," J. High Energy Phys. 09, 053.

Sirunyan, A. M., *et al.* (CMS Collaboration), 2017n, "Search for dark matter produced with an energetic jet or a hadronically decaying W or Z boson at $\sqrt{s} = 13$ TeV," J. High Energy Phys. 07, 014.

Sirunyan, A. M., *et al.* (CMS Collaboration), 2017o, "Search for associated production of dark matter with a Higgs boson decaying to b$\bar{\text{b}}$ or $\gamma\gamma$ at $\sqrt{s} = 13$ TeV," J. High Energy Phys. 10, 180.

Sirunyan, A. M., *et al.* (CMS Collaboration), 2017p, "Searches for W' bosons decaying to a top quark and a bottom quark in proton-proton collisions at 13 TeV," J. High Energy Phys. 08, 029.

Sirunyan, A. M., *et al.* (CMS Collaboration), 2018a, "Observation of $t\bar{t}H$ production," Phys. Rev. Lett. **120**, 231801.

Sirunyan, A. M., *et al.* (CMS Collaboration), 2018b, "Observation of Higgs boson decay to bottom quarks," Phys. Rev. Lett. **121**, 121801.

Sirunyan, A. M., *et al.* (CMS Collaboration), 2018c, "Identification of heavy-flavour jets with the CMS detector in pp collisions at 13 TeV," J. Instrum. **13**, P05011.

Sirunyan, A. M., *et al.* (CMS Collaboration), 2018d, "Search for vectorlike light-flavor quark partners in proton-proton collisions at $\sqrt{s} = 8$ TeV," Phys. Rev. D **97**, 072008.

Sirunyan, A. M., *et al.* (CMS Collaboration), 2018e, "Measurement of jet substructure observables in $t\bar{t}$ events from proton-proton collisions at $\sqrt{s} = 13$ TeV," Phys. Rev. D **98**, 092014.

Sirunyan, A. M., *et al.* (CMS Collaboration), 2018f, "Search for supersymmetry in proton-proton collisions at 13 TeV using identified top quarks," Phys. Rev. D **97**, 012007.

Sirunyan, A. M., *et al.* (CMS Collaboration), 2018g, "Search for physics beyond the standard model in events with high-momentum Higgs bosons and missing transverse momentum in proton-proton collisions at 13 TeV," Phys. Rev. Lett. **120**, 241801.

Sirunyan, A. M., *et al.* (CMS Collaboration), 2018h, "Search for new physics in final states with an energetic jet or a hadronically decaying W or Z boson and transverse momentum imbalance at $\sqrt{s} = 13$ TeV," Phys. Rev. D **97**, 092005.

Sirunyan, A. M., *et al.* (CMS Collaboration), 2018i, "Search for Higgs boson pair production in events with two bottom quarks and two tau leptons in proton-proton collisions at $\sqrt{s} = 13$ TeV," Phys. Lett. B **778**, 101.

Sirunyan, A. M., *et al.* (CMS Collaboration), 2018j, "Search for massive resonances decaying into WW, WZ, ZZ, qW, and qZ with dijet final states at $\sqrt{s} = 13$ TeV," Phys. Rev. D **97**, 072006.

Sirunyan, A. M., *et al.* (CMS Collaboration), 2018k, "Evidence for the Higgs boson decay to a bottom quark-antiquark pair," Phys. Lett. B **780**, 501–532.

Sirunyan, A. M., *et al.* (CMS Collaboration), 2018l, "Inclusive search for a highly boosted Higgs boson decaying to a bottom quark-antiquark pair," Phys. Rev. Lett. **120**, 071802.

Sirunyan, A. M., *et al.* (CMS Collaboration), 2018m, "Search for single production of a vector-like T quark decaying to a Z boson and a top quark in proton-proton collisions at $\sqrt{s} = 13$ TeV," Phys. Lett. B **781**, 574–600.

Sirunyan, A. M., *et al.* (CMS Collaboration), 2018n, "Search for pair production of vector-like quarks in the $bW\bar{b}W$ channel from proton-proton collisions at $\sqrt{s} = 13$ TeV," Phys. Lett. B **779**, 82.

Sirunyan, A. M., *et al.* (CMS Collaboration), 2018o, "Measurements of the differential jet cross section as a function of the jet mass in dijet events from proton-proton collisions at $\sqrt{s} = 13$ TeV," J. High Energy Phys. 11, 113.

Sirunyan, A. M., *et al.* (CMS Collaboration), 2018p, "Search for low mass vector resonances decaying into quark-antiquark pairs in proton-proton collisions at $\sqrt{s} = 13$ TeV," J. High Energy Phys. 01, 097.

Sirunyan, A. M., *et al.* (CMS Collaboration), 2018q, "Search for $Z\gamma$ resonances using leptonic and hadronic final states in proton-proton collisions at $\sqrt{s} = 13$ TeV," J. High Energy Phys. 09, 148.

Sirunyan, A. M., *et al.* (CMS Collaboration), 2018r, "Search for dark matter in events with energetic, hadronically decaying top quarks and missing transverse momentum at $\sqrt{s} = 13$ TeV," J. High Energy Phys. 06, 027.

Sjostrand, T., S. Mrenna, and P. Z. Skands, 2006, "PYTHIA 6.4 Physics and Manual," J. High Energy Phys. 05, 026.

Sjostrand, T., S. Mrenna, and P. Z. Skands, 2008, "A Brief Introduction to PYTHIA 8.1," Comput. Phys. Commun. **178**, 852–867.

Skands, P. Z., 2010, "Tuning Monte Carlo generators: The Perugia Tunes," Phys. Rev. D **82**, 074018.

Soper, D. E., and M. Spannowsky, 2011, "Finding physics signals with shower deconstruction," Phys. Rev. D **84**, 074002.

Soper, D. E., and M. Spannowsky, 2013, "Finding top quarks with shower deconstruction," Phys. Rev. D **87**, 054012.

Soyez, G., G. P. Salam, J. Kim, S. Dutta, and M. Cacciari, 2013, "Pileup subtraction for jet shapes," Phys. Rev. Lett. **110**, 162001.

Sterman, G., and S. Weinberg, 1977, "Jets from Quantum Chromodynamics," Phys. Rev. Lett. **39**, 1436.

Thaler, J., and K. Van Tilburg, 2011, "Identifying boosted objects with N-subjettiness," J. High Energy Phys. 03, 015.

Thaler, J., and K. Van Tilburg, 2012, "Maximizing boosted top identification by minimizing N-subjettiness," J. High Energy Phys. 02, 093.

Thaler, J., and L.-T. Wang, 2008, "Strategies to Identify Boosted Tops," J. High Energy Phys. 07, 092.

Waalewijn, W. J., 2012, "Calculating the charge of a jet," Phys. Rev. D **86**, 094030.

Wobisch, M., and T. Wengler, 1998, "Hadronization corrections to jet cross-sections in deep inelastic scattering," in *Monte Carlo generators for HERA physics. Proceedings, Workshop, Hamburg, Germany, 1998–1999* (DESY, Hamburg, Germany), p. 270.